POLITECNICO DI TORINO

Master of Science in Electronic Engineering

Master Thesis

Analysis and Simulation of the Sinusoidal Clocking Field in Molecular FCN

Supervisors:
Prof. Gianluca Piccinini
Prof. Mariagrazia Graziano

Candidate:
Giovanni Sanclemente

April 2019

Compiled with LaTeX on April 3, 2019.

Computers are incredibly fast, accurate and stupid. Humans are incredibly slow, inaccurate and brilliant. The combination of two constitutes an incalculable force.."

Albert Einstein

Acknowledgements

At the end of this formative path, I wish to thank all those people who have been close to me, with sincere affection, sharing the stages of this road. I would like these thanks to be a point of arrival on one side, but also a starting point, because I believe that we will never stop growing and I hope to be able to reach new important goals in my life and above all in my work.
First of all, I thank my parents for giving me the opportunity to arrive here, without their moral and economic support, all this would not have been possible, they believed in me allowing me to reach this important goal. I thank my brother Vito who always gave me a hand to overcome this difficult but stimulating journey.
A special thank goes to my girlfriend Alessandra whom most of all supported me, allowing me to reach my maximum potential and making me happy like no one else has done. I also thank my supervisors, Prof. Piccinini and Prof. Graziano, for guiding me with their great wisdom and for the help given to me during this thesis work, but in particular, I want to thank the PhD student Yuri Ardesi for his incredible availability, for the excellent advice and for having followed me during the thesis work, despite the many commitments arising from the PhD.
I would like to thank all my university friends including Luca, Marco and Davide for their great sympathy but also my housemate Antonino, with whom I established a good friendship. And last but not least my two cousins Vincenzo and Giovanni, who are brothers to me, to whom I want a world of good.

Summary

Moore's Law states that the number of transistors per chip doubles roughly every two years. For decades, semiconductor industry has succeeded in shrinking transistor dimensions, keeping up with this law and getting ever more powerful laptops, tablets, and smartphones. However, ITRS roadmap has predicted that Moore's law will reach natural end in 2020, due to the impossibility of miniaturization of electronic devices since the physical limits of the semiconductor-based technology are achieved, such as unbearable power consumption and leakage current.

With the aim of overcoming these scaling constraints, different technologies projected towards nanometric scales are being researched, among these the most promising are FCN technologies (Field-Coupled NanoComputing). These new transistorless technologies do not exploit standard current-voltage paradigm but only local field interactions, not involving charge transport for binary information transfer. In particular, among these FCN paradigms, the Molecular QCA (Quantum Cellular Automata) technology represents a very interesting candidate where the basic building block is a cell formed by molecules.

Exploiting the redox centers of molecules as electron containers well-known charge arrangements are possible inside the QCA cells allowing binary encoding information. In general, the *Three-Phase Clocking* is needed to ensure correct switching behaviour of QCA cells and adiabatic propagation of information, avoiding the fall of circuit in a metastable state. In particular, in this thesis a full characterization of all basic QCA devices with a new *Sinusoidal Clocking* is performed verifying the feasibility and correct propagation of information with this novel clocking mechanism.

Thesis Organization

- **Chapter 1: Introduction**
  In Chapter 1 the basic operating principles of QCA cells are discussed, as well as, how the binary information is encoded and transmitted. Moreover, the basic logic QCA gates are treated and illustrated. In the final part of chapter, an explanation of Three-Phase Clocking in a QCA Wire is performed.

- **Chapter 2: Possible Physical Implementations of QCA Device**
  In Chapter 2 the various possible implementations of QCA Device are treated, giving a brief description of each of them and explaining why the molecular QCA is one of the major implementations under investigation.

- **Chapter 3: Candidate Molecules for MQCA**
  In Chapter 3 the various candidate Molecules for MQCA are analysed leading to a deepening on why the *Bis-ferrocene* molecule has been chosen for QCA circuit implementation. In particular, the description on the effect of *Switching field* and *Clock field* on this molecule, as well as, a hint on Molecule-Molecule Interactions, Write-In and Read-Out Systems is carried out.

- **Chapter 4: Sinusoidal Clocking Mechanism**
  In Chapter 4 the new Sinusoidal Clocking Mechanism is explained highlighting the differences and advantages with respect to the Three-Phase Clocking one. Chapter 4 also introduces the simulation MATLAB® program called SCERPA and the code designed to apply the Sinusoidal Clock to the different QCA devices.

- **Chapter 5: Sinusoidal Clocking Simulation Analysis and Results**
  In Chapter 5 results concerning Sinusoidal Clocking simulation in the different MQCA functional blocks are discussed. Moreover, an improvement of QCA device layouts is performed, as well as, the designing of new QCA Inverter.

- **Chapter 6: Sinusoidal Clocking Simulation of MQCA Circuit: Half Adder**
  In Chapter 6 results concerning Sinusoidal Clocking simulation in the Half Adder are reported demonstrating a possible application of the Sinusoidal Clock on functional QCA circuit.

- **Chapter 7: MQCA Wire Noise Analysis**
  In Chapter 7 a first model of thermal noise is proposed. The noise is generated according to Gaussian distribution and applied on MQCA Wire in order to simulate more realistic conditions.

Contents

List of Figures VIII

List of Tables IX

1 Introduction 1

1.1 Beyond CMOS Technologies . . . 1
1.2 Quantum-Dot Cellular Automata . . . 4
1.2.1 Single QCA Cell . . . 4
1.2.2 Cell Coupling . . . 6
1.2.3 Basic QCA Building Blocks . . . 8
1.2.4 Four-Phase Clocking QCA System . . . 11

2 Possible Physical Implementations of QCA Device 15

2.1 Metal-Dot QCA . . . 16
2.2 Semiconductor-Dot QCA . . . 16
2.3 Magnetic QCA or Nanomagnet Logic (NML) . . . 17
2.4 Molecular QCA . . . 19

3 Candidate Molecules for MQCA 23

3.1 Diallyl-Butane Molecule . . . 24
3.2 Decatriene Molecule . . . 26
3.3 Bis-Ferrocene Molecule . . . 26
3.3.1 Effects of Switching and Clock Fields . . . 29
3.3.2 Driver-Molecule and Molecule-Molecule Interactions . . . 32
3.3.3 Write-In and Read-Out Systems . . . 36
3.3.4 MQCA Clock System: Three-Phase Clock . . . 38

4 Sinusoidal Clocking Mechanism 41

4.1 Sinusoidal Clock Simulation with SCERPA . . . 43
4.2 Algorithm section . . . 44
4.3 Layout section . . . 44
4.3.1 Molecule Settings . . . 45
4.3.2 Sinusoidal Clock Settings . . . 46

4.3.3 Driver Definition 47
4.3.4 Process Variation 48
4.3.5 Layout QCA Circuit 49
4.3.6 “Fake” Sinusoidal Clock Phases 56

5 Sinusoidal Clocking Simulation Analysis and Results 67
5.1 Simulation Results: Wire Structure 67
5.1.1 Minimum Lambda of Sinusoidal Clock 69
5.1.2 Maximum Lambda of Sinusoidal Clock 71
5.2 Simulation Results: Angle Structure 76
5.3 Simulation Results: T-shape Structure 82
5.4 Simulation Results: Majority Voter 87
5.5 Simulation Results: Inverter 91
5.5.1 Inverter behaviour with Three-Phase Clock 91
5.5.2 Inverter behaviour with Sinusoidal Clock 95
5.6 Lower Bound of Sinusoidal Clock Wavelength 100

6 Sinusoidal Clocking Simulation of MQCA Circuit: Half Adder 105
6.1 Sub-Circuit of Half Adder 105
6.2 Half Adder 113
6.2.1 Simulation Results: Half Adder 115

7 MQCA Wire Noise Analysis 121
7.1 Simulation Methodology and Results 122

8 Conclusion and Future Perspectives 129

References 132

List of Figures

1.1 Moore's Law. 1
1.2 Relationship of "More Moore","More than Moore" and "Beyond CMOS". 3
1.3 Standard Logic dots indexing in QCA cell. 5
1.4 QCA cell structure and logic state encoding. 5
1.5 Maximum and minimum electrostatic repulsion conditions in QCA cell. 6
1.6 State transfer between two adjacent cells. 7
1.7 QCA Binary Wire. 8
1.8 Propagation of information in a QCA Wire. 8
1.9 QCA Inverter. 9
1.10 Propagation of information in a QCA Inverter. 9
1.11 QCA Majority Voter. 10
1.12 QCA AND Gate. 10
1.13 QCA OR Gate. 11
1.14 Four phase Clock signal waveform. 12
1.15 Application of Clock signal to the QCA Cell. 13
1.16 Different phases of trapezoidal signal applied to the clock zones of QCA Wire. 13

2.1 Main types of Quantum Cellular Automata. 15
2.2 Metal-Dot QCA binary representation. 16
2.3 NML binary representation. 18
2.4 (A) Anti-ferromagnetically coupled binary wire, (B) Ferromagnetically coupled binary wire. 19
2.5 Schematic of a magnetic three-input majority-logic gate. 19
2.6 State encoding of 2-dots oxidized molecule: (A) logic state "1"; (B) switching state and (C) logic state "0". 20
2.7 State encoding of 3-dots oxidized molecule: (A) logic state "0"; (B) logic state "1" and (C) NULL state [18]. 21
2.8 Complete MQCA cell: (A) 3D view, (B) top view. 21
2.9 Horizontal and Vertical Interaction in 1D implementation. 22

3.1 Diallyl-butane molecule (A) molecular structure [41], (B) schematic representation. . . . 24
3.2 Binary representation in the MQCA cell: (A) Diallyl-butane molecules with molecular orbital localization [18] and (B) corresponding scheme. 25
3.3 Molecule with 3 Allyl groups (A) molecular structure [28], (B) schematic representation. . . . 26
3.4 Decatriene Molecule (A) molecular structure [41], (B) schematic representation. . . . 27
3.5 Bis-Ferrocene Molecule (A) molecular structure [43], (B) schematic representation. . . . 27
3.6 Bis-Ferrocene Molecule (A) Ground state HOMO, (B) HOMOs of logic state "1", (C) HOMOs of logic state "0" [15]. (D),(E) and (F) corresponding schematic representation. . . . 28
3.7 MQCA cell Binary encoding: (A) Bis-ferrocene molecules with molecular orbital localization [17] and (B) corresponding schematic representation. . . . 29
3.8 (A) Switching Field for single bis-ferrocene molecule; (B) Charge localization with positive Switching Field and (C) Charge localization with Negative one. . . . 30
3.9 (A) Clock Field for single bis-ferrocene molecule; (B) Available charge localizations with Positive Clock Field and (C) Charge localization with Negative one. . . . 31
3.10 (A) Charge localization example with positive Clock Field and positive Switching Field; (B) Charge configuration deriving from molecular coupling achievable thanks positive clock field; (C) Charge localization with negative Clock Field and Positive/Negative Switching Field and (D) Charge localization with negative Clock Field depicting the molecular interaction suppression. . . . 31
3.11 Driver-molecule interactions model: (A) 3D view and (B) top view. 32
3.12 (A) Charge distributions by means of ESP computation[4] (B) Aggregated charges definition for bis-ferrocene molecule dots. . . . 33
3.13 Molecule-Molecule interactions model: (A) 3D view and (B) top view. 33
3.14 Electric field generated by the distribution of: (A) Point charges of ideal driver (B) Aggregated charge of a bis-ferrocene molecule and the corresponding V_{IN}. . . . 34
3.15 V_{IN}–V_{OUT} schematic representation: (A) Point charges of ideal driver (B) Aggregated charge of a bis-ferrocene molecule and the corresponding V_{IN} (for the sake of clarity the left part of generated electric field by the MUT is not reported). . . . 35
3.16 Write-in and Read-out system for a MQCA wire. . . . 36
3.17 Aggregated charge analysis on the three dots vs. the Switching Field [15]. . . . 37

3.18 (A) Scheme of physical implementation of MQCA clock system (B) Almost vertical Clock field generated by the designed clock system. 38
3.19 Scheme representation of MQCA physical implementation: (A) 3D view (B) Top view with Clock Zone partition. 39
3.20 Schematic example of information propagation in MQCA Wire. . . 40

4.1 (A) Clock systems comparison: Three-Phase Clock schematic (left) Sinusoidal Clock schematic (right), (B) corresponding Clock voltages. 41
4.2 Sinusoidal Clock physical implementation proposed in [24]: (A) 3D view, (B) Transversal view with schematic representation of induced sinusoidal clock field. 42
4.3 Flux lines of electric field generated by nanoelectrodes obtained through COMSOL program 43
4.4 Discretization of the Sinusoidal Clock to the QCA Wire. 44
4.5 Flow chart of SCERPA for MQCA simulations. 45
4.6 Schematic representation of `dist_z` and `dist_y` (top view) 50
4.7 Layout of the MQCA Wire obtained with the instructions in `Qca_wire` box. 50
4.8 Layout of the MQCA Majority Voter obtained with the instructions in `Qca_majority_voter` box (two Clock Zone are enough). 52
4.9 Layout of the MQCA Wire obtained with the instructions in `Qca_wire_sinusoidal_ck` box. 54
4.10 Layout of the MQCA Majority Voter obtained with the instructions in `Qca_majority_voter_sinusoidal_ck` box. 55
4.11 Simulation of MQCA Wire formed by 24 molecules with Three-Phase Clock. 57
4.12 Comparison between the defined sinusoidal Clock and MQCA Wire. 59
4.13 Possible initial configuration of Wire with Sinusoidal Clock. 60
4.14 Correct initial configuration of Wire with Sinusoidal Clock, in the left the layout is present at different time instants, in the right the corresponding charge distribution along the Wire. 61
4.15 Schematic representation of voltage values updating with `num_mol_update = 4`. 62
4.16 Schematic representation of voltage values updating with `num_spatial_step_update = 6` (in the picture $n = 6$). 63

5.1 Wire simulation formed by 24 molecules and Sinusoidal Clock application with a wavelength $\lambda = 24\ nm$. 68
5.2 Maximum number of activated molecules in a Wire of 24 molecules with Sinusoidal Clock application at wavelength $\lambda = 24\ nm$ and at fixed time instant: Above a schematic representation, below the corresponding charge distribution. 69

5.3 Sinusoidal Clocked behaviour of Wire with 50 molecules at wavelength $\lambda = 10\ nm$ and at fixed time instant: Above the structure layout, below the corresponding charge distribution. 70
5.4 Sinusoidal Clocked behaviour of Wire with 50 molecules at wavelength $\lambda = 12\ nm$ and at fixed time instant: Above the structure layout, below the corresponding charge distribution. 71
5.5 Sinusoidal Clocked behaviour of Wire with 100 molecules at wavelength $\lambda = 12\ nm$ and at fixed time instant: charge distribution. . . 72
5.6 Sinusoidal Clocked behaviour of Wire with 50 molecules at wavelength $\lambda = 1\ \mu m$ and at fixed time instant (charge distribution). . . 72
5.7 Sinusoidal Clocked behaviour of Wire with 50 molecules at wavelength $\lambda = 100\ \mu m$ and at fixed time instant (charge distribution). . 73
5.8 Sinusoidal Clocked behaviour of Wire with 100 molecules at wavelength $\lambda = 1\ \mu m$ and at fixed time instant (charge distribution). . . 73
5.9 Sinusoidal Clocked behaviour of Wire with 100 molecules at wavelength $\lambda = 100\ \mu m$ and at fixed time instant (charge distribution). . 74
5.10 Sinusoidal Clocked behaviour of Wire with 300 molecules at wavelength $\lambda = 1\ \mu m$ and at fixed time instant (charge distribution). . . 74
5.11 Sinusoidal Clocked behaviour of Wire with 300 molecules at wavelength $\lambda = 100\ \mu m$ and at fixed time instant (charge distribution). . 75
5.12 Wavefronts schematic representation. 76
5.13 Schematic layout of Angle structure and direction propagation of wavefronts. 76
5.14 Sinusoidal Clocked behaviour of Angle at wavelength $\lambda = 12\ nm$ with logic input state “0”. 77
5.15 Top view of Sinusoidal Clocked behaviour of Angle at wavelength $\lambda = 12\ nm$, with logic input state “0”: (A) Before information corruption, (B) After information corruption. 78
5.16 Sinusoidal Clocked behaviour of Angle at wavelength $\lambda = 50\ nm$ with logic input state “0”. 78
5.17 Sinusoidal Clocked behaviour of Angle at wavelength $\lambda = 1\ \mu m$ with logic input state “1”. 79
5.18 Top view of Sinusoidal Clocked behaviour of Angle at wavelength $\lambda = 1\ \mu m$, with logic input state “1”: (A) inside transition window, (B) outside transition window. 80
5.19 Sinusoidal Clocked behaviour of Angle at wavelengths $\lambda = 12\ nm$, $\lambda = 50\ nm$, $\lambda = 1\ \mu m$, at fixed time instants and with logic input state “0” (left column) and “1” (right column). 81
5.20 Schematic layout of T-shape structure and direction propagation of wavefronts. 82
5.21 Sinusoidal Clocked behaviour of T-shape structure at wavelength $\lambda = 12\ nm$ with logic input state “0”. 83

5.22 Sinusoidal Clocked behaviour of T-shape structure at wavelength $\lambda = 50\ nm$ with logic input state “0”. 84
5.23 Sinusoidal Clocked behaviour of T-shape structure at wavelength $\lambda = 1\ \mu m$ with logic input state “0”. 85
5.24 Comparison between the standard T-shape structure and the enhanced one at the same time instant (inside the transition window). 85
5.25 Sinusoidal Clocked behaviour of T-shape structure at wavelengths $\lambda = 12\ nm$, $\lambda = 50\ nm$, $\lambda = 1\ \mu m$, at fixed time instants and with logic input state “0” (left column) and “1” (right column). 86
5.26 Schematic layout of Majority Voter and direction propagation of wavefronts. 87
5.27 Sinusoidal Clocked behaviour of Majority Voter at wavelength $\lambda = 12\ nm$, at fixed time instants and with the eight logic input states reported in Table 5.1. 88
5.28 Polarization error of intersection cell with input pattern $A = 0$, $B = 1$, $C = 0$ at $\lambda = 12\ nm$: (A) Top view of Figure 5.27.b, (B) Central and peripheral cells definition. 89
5.29 Sinusoidal Clocked behaviour of Majority Voter at wavelength $\lambda = 50\ nm$, at fixed time instants and with the eight logic input states reported in Table 5.1. 90
5.30 Sinusoidal Clocked behaviour of Majority Voter at wavelength $\lambda = 1\ \mu m$, at fixed time instants and with the eight logic input states reported in Table 5.1. 91
5.31 Schematic layout of Inverter structure used for Three-phase Clock analysis. 92
5.32 Three-Phase Clocked behaviour of Inverter with logic input state “0”. 92
5.33 Three-Phase Clocked behaviour of Inverter with logic input state “1”. 93
5.34 Structures’ comparison: (A) Standard Inverter, (B) new Enhanced Inverter structure, highlighting the corresponding modifications with respect standard structure. 93
5.35 Three-Phase Clocked behaviour of new Enhanced Inverter with logic input state “0”. 94
5.36 Three-Phase Clocked behaviour of new Enhanced Inverter with logic input state “1”. 95
5.37 Schematic layout of Enhanced Inverter structure used for Sinusoidal Clock analysis and direction propagation of wavefronts. 96
5.38 Sinusoidal Clocked behaviour of Enhanced Inverter at wavelength $\lambda = 12\ nm$ with the logic input state “0”. 97
5.39 Sinusoidal Clocked behaviour of Enhanced Inverter at wavelength $\lambda = 50\ nm$ with the logic input state “1”. 98
5.40 Sinusoidal Clocked behaviour of Enhanced Inverter at wavelength $\lambda = 1\ \mu m$ with the logic input state “0”. 99

5.41 Error corruption in Enhanced Inverter with Sinusoidal Clock at wavelength $\lambda = 1\ \mu m$: (A) Top view and cell x, cell y definition, (B) and (C) Schematic representation of the parties responsible for the error. 100
5.42 Sinusoidal Clocked behaviour of Wire with 100 molecules at wavelength $\lambda = 20\ nm$ and at fixed time instant: charge distribution. . . 101
5.43 Sinusoidal Clocked behaviour of Angle at wavelength $\lambda = 20\ nm$, at fixed time instant and with both logic input states. 101
5.44 Sinusoidal Clocked behaviour of T-shape structure at wavelength $\lambda = 20\ nm$, at fixed time instant and with both logic input states. . 102
5.45 Sinusoidal Clocked behaviour of Majority Voter at wavelength $\lambda = 20\ nm$, at fixed time instant and with the eight logic input states reported in Table 5.1. 102
5.46 Sinusoidal Clocked behaviour of Enhanced Inverter at wavelength $\lambda = 20\ nm$ with the logic input "1". 103
5.47 Sinusoidal Clocked behaviour of Enhanced Inverter at wavelength $\lambda = 20\ nm$ with the logic input "0". 104

6.1 Left: Schematic diagram of Half Adder, Right: The Schematic diagram of Half Adder used to design the MCQA Half Adder, where is visible the schematic of XOR gate. 105
6.2 Schematic layout of Half Adder Sub-Circuit. 106
6.3 Sinusoidal Clocked behaviour of Half Adder Sub-Circuit at wavelength $\lambda = 50\ nm$ with the logic input configurations $A = 0$, $B = 0$ and and $Output = 0$. 107
6.4 Sinusoidal Clocked behaviour of Half Adder Sub-Circuit at wavelength $\lambda = 50\ nm$ with the logic input configurations $A = 0$, $B = 1$ and $Output = 1$. 108
6.5 Sinusoidal Clocked behaviour of Half Adder Sub-Circuit at wavelength $\lambda = 50\ nm$ with the logic input configurations $A = 1$, $B = 0$ and $Output = 0$. 109
6.6 Sinusoidal Clocked behaviour of Half Adder Sub-Circuit at wavelength $\lambda = 50\ nm$ with the logic input configurations $A = 1$, $B = 1$ and $Output = 0$. 110
6.7 Reliability verification of Enhanced Inverter at different distances between the branches and its final part. 112
6.8 Schematic layout of Half Adder (3D view). 113
6.9 Schematic layout of Half Adder(top view). 114
6.10 Sinusoidal Clocked behaviour of Half Adder at wavelength $\lambda = 50\ nm$ and with all four input pattern configurations. 119

7.1 Bis-ferrocene Transcharacteristics: Aggregated Charges - Applied Electric Field relation. 122

7.2 Charge distributions at different time instants of Sinusoidal Clocked Ideal Wire during transmission of one frame, with $\Delta V_{in} = 0\ mV$, $\lambda = 20\ nm$ and $d = 1\ nm$. 124
7.3 Charge distributions at different time instants of Sinusoidal Clocked Noisy Wire during transmission of one frame, with $\Delta V_{in} = 81.8\ mV$, $\lambda = 20\ nm$ and $d = 1\ nm$. 125
7.4 Charge distributions at different time instants of Sinusoidal Clocked Noisy Wire during transmission of one frame, with $\Delta V_{in} = 40.9\ mV$, $\lambda = 20\ nm$ and $d = 1\ nm$. 125
7.5 Charge distributions at different time instants of Sinusoidal Clocked Noisy Wire during transmission of one frame, with $\Delta V_{in} = 27.3\ mV$, $\lambda = 20\ nm$ and $d = 1\ nm$. 126
7.6 Charge distributions at different time instants of Sinusoidal Clocked Ideal Wire during transmission of one frame, with $\Delta V_{in} = 0\ mV$, $\lambda = 16\ nm$ and $d = 0.8\ nm$. 126
7.7 Charge distributions at different time instants of Sinusoidal Clocked Noisy Wire during transmission of one frame, with $\Delta V_{in} = 81.8\ mV$, $\lambda = 16\ nm$ and $d = 0.8\ nm$. 127
7.8 Charge distributions at different time instants of Sinusoidal Clocked Noisy Wire during transmission of one frame, with $\Delta V_{in} = 40.9\ mV$, $\lambda = 16\ nm$ and $d = 0.8\ nm$. 127

List of Tables

4.1 Possible initial charge configurations of Bis-ferrocene molecule. . . . 46
4.2 Generated matrix by the instructions in the `Fake_ck_phases` box. . . . 56
4.3 Generated `ck_table` matrix when $\Delta x >$ *intermolecular distance* and `num_mol_update = 4` considering a MQCA Wire formed by arrangement of 24 molecules. 64
4.4 Generated `ck_table` matrix when $\Delta x <$ *intermolecular distance* and `num_spatial_step_update = 3` considering a MQCA Wire formed by arrangement of 24 molecules. 65

5.1 Truth table of Majority Voter. 87

6.1 Truth table of Half Adder Sub-Circuit. 106
6.2 Truth table of Half Adder. 113

Chapter 1

Introduction

1.1 Beyond CMOS Technologies

For the past 50 years, the Semiconductor Industry has followed the pace of Moore's Law (Figure 1.1), according to which, every two years the number of transistors per chip doubles, due to the transistor scaling. As a consequence, the ability of the semiconductor industry to continuously scale down the transistors translates into their switching from the off to the on state at faster rates, and in increasingly cheaper manufacture.

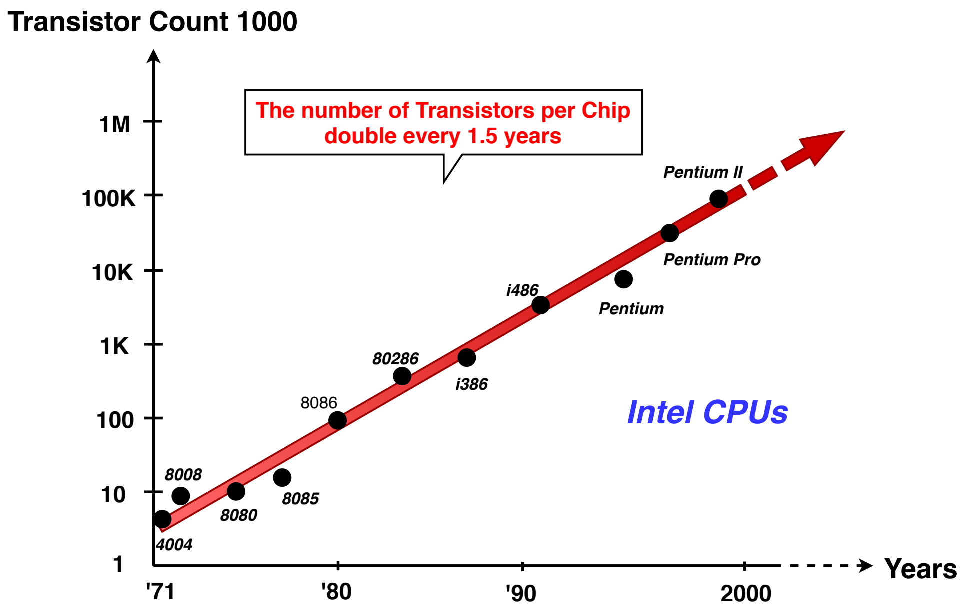

Figure 1.1. Moore's Law.

Through the years nobody paid too much attention to the fact that power consumption of *Integrated Circuits* (IC_s) kept on increasing with any new technology generation since the industry motto was: ***"Performance at any cost"***[5]. However, it has been shown that it has become practically impossible to increase both working frequency and number of transistors, due to physical limitations on power dissipation. Therefore, one of the two feature, the frequency, was chosen as the sacrificial victim since an increase of it leads also to a higher dynamic power, so it has stalled in the few GHz, in order to make the IC_s capable to operate under practical thermal conditions [5].

The current-switch paradigm at the base of *Complementary Metal-Oxide Semiconductor* (CMOS) technology, according to which the binary information is represented by turning current switches on or off, meets serious limitations as transistor sizes are reduced to the nanometers scale [33]. When the switch shrinking occurs, there are several challenges to overcome including the leakage currents through the gate oxide, the less capability to turn the current off and on cleanly, low on/off ratios due to *Drain Induced Barrier Lowering* (DIBL), the increasing charge time of the interconnect lines due to the smaller current through a single switch, and very high power dissipation.

In order to overcome these fundamental restrictions, several new alternative information processing devices and computational paradigms for existing or new functions are being explored, leading to an evolution of two technology domains [5]:

1. Extending the functionality of the CMOS platform via *heterogeneous integration* of new technologies (a.k.a **"More than More"**). In this case, added value to devices is provided by incorporating functionalities that do not necessarily scale according to Moore's Law.

2. Stimulating invention of new information computing paradigms (a.k.a **"Beyond CMOS"**).

The relation between these two domains is schematically illustrated in Figure 1.2.

The dimensional and functional scaling of the CMOS platform is often called *"More Moore"*, where functional scaling means that a system has been realized to execute a specific function in current technology and it has scaled functionality if it is realized in an alternate technology such that it performs the identical function as the original system and offers improvements in at least one of size, power, speed or cost, and does not degrade in any of the other metrics. The CMOS platform can be further extended by the "More than Moore" approach, which was first introduced into *Emerging Research Devices* (ERD) chapter in 2011.

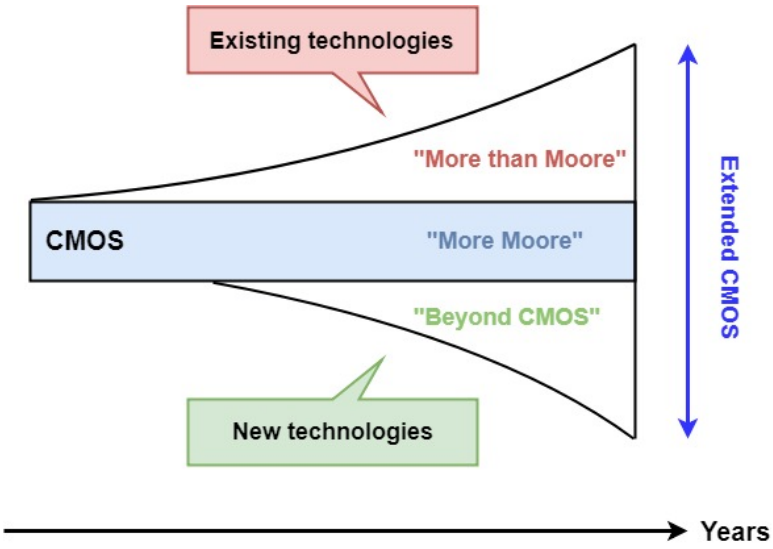

Figure 1.2. Relationship of “More Moore”,“More than Moore” and “Beyond CMOS”.

On the other hand, new information processing and architectures are called “Beyond CMOS” technologies. The heterogeneous integration of “Beyond CMOS”, as well as “More than Moore”, into “More Moore” will extend the CMOS platform functionality forming ultimate **“Extended CMOS”** [5].

1.2 Quantum-Dot Cellular Automata

Since the scaling of the current CMOS technology will reach the fundamental limit in the near future the era of “Beyond CMOS” will start. In particular, among all of these evolving nanotechnologies, *Field-Coupled Nanocomputing* (FCN) paradigms show great potential and they are viable candidate for “Beyond CMOS” device technology. In FCN paradigms information encoding, transmission and computation are achieved, not using transistors, but via local field interactions between nanoscale building blocks arranged in array form.

Several FCN paradigms are currently under active investigation, including *Quantum-dot Cellular Automata* (QCA), *Molecular Quantum-dot Cellular Automata* (MQCA), *NanoMagnetic Logic* (NML), and *Atomic Quantum Cellular Automata* (AQCA). Each of these paradigms presents features that make it a good candidate for Beyond-CMOS technologies, but each of them must face great obstacles to realization and fabrication [3].

The QCA is a FCN based architecture that has been proposed by C.S. Lent and his co-worker at early 1990s derived from the confluence of four concepts [3]:

1. The ability to realize configurations of quantum dots able to localize charge.
2. The practical device would need bistable saturation in the information transfer function, argued by Landauer.
3. The charge quantization leads to non-linearity of charge tunneling between such dots.
4. The notion of a locally coupled architecture in analogy to *Cellular Automata* (CA).

Which means that the binary information is encoded using an elementary unit called **QCA Cell**, in which the state of each cell is determined by the state of the neighbouring cells. The information propagation occurs through field coupling, either electrostatic or magnetic, of such QCA cells, not requiring charge transport among them. The power dissipation is significantly reduced with respect to standard CMOS technology where current flow is present, and high device density and working frequency up to THz are achievable.

1.2.1 Single QCA Cell

The basic QCA cell is a squared nanostructure of potential wells confining free electrons. Each cell is constructed from six quantum dots (or four quantum dots depending on the implementation technology), which can ideally hold a mobile charge per dot, and binary information is represented by the arrangement of these charges (or magnetic dipoles) inside this cell. Importantly, cells are designed to have a bistable charge configuration, which means to have two low energy states with different dipole or quadrupole orientation that can encode a binary logic states "1" or "0", and no current flows into or out of the cell. Using indexing convention illustrated in Figure 1.3, *cell polarization* is defined as:

$$P = \frac{(\rho_1 + \rho_3) - (\rho_2 + \rho_4)}{\rho_1 + \rho_2 + \rho_3 + \rho_4} \tag{1.1}$$

where ρ_i is the charge density at dot i and its value represents the average number of electrons occupying dot i [34].

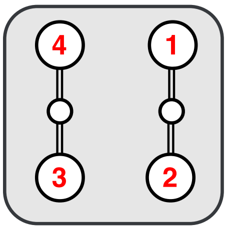

Figure 1.3. Standard Logic dots indexing in QCA cell.

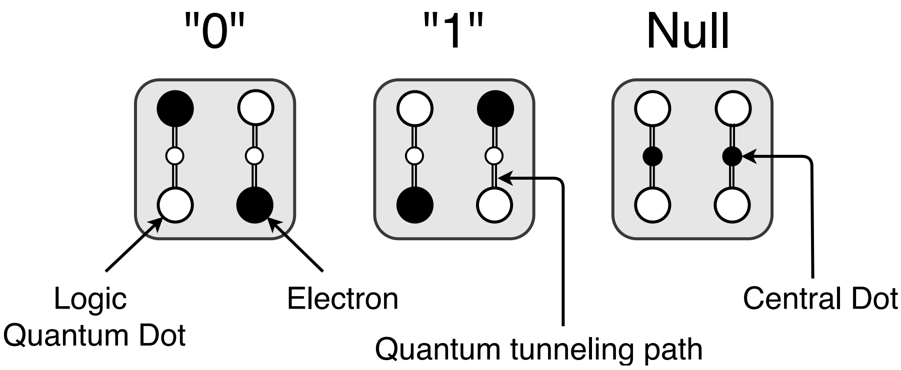

Figure 1.4. QCA cell structure and logic state encoding.

When the two free electrons lie in the main diagonal of the cell the logic state "0" is reached and the cell is negatively polarized ($P = -1$), vice versa if they lie in the anti-diagonal the logic state "1" is reached and the cell is positively polarized ($P = +1$) . The third state represents the condition when the two free electrons are forced to occupy the two central dots, representing the so-called *NULL state* ($P = 0$) because in this configuration the cell is unpolarized and no binary information holds in it. Apparently it may seem useless, nevertheless it is fundamental to fix switching issue and favour the transition between the logic states, moreover, in the future can be used to create a ternary logic system.

The working principle of QCA relies on quantum mechanical inter-dot tunneling of the electrons localized in the *Logic Quantum Dots* (physically they are wells), and on coulombic interaction between these mobile charges.
The barrier potential between dots should be high enough so that charge can only tunnel through the barrier, allowing the localization and confinement in the dots and not in the tunneling paths. The electrons arrangement in the QCA cell is ruled by the Coulomb's law according to which the electrons tend to occupy the Logic Quantum Dots with maximum distance, minimizing electrostatic repulsion between them and reaching the minimum energy condition [8].
Therefore, there are the only two possible configurations of the electrons because all other arrangements lead to maximum repulsion as shown in Figure 1.5.

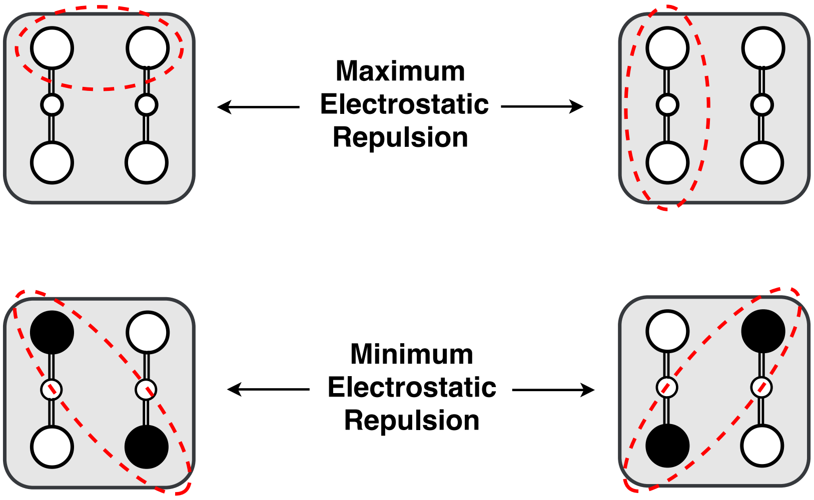

Figure 1.5. Maximum and minimum electrostatic repulsion conditions in QCA cell.

1.2.2 Cell Coupling

In order to understand how the information is transferred it is necessary to examine the coupling between two adjacent cells. When two QCA cells are placed close enough to each other, always by means coulombic interaction, the first cell (*Driver* *cell*) induce the second cell (*Target cell*) to assume the same polarity reaching the minimum energy condition.

The electrostatic cell-cell coupling can be described by the so-called *kink energy*, E_{kink}, associated with the energetic cost of two neighbouring cells having opposite polarization [31]. The electrostatic interaction between charges in two four-dot cells, A and B, is:

$$E_{A,B} = \frac{1}{4\pi\varepsilon} \sum_{i=1}^{4} \sum_{j=1}^{4} \frac{q_i^A q_j^B}{|r_i^A - r_j^B|} \tag{1.2}$$

where q_i^A and q_i^B is the charge in dot i of cell A and B, respectively. While r_i^A and r_i^B is the position of dot i in cell A and B, respectively. The kink energy is defined as the difference in energy between two cells that have opposite polarization and those same two cells having the same polarization:

$$E_{A,B}^{kink} = E_{A,B}^{opposite\ pol} - E_{A,B}^{same\ pol} \tag{1.3}$$

Actually, there are two positive background charges distributed underneath the cell to represent the *counter-ion* and ensure charge neutrality of the system. These charges must also be included in the expression 1.3, and it can be shown that the kink energy has a decaying behaviour proportional to the fifth power of the distance between cells [48]. This property can be useful to evaluate the possible *crosstalk* between QCA circuits.

Therefore, the state of a particular cell is transferable to another cell as shown in Figure 1.6, and aligning several cells like an array it is able to propagate information since all successive cells must change their polarization to achieve the new minimum energy condition, like *Domino effect*. Whenever the i-th driver cell switches his polarity a polarization refresh of the target cell occurs, reducing the need to have repeaters in the QCA circuits.

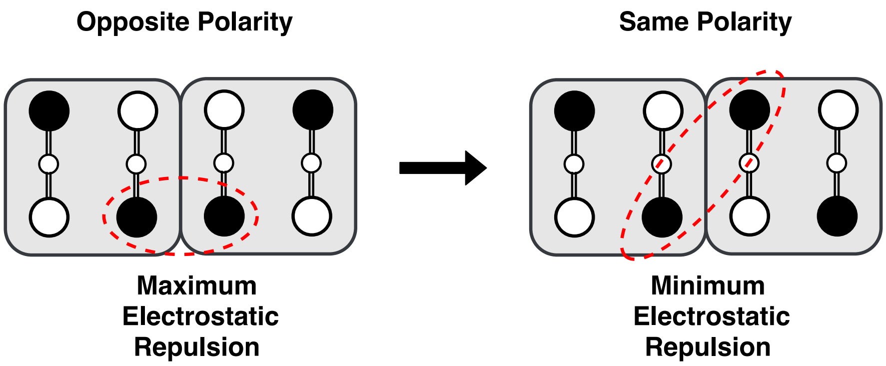

Figure 1.6. State transfer between two adjacent cells.

1.2.3 Basic QCA Building Blocks

The most elementary building block in QCA technology is the **QCA Wire** that consists in an array of QCA cells aligned in order to form a row (Figure 1.7). Unlike CMOS technology, where the interconnections have their own set of principles and designs, in this technology the wire represents a processing element since the propagation of binary information depends on the correct polarity of each single QCA cell. An example how the information travels in the binary QCA Wire is shown in Figure 1.8, in which is highlighted the chain reaction that starts when the logic state of the first cell (the input) is changed.

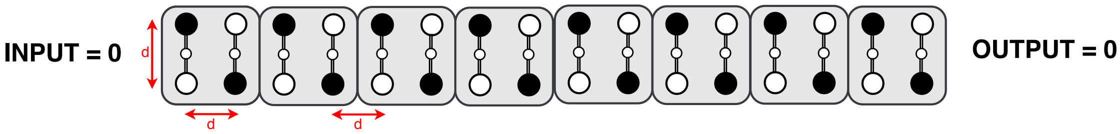

Figure 1.7. QCA Binary Wire.

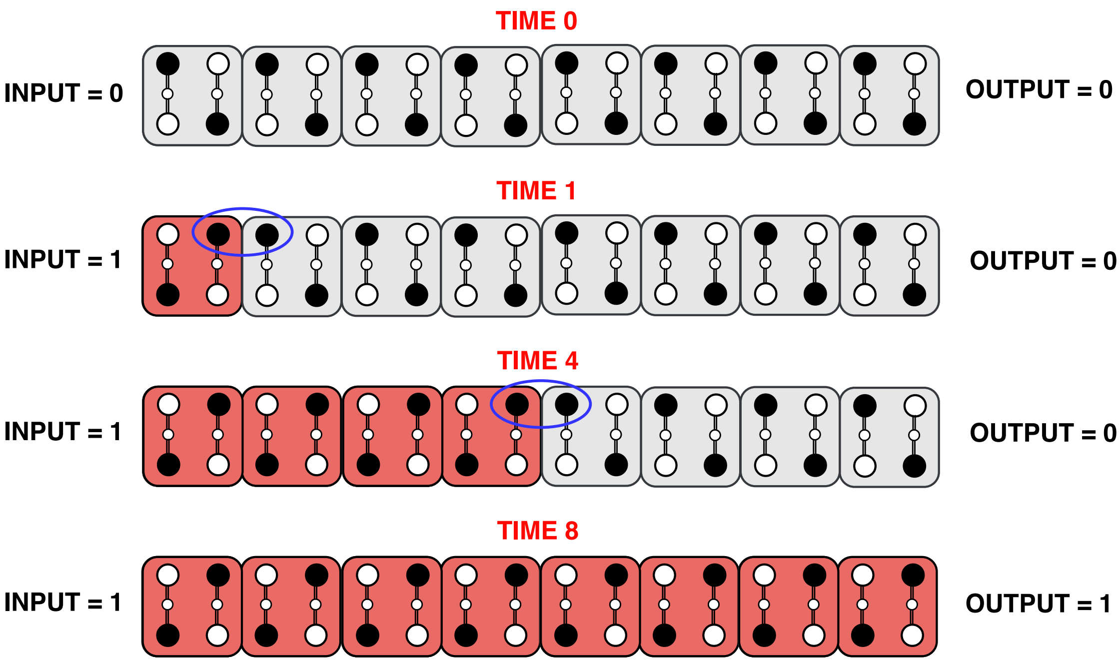

Figure 1.8. Propagation of information in a QCA Wire.

Other important basic elements such as the **QCA Inverter** (Figure 1.9) and **QCA Majority Voter** (Figure 1.11) can be implemented. The QCA Inverter exploits the electrostatic corner interaction (or diagonal coupling) to reverse the propagating state as illustrated in Figure 1.10.

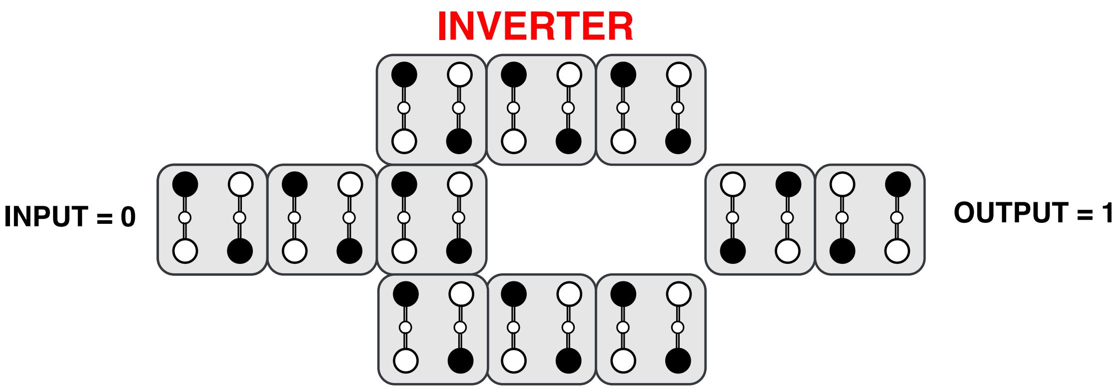

Figure 1.9. QCA Inverter.

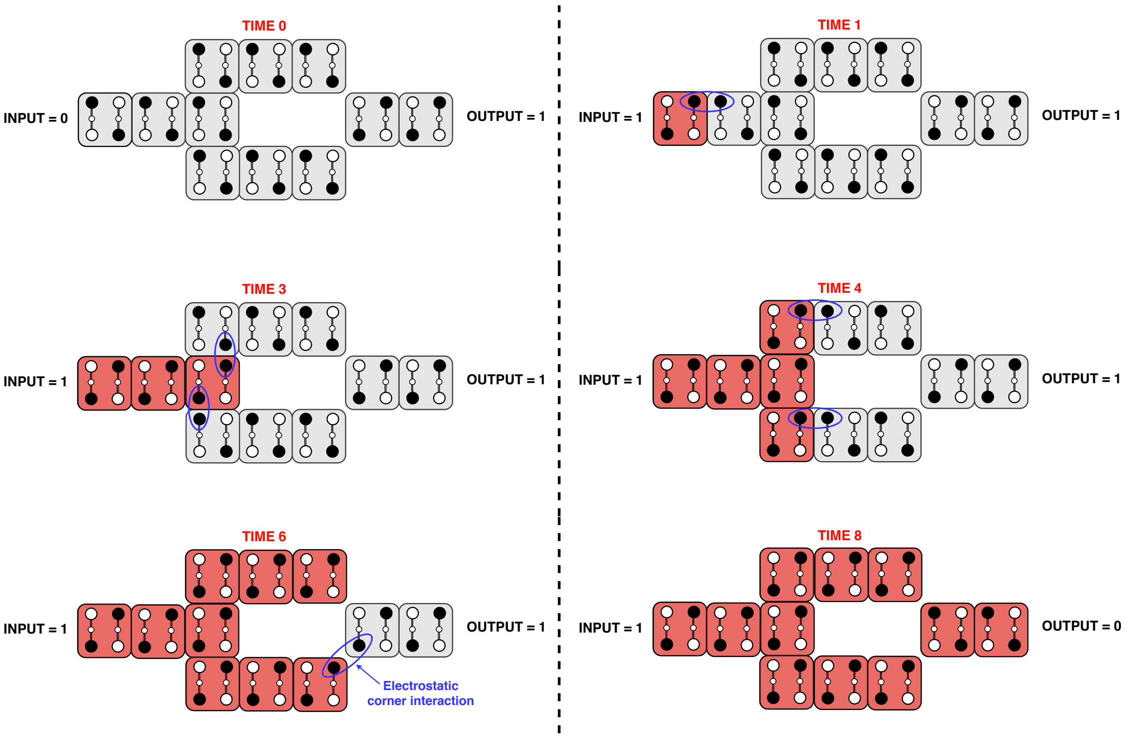

Figure 1.10. Propagation of information in a QCA Inverter.

The Majority Voter is a logic circuit which has three inputs and one output, the output is determined by the simple *majority rule*, according to which the output state is the polarization that has the majority at the three inputs.
This basic device performs the following boolean function $OUT = AB + AC + BC$ and it has great importance because forcing one of the inputs to the logic state "0", the block acts as the **AND gate** since the output is equal to the logic "1" only if the other two inputs are "1" (Figure 1.12). On the other hand, with one input forced to "1", the **OR gate** is implemented, since the output is equal to the logic "0" only if the other two inputs are "0" (Figure 1.13).
Therefore, having the possibility to implement the three fundamental blocks of the combinational logic (Inverter, AND, OR), any Boolean functions could be constructed using majority voters and inverters.

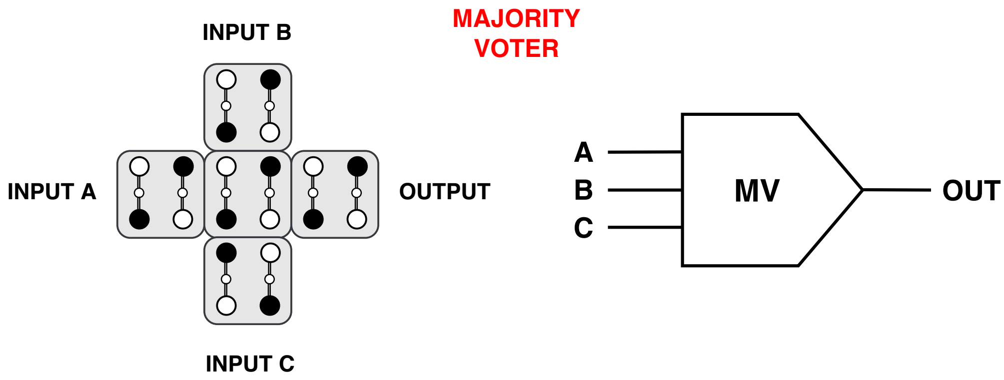

Figure 1.11. QCA Majority Voter.

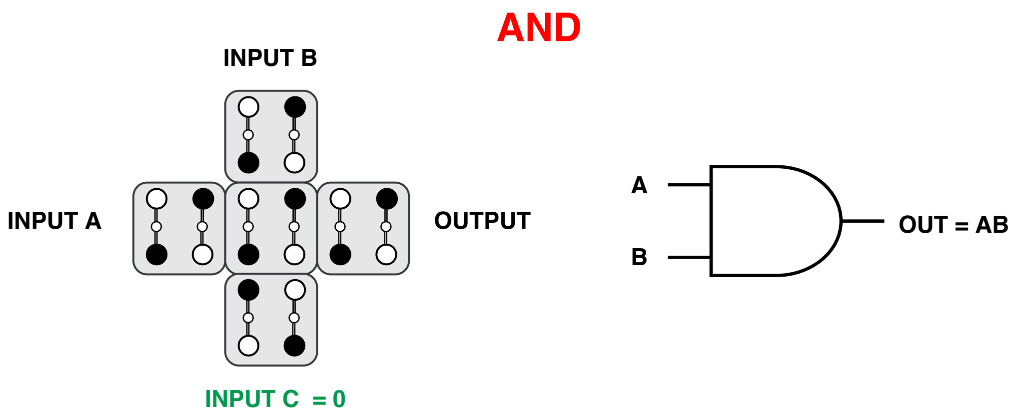

Figure 1.12. QCA AND Gate.

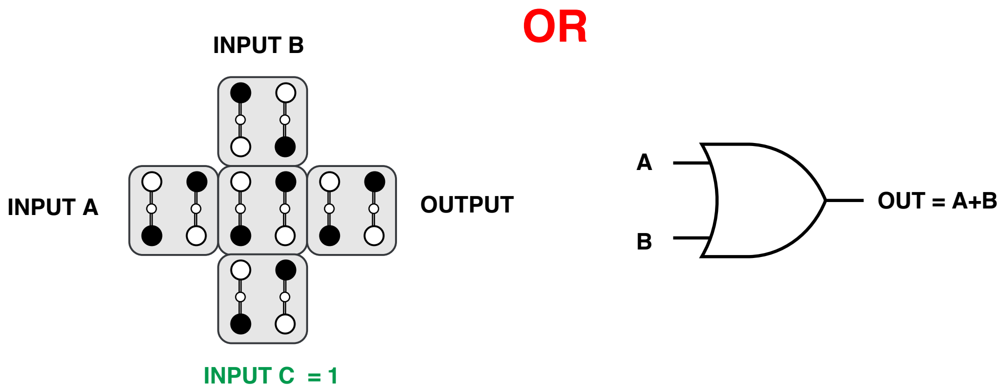

Figure 1.13. QCA OR Gate.

1.2.4 Four-Phase Clocking QCA System

Ideally, using an *edge-driven* approach, which means changing the boundary condition (the input) of the circuit, the information flow occurs without any problem thanks to Domino effect mentioned in the previous section. However, this approach limits the size of the circuit, since larger circuits tend to stabilize in one of many unwanted metastable states corrupting the information flow [31].
Indeed, as explained in [46] to guarantee correct computation can be used only a maximum number of cells.

With the aim to overcome this computational limitation, *Adiabatic switching* mechanism was proposed in [45, 31]. According to this mechanism, QCA Circuit partition in smaller sections called *Clock Zones* is performed, in which in each of them a vertical multi-phase clock field is applied to help the cell state transition, e.g., switching the cells between a NULL state and Logic states without metastability.

The QCA Clock, usually applied and controlled using coupled electrodes, is carried out in four phases (**Switch**, **Hold**, **Release** and **Relax**) as shown in Figure 1.14, and it is able to vary the potential barriers between the quantum dots of the cell [3], which in turn controls the transfer of charges:

1. **Switch Phase**: The clock field starts to rise slowly increasing the inter-dot potential barriers and, at the same time, forcing the mobile charges to tunnel from the quantum dots representing the NULL state towards the Logic Dots (Figure 1.15.A), according to the polarization of neighbouring cells. During this phase, the information is encoded and propagated.

2. **Hold Phase**: The potential barriers reach the maximum value, full polarizing the QCA cells. In this phase the cells are locked in their previous logic states, any kind of tunneling is suppressed and, ideally, no logical switching is possible. The locked cell act as a driver to the next stage.

3. **Release Phase**: The clock field starts to decrease slowly and the mobile charges are free to tunnel from Logic Dots to central dots (Figure 1.15.B). At the end of this phase, the QCA cells lose their polarization assuming the NULL state configuration.

4. **Relax Phase**: The potential barriers reach the minimum value locking the QCA cells in the NULL state. Due to the loss of polarization, the cells inside this clock zone do not influence the cells of the other clock zones.

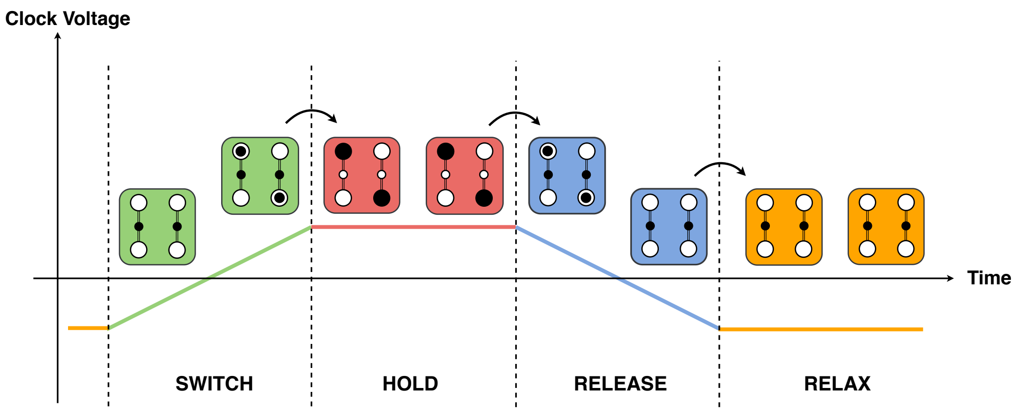

Figure 1.14. Four phase Clock signal waveform.

Considering a wire, which is clocked from left to right with increasing Clocking Zones, the application of a trapezoidal clock signal with delay of 90 degrees in phase between adjacent zones, as depicted in Figure 1.16, enables adiabatic propagation as well as correct QCA computation. This clock mechanism is called *Four-Phase Clock*, recalling the number of phases induced by the trapezoidal signal in each clock zone. As a result, the QCA wire is pipelined at the clocking zone level and behaves like a shift register.

Finally, it is important to remark that the main advantage of this computing paradigm is that the interaction between cells is electrostatic, which means through a field, not involving conduction of charges in the information flow. As a consequence, this property translates into a strong limitation of power consumption, especially with respect to CMOS technology [41].

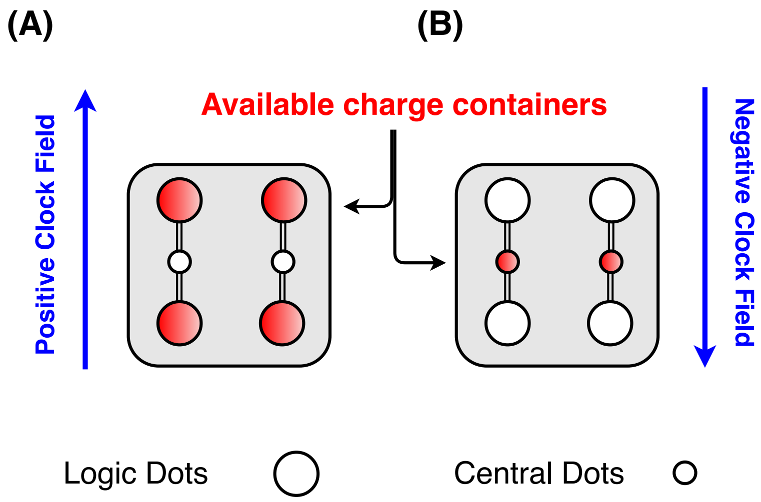

Figure 1.15. Application of Clock signal to the QCA Cell.

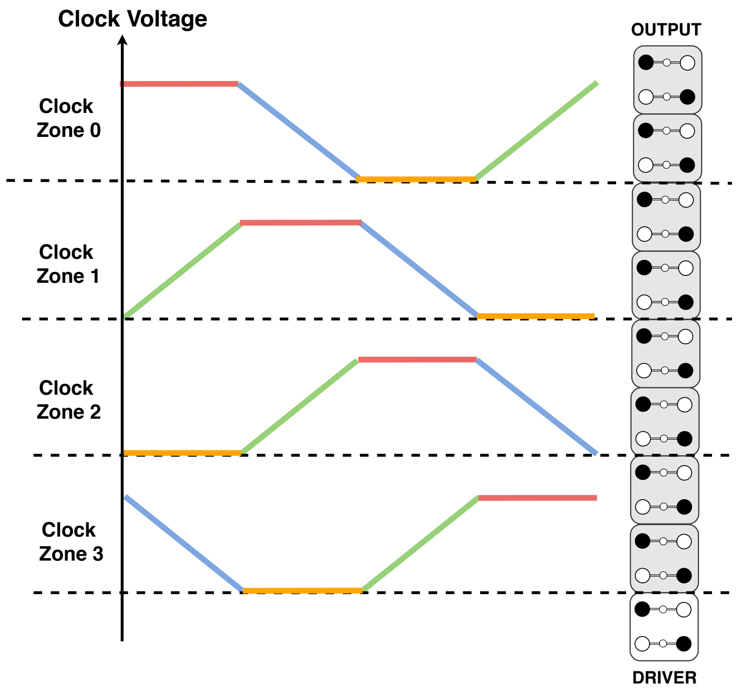

Figure 1.16. Different phases of trapezoidal signal applied to the clock zones of QCA Wire.

Chapter 2

Possible Physical Implementations of QCA Device

As mentioned in the previous chapter the binary information is encoded with charge configuration of the cell and in particular by the confinement and localization of the two charges in the Quantum Dots.
The Quantum Dot is a region of space with potential barriers surrounding it sufficiently tight and high to induce charge quantization to a multiple of the elementary charge within itself. Of course, at a certain point, it is necessary to lower the barrier so that a charge can quantum mechanically tunnel from one dot to another [33].
During the years several approaches have been published to create QCA cell and in the following, some of these are discussed according to the schematic classification reported in Figure 2.1.

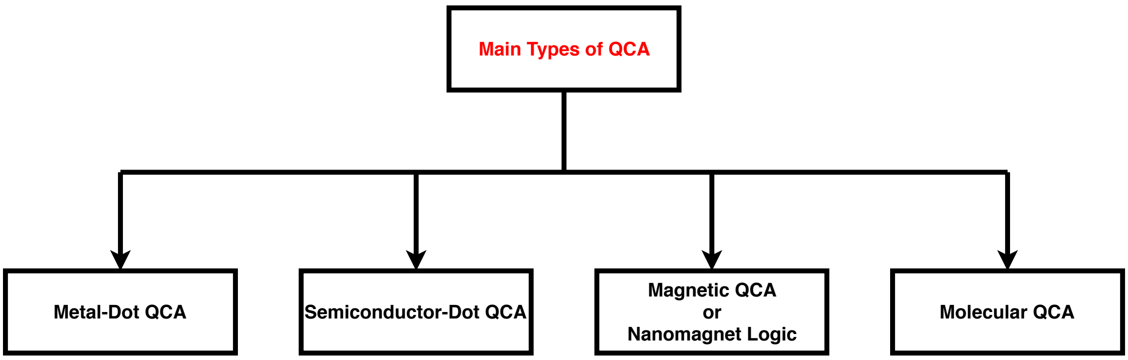

Figure 2.1. Main types of Quantum Cellular Automata.

2.1 Metal-Dot QCA

In metal-dot QCA implementation the dot is created by small metal islands (Al) on an insulating substrate (SiO_2) and tunnel junction are used to create connection between two dots, as shown in Figure 2.2. The Metal-Dot QCA is the first fabrication done to implement the QCA cell [42]. Unfortunately, up to now, the current techniques do not allow to scale the metal islands to nanoscale, needing cryogenic temperature ($70\,mK$ [34]) to work properly and the maximum operating frequency is in the range of MHz [43].
The reason why this approach is under study, despite the strong limitations described above, is that the electron population inside them is quantized allowing analogous behaviour of quantum dot.

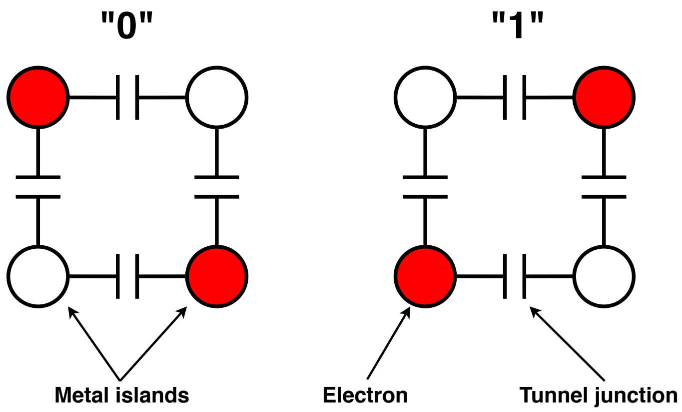

Figure 2.2. Metal-Dot QCA binary representation.

2.2 Semiconductor-Dot QCA

Another solution consists of exploiting Semiconductor QCA structures, fabricated with advanced CMOS fabrication processes, to create the dots in order to contain mobile charge. The advantage of using semiconductor QCA is that it is based on materials that are very well understood and several fabrication techniques have been created to work with them. Different approaches are used in order to demonstrate semiconductor based QCA operation:

- SOI Technology (chapter 7 [33]),
- GaAs Technology (chapter 8 [33]),

- GaAs/AlGaAs heterostructures with confining top-gate electrodes and high-mobility 2-D electron gas below the surface (from Cavendish group of Smith et al.) [9],
- Silicon technology creating the dots using an etching technique (from the group of Kern et al.) [13]-[11],
- A new method in which small clusters of phosphorus donors in silicon are used to create dots (from the group of Mitic et al.) [12].

The dots structures can be formed using 3-Dimensional Quantum wells [42], created through patterning of the semiconductor surface [33], permitting energy quantization effect of the charge population inside the dot itself. Unlike the Metal-Dots, in this case, the dimensions and distance are both of the order of nanometer scale and no longer micrometer one. Also here there are the same limitations of Metal-Dot solution since room temperature operation is expected only when the sizes are reduced to the molecular scale ($\approx 1\,nm$), and the energy levels are very strongly affected by the size of the well presenting an extreme sensitivity to geometry variations [33].
Therefore it is possible to summarize the challenges of all semiconductor implementations in two aspects:

1. From the lithographic point of view, the feasible quantum dot sizes are large enough that kink energies [3],
2. Semiconductor QCA devices are never free from fabrication imperfections and in ideal case (single electron occupancy) the dots become very sensitive to the variations of the electronic environment [3].

Research on both Metal-Dot and Semiconductor-Dot has almost been abandoned in favour of Magnetic and Molecular QCA since they overcome the main drawbacks of these types of physic implementations.

2.3 Magnetic QCA or Nanomagnet Logic (NML)

In general magnetic phenomena are used for data storage and hard disk implementation because *ferromagnetism* phenomenon is non-volatile, meaning that magnetization state can be preserved even without power. A lot of research efforts have been performed during the years in order to implement magnetic logic due to the attractive feature that consists in eliminating standby power consumption.
Another advantage of the magnetic device is that its intrinsic switching energy can be orders of magnitude lower than a current-based CMOS device due to its non-volatile constitution [3].

Presented and developed for the first time by Cowburn and Welland [35] and highly explored by Porod group [10], Magnetic QCA cell is composed of nanomagnet or magnetic nano-particle in which the coupling between them is *ferromagnetic* (the individual nanomagnets tend to be magnetized in the same direction) or *anti-ferromagnetic* (the individual nanomagnets tend to be magnetized in the opposite direction), unlike other types of QCA where the coupling is *electrostatic* one.

To encode the binary information the magnetization orientation of QCA cell is utilized, when it is magnetized along "up" or "down" direction the logic state "1" or "0" is achieved, respectively. While the NULL state is encoded forcing the magnetic orientation along the short axis of the cell (Figure 2.3).

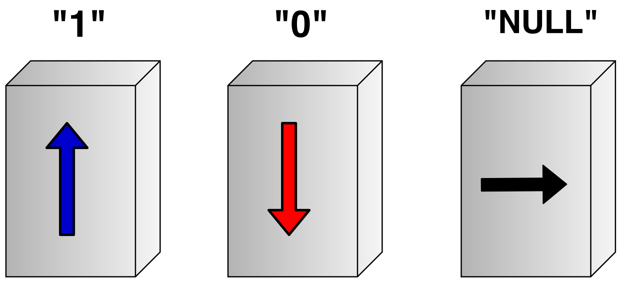

Figure 2.3. NML binary representation.

Computing devices are performed by arranging a chain of these elongated nanomagnets with small separation, in which each of them is able to contain single magnetic dipole; in particular the version fabricated by the Cowburn et al. group is a single circular nanodot made up of magnetic Supermalloy Ni, created through high-resolution *Electron Beam Lithography* (EBL). This nanodot presents a diameter of 110 nm, thickness of 10 nm and size of 100 nm, with interspacing between other nanodots equal to 20 nm [35]. Additionally, a cartoon example of Ferromagnetically and Anti-ferromagnetically coupled binary wire are depicted in Figure 2.4.

The main advantages of Magnetic QCA are that they can be operated in room temperature, require fewer fabrication requirements compared to QCA, very low power consumption, high thermal robustness and 3D architectures are possible. Nevertheless, when the nanomagnets are made under 20 nm stability issues are present and the working frequency is lower with respect to existing technologies [42].

Indeed, it is experimentally demonstrated the operation of majority-logic gates at ambient temperature in [25] and shown in Figure 2.5, where the predicted frequency reach a speed of about 100 MHz .

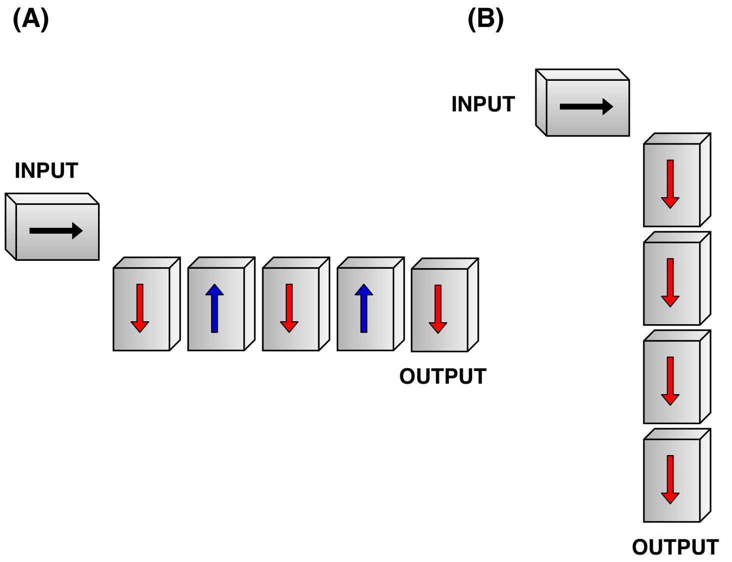

Figure 2.4. (A) Anti-ferromagnetically coupled binary wire, (B) Ferromagnetically coupled binary wire.

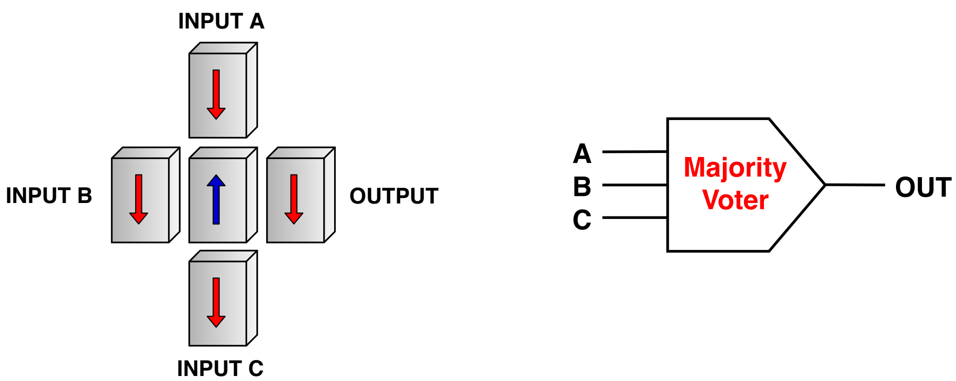

Figure 2.5. Schematic of a magnetic three-input majority-logic gate.

2.4 Molecular QCA

One of the most attractive QCA approaches, apart from the magnetic one, consists of using molecules as structured charge containers, because molecules represent the smallest artificial structures that can be engineered by humans [33]. In MQCA implementation the Quantum Dots are formed by redox-active sites, that are regions inside the molecule itself able to release or to accept an electron without breaking the chemical bonds that hold the molecule together. In the former case, the site is **oxidized** namely positively charged, while in the latter it is **reduced** namely negatively charged.

As shown in Figure 2.6, to perform the binary encoding at least two redox centers are needed and they are connected by a bridging group (stretched grey rhombus) in which mechanical tunneling can occur [18]. This allows creating a link that has a role of the channel to promote the exchange of electrons or a separator/barrier to stop their passage when necessary. The oxidation/reduction charge resultant on the left molecule dot or on the right one gives the logic state "1" or "0", respectively.

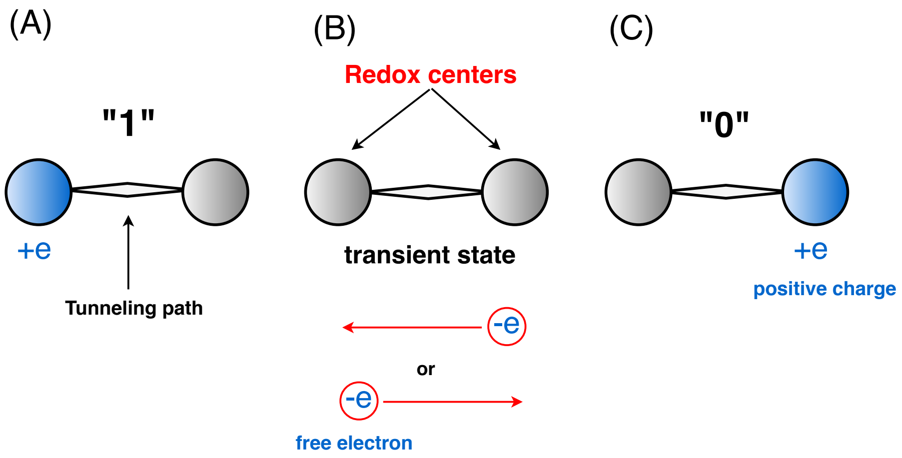

Figure 2.6. State encoding of 2-dots oxidized molecule: (A) logic state "1"; (B) switching state and (C) logic state "0".

With the purpose of avoiding meta-stability switching problems, an extra third redox site is necessary to encode the NULL state in which the positive charge (the oxidized molecule is considered) $+e$ is localized in the central dot and it is used to synchronize the propagation and guarantee stability [3, 43]. Specifically, this single 3-dots molecule (Figure 2.7) constitutes the *half QCA cell* and approaching an identical molecule on its side the complete QCA structure is built, as depicted in Figure 2.8.

Since a molecule is neutral, to improve performance and increase the polarization it is convenient to use its reduced or oxidized form, in this way when an electron is missing the oxidative configuration is achieved and its net charge is positive; vice versa if an electron is acquired the reduced configuration is achieved leading to a net negative charge[18].

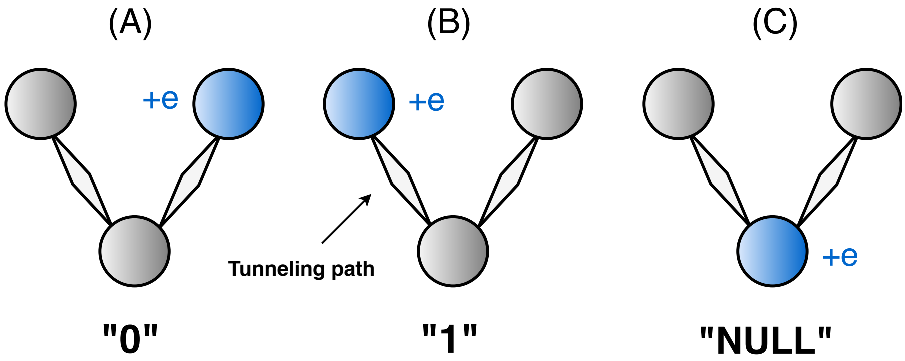

Figure 2.7. State encoding of 3-dots oxidized molecule: (A) logic state “0”; (B) logic state “1” and (C) NULL state [18].

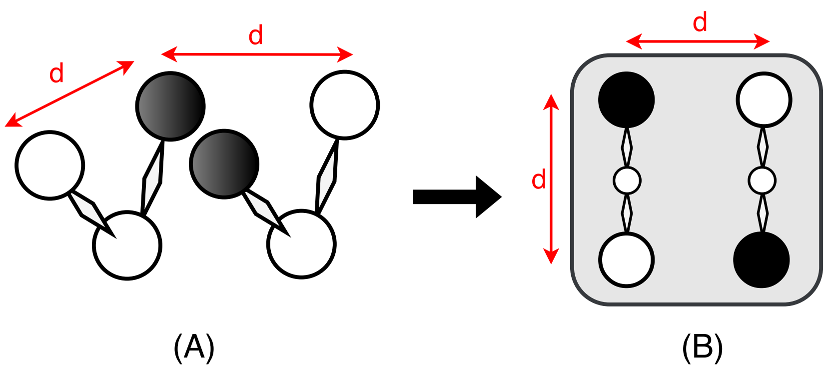

Figure 2.8. Complete MQCA cell: (A) 3D view, (B) top view.

In any case charge neutrality of the molecule (which would likely be preferable) or at least the molecule plus substrate must hold [33], in order to avoid unwanted vertical interactions (Figure 2.9) between molecules, which are negligible in the case of 1D devices, because the molecules are deposited next to each other only along one direction and mainly horizontal interactions are present, but they are fundamental in a potential 2D implementation in which the molecules are also deposited in the vertical direction. Consequently, the counterion is introduced during the molecule synthesis process forming a molecule + counterion neutral system.

The electrostatic coupling present when two half-cells are put at a reasonable distance, such that the six dots form a square, is able to switch the logic state of the molecule and the same time, going to a higher level, provides cell-cell coupling (as mentioned in Section 1.2.2). Indeed, only two possible states are available due to the Coulombic repulsion, leading to the minimization of cell energy and no current

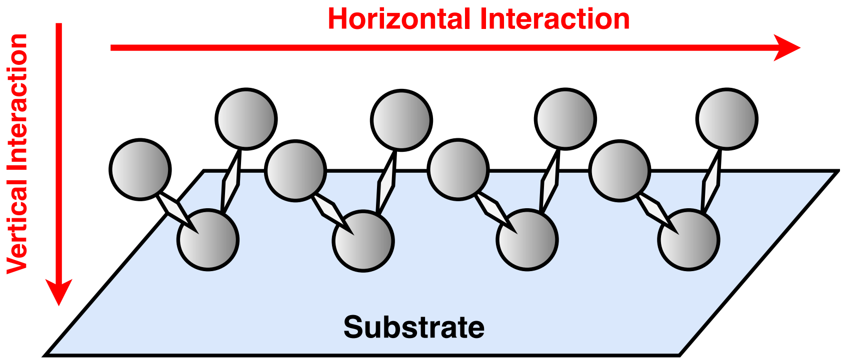

Figure 2.9. Horizontal and Vertical Interaction in 1D implementation.

flow between molecules is required.

MQCA implementation is one of the most promising technology for electronic device miniaturization because:

- Using chemical synthesis the molecules are all identical, overcoming the process variations typical of all lithographic device fabrication techniques [33]. This permit great uniformity in the mass production of devices at nanoscale [4].
- The interaction energies between the cells grow as the size decreases, thus due to the molecular dimensions involved these Coulomb energies are expected to be in the $0.2 - 0.5\,eV$ range. Since these energies are greater than the thermal ambient energy $K_B T \approx 25meV$ (K_B is Boltzmann's constant and T is the temperature in Kelvin) room working temperature operations are available [40].
- In contrast to Metal-Dot and Semiconductor-Dot QCA cells, due to the molecular dimensions involved, the density in the range of $10^{11} \div 10^{14}$ devices cm^{-2} is expected [32].
- Thanks to the lack of current flow in information transmission and adiabatic switching, the power dissipation is extremely reduced with respect standard current technologies [44].
- The expected operating frequency of the order of few THz is achievable [30].
- QCA cell act both as processing elements and as storage elements, not requiring the rigid separation needed in today's electronics [4].

However, current technological processes do not allow enough control and precision to achieve proper working device.

Chapter 3

Candidate Molecules for MQCA

In order to construct a molecular implementation of a QCA cell, a molecule candidate must exhibit several features:

1. Parts of the molecule must realize *charge localization* creating the Dots. In MQCA the redox centers play the role of the Dots, with bridging ligands between them providing the tunneling barrier which causes the localization [33].

2. The molecule must show bistable behaviour and charge must be able to tunnel between dots to enable switching. The switching frequency depends on the tunneling time through the bridging groups [33].

3. The Coulomb field produced by driver molecule must be able to switch the state of a neighbouring molecule. The molecular bistable response of target molecule to variations in the electric field produced by neighbouring driver molecule or external perturbations is expected to be *non-linear*, as demonstrated in [26].

Apart from these elementary characteristics, many efforts must be addressed to achieve physical implementation of MQCA like the absence of a binding element for deposition on substrates [18]. Consequently, anchor groups that allow binding and orientation on a substrate surface in a controlled way are needed in actual QCA molecules.
As explained into Introduction, clock system is necessary and can be accomplished by having middle NULL dots within the molecule. This requirement, in the case of MQCA, arises from the fact that a single cell is not influenced only by the previous and the next cell, but by other molecules in the device.

3.1 Diallyl-Butane Molecule

The first candidate molecule which has been proposed for MQCA implementation is the *Diallyl-Butane* in [26]. This molecule first proposed by Aviram [6] and later studied by Hush et al. [7] consists of two *Allyl* groups (representing the Logic Dots) connected by a *Butyl* bridge (representing the tunneling path), as depicted in Figure 3.1.

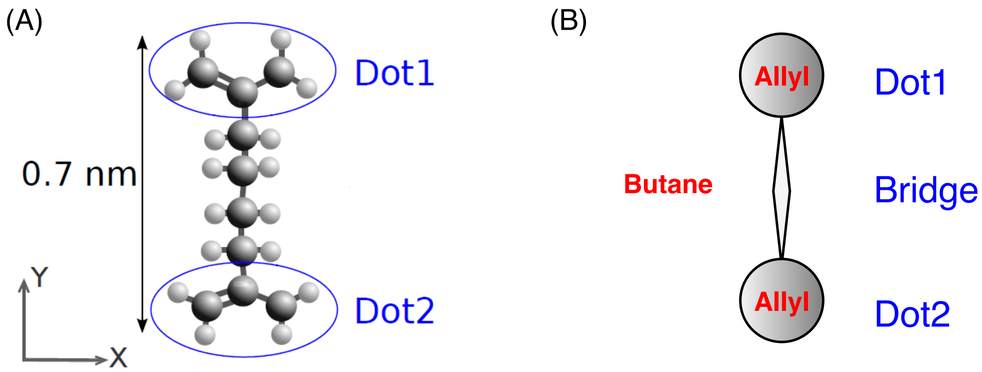

Figure 3.1. Diallyl-butane molecule (A) molecular structure [41], (B) schematic representation.

Authors in [26] have studied the cationic form of the molecule for which one allyl group is a neutral radical and the other is cationic because of the unpaired electron, forming the neutral radical it can be transferred from one end-group to the other through the tunneling path formed by the butane bridge. The missing electron from the HOMO level in one end-group with respect to the neutral one develops a dipole moment formed by the electronic configuration *donor-bridge-acceptor*, that is reversed in *acceptor-bridge-donor* when an electric field is applied and the electron is forced to tunnel from one end-group to the opposite one [18, 48, 26].

Therefore, the cationic form and the potential barrier provided by butane bridging group gives the possibility to have the bistable charge molecule configuration. This molecule represents only the QCA half-cell and its dipole field induces a change of sign in the dipole moment of the neighbouring molecule, giving entire MQCA cell (Figure 3.2).

Although the molecule exhibits non-linear response as a function to the external dipole moment, molecule–molecule electrostatic interactions necessary for information transmission and good charge confinement, the absence of the third dot preventing the possibility of encoding a NULL state and together with the lack

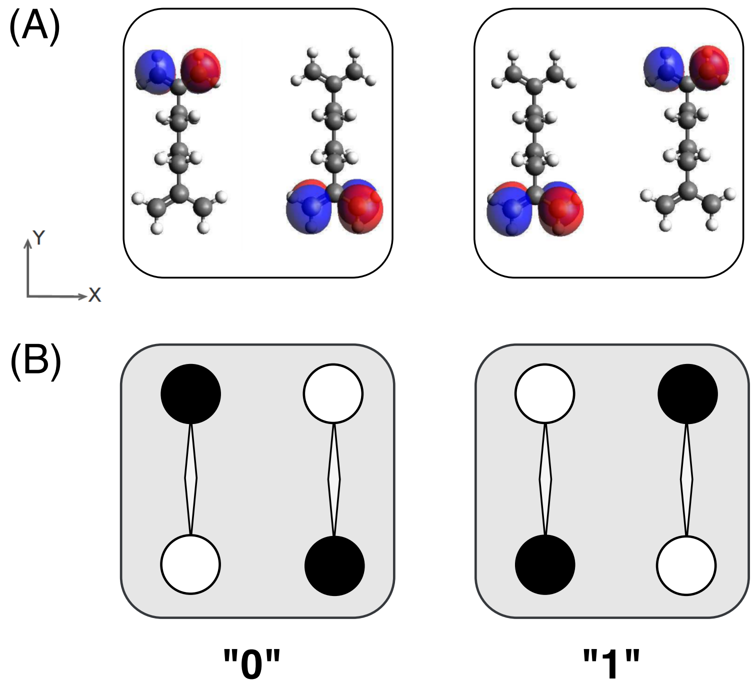

Figure 3.2. Binary representation in the MQCA cell: (A) Diallyl-butane molecules with molecular orbital localization [18] and (B) corresponding scheme.

of binding group for attachment to a substrate, make this molecule unsuitable for actual applications [18].

It is possible to extend the molecule including an additional allyl group implementing the common “V” shaped molecule, as presented in [28] and shown in Figure 3.3. Also here the cationic form is considered, according to which two allyl groups are neutral and one allyl group has a positive charge [28] and tunneling through alkyl bridges can occur.

This extended 3-Dots molecule provides a first example of clocked molecular QCA half-cell [33], due to the possibility of NULL state encoding and adiabatic switching thanks to the application of vertical electric field to induce a potential difference between the upper sites (the two ends of the V) and the lower site (the vertex of the V) [48]. Simulations in [28] demonstrate that the whole molecular QCA cell to switch from the NULL state to one of the two Logic states requires a clock field of $1.3\,V/nm$. The Logic state assumed by the two molecules depends on the polarization field generated by neighbouring cell or drivers placed a single cell distance away. Even if the explained molecule has the necessary non-linear response function and enables clocked QCA computing, the absence of the necessary

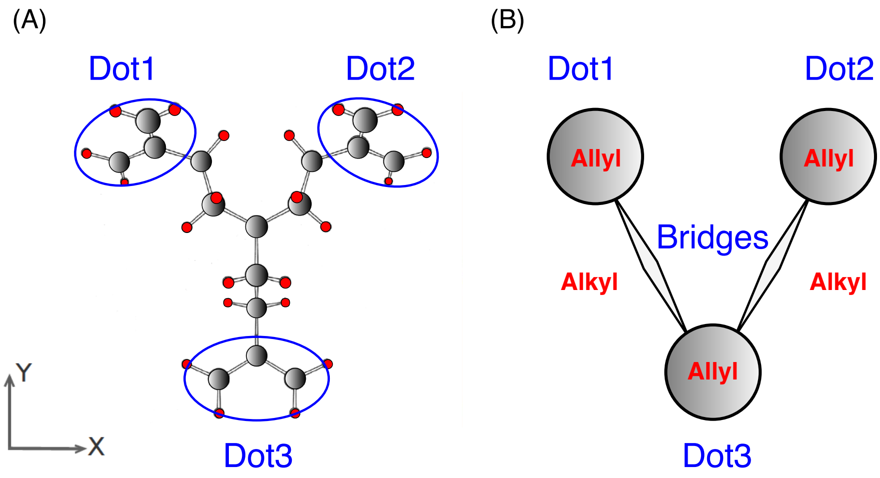

Figure 3.3. Molecule with 3 Allyl groups (A) molecular structure [28], (B) schematic representation.

substrate binding structure remains [48].

3.2 Decatriene Molecule

Another possible candidate able to overcome the limitations of Diallyl-butane is the *Decatriene cation molecule*. The molecule constitutes only QCA half-cell and it presents three dots as highlighted in Figure 3.4, where each dot is formed by an ethylene group and equivalently to the molecule with three allyl groups, three stable orbital localizations are available corresponding to the NULL state and the Logic states "0" and "1", as sketched in Figure 2.7.
Although adiabatic switching is applicable with a clock field equal to $10\,V/nm$ [30], unfortunately, also here no element is able to guarantee molecules' attachment on the substrate [18], however, Decatriene molecule is under research because of its realistic physical implementation and the lower number of atoms with respect to other molecules like *Bis-Ferrocene* explained in the next section.

Particular attention is needed in redox processes since all the molecules already discussed are in cationic form, thus they need to be oxidized or reduced in order to have non-zero net charge and as a consequence, to realize the QCA paradigm.

3.3 Bis-Ferrocene Molecule

Bis-Ferrocene molecule is a novel candidate molecule that has been proposed and analysed in [49, 47, 17, 19, 14, 15]. The molecule shown in Figure 3.5 has been

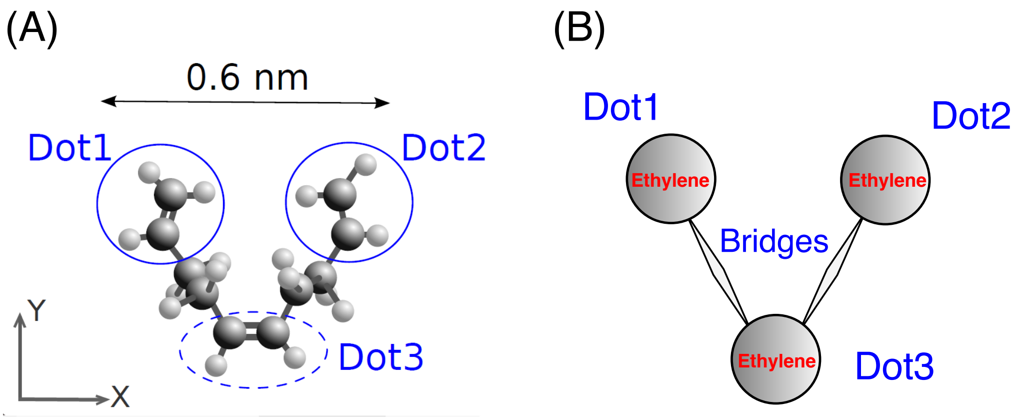

Figure 3.4. Decatriene Molecule (A) molecular structure [41], (B) schematic representation.

specifically synthesized for QCA paradigm and to implement real experimental applications, thanks to a collaboration among ST Microelectronics (Italy), University of Bologna and Politecnico di Torino (Italy).

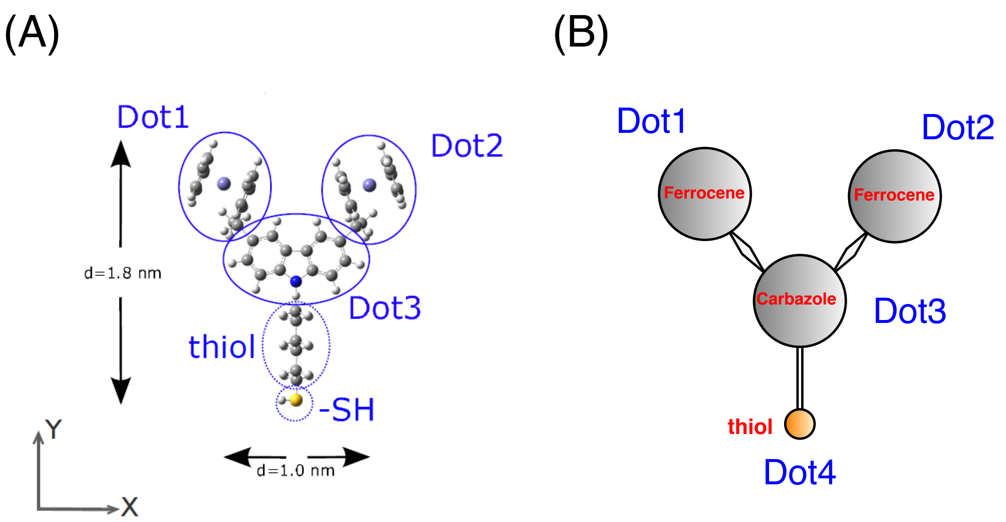

Figure 3.5. Bis-Ferrocene Molecule (A) molecular structure [43], (B) schematic representation.

It is composed by ninety one atoms divided in two ferrocene redox sites acting as the Logic Dots, a carbazole bridge representing the third dot for the NULL

state and, additionally, an alkyl chain is present as an anchoring element in order to connect the molecule to the ending thiol (-SH) group, which in turn it is able to attach molecules to a gold surface. The molecule is 1 *nm* wide, considering the distance of two centralized iron atoms present inside the ferrocene groups and 1.8 *nm* high. As the previous molecules, bis-ferrocene molecule in cationic state is employed performing chemical oxidation introducing iodine atoms as counterions or electrical oxidation through cyclic-voltammetry (CV) technique [47].
The whole QCA cell is realized aligning two bis-ferrocene molecules at *intermolecular distance* equal to 1 *nm* from each other originating squared QCA cell (Figure 3.7), in which every single molecule enables the three typical charge layouts of 3-dots oxidized molecule, as depicted in Figure 3.6.

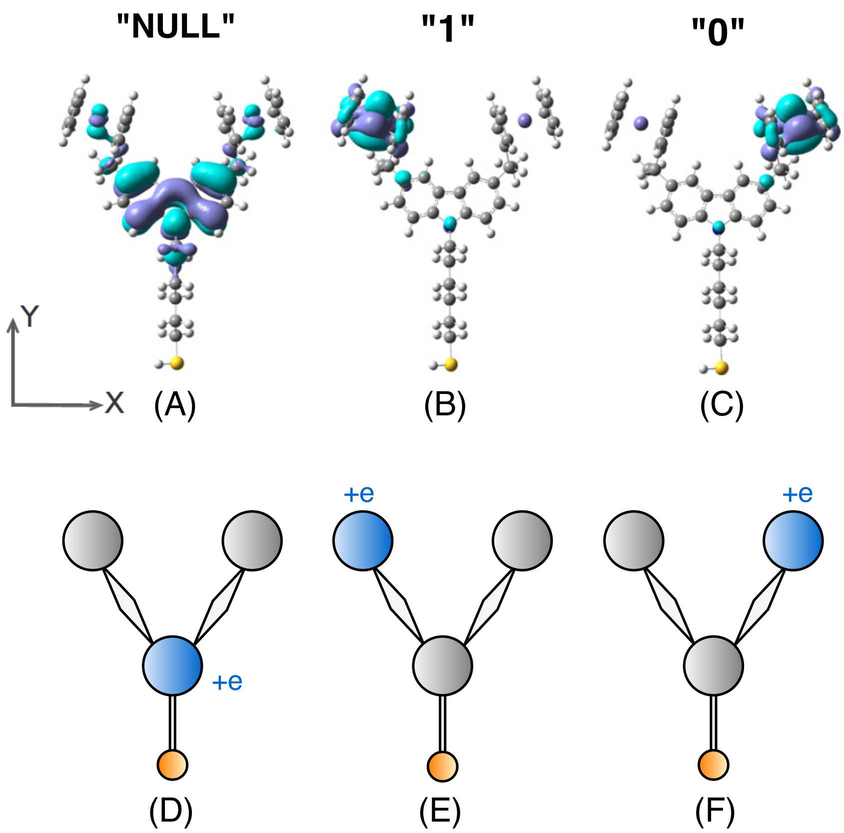

Figure 3.6. Bis-Ferrocene Molecule (A) Ground state HOMO, (B) HOMOs of logic state “1”, (C) HOMOs of logic state “0” [15]. (D),(E) and (F) corresponding schematic representation.

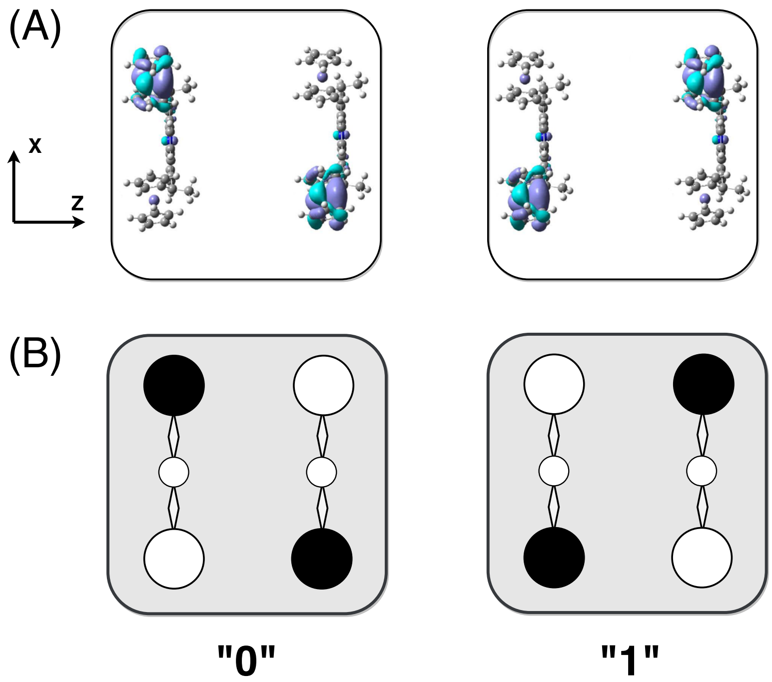

Figure 3.7. MQCA cell Binary encoding: (A) Bis-ferrocene molecules with molecular orbital localization [17] and (B) corresponding schematic representation.

3.3.1 Effects of Switching and Clock Fields

Bis-ferrocene molecule is not conductive because the charge centers are effectively insulated from conducting substrates thanks to the groups of atoms that surround them [3]. However, this insulation does not occur with the application of an external electric field, making possible to re-arrange the charge distribution of the molecule forcing the desired state on it. In particular, two types of biasing conditions are created, *Switching Field* [29] and *Clock Field* [28]. The simultaneous application of both allows imposing one of the three possible molecule states.

Switching Field

The switching field is an electric field parallel to the active dots axis (X-axis) of the molecule and it is able to impose charge localization in one of the two logic dots defining the desired logical molecule polarization, as shown in Figure 3.8. With positive switching field the free positive charge tends to position itself on Dot2, vice versa negative switching field generates charge localization on Dot1, writing logic state “0” or “1” to the single molecule.

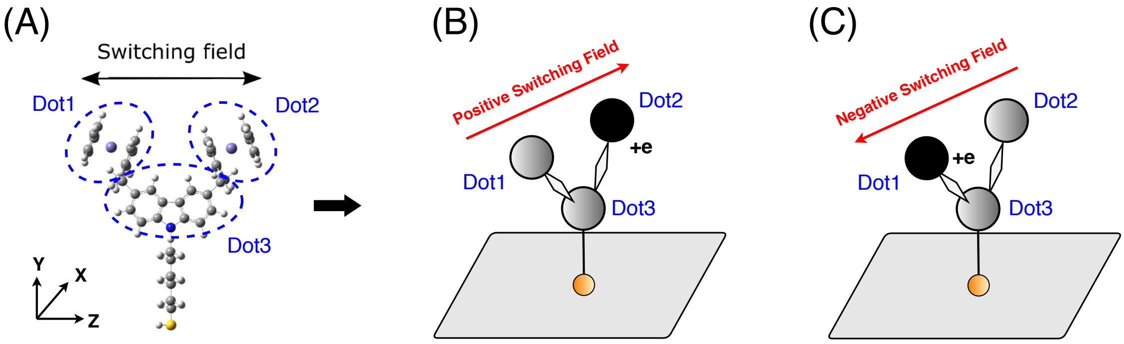

Figure 3.8. (A) Switching Field for single bis-ferrocene molecule; (B) Charge localization with positive Switching Field and (C) Charge localization with Negative one.

Clock Field

The clock field is an electric field applied along the vertical axis of the molecule (Y-axis) and, as mentioned before, this field is necessary to apply adiabatic switching. In case of Bis-ferrocene molecule, or more in general the three-dot molecules, the application of the clock signal has the effect of to enhance or impede the communication between nearby molecules (Figure 3.9). When a positive vertical field is applied to the molecule the excited states are available, it becomes sensitive to external perturbations and the positive charge is able to tunnel between the Logic Dots. When this happens two situations can take place:

1. Switching field is present and the desired Logic state is written;
2. The molecule can interact with other molecules changing its polarity transmitting the information.

With negative clock field the free positive charge down to central Dot3, freezing the molecule to NULL state (no information is stored) hindering the interactions among the molecules or screening it from switching field preventing the writing. All these conditions are illustrated in Figure 3.10.

To evaluate the effective clock signal control on molecular interaction, simulations with simultaneous usage of Switching and Clock fields are needed [18, 43]. In particular, has been demonstrated in [22] that the optimal charge distribution to encode logic state in oxidized bis-ferrocene molecule is obtained with clock signal equal to $2\,V/nm$, because in this condition almost zero charges on the central Dot3 is present and the remaining positive net charge is equally distributed on two working dots ensuring proper logic switching between nearby molecules.

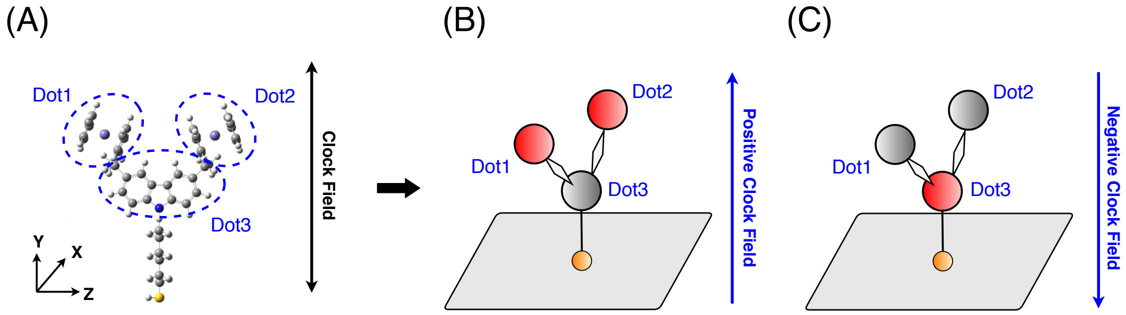

Figure 3.9. (A) Clock Field for single bis-ferrocene molecule; (B) Available charge localizations with Positive Clock Field and (C) Charge localization with Negative one.

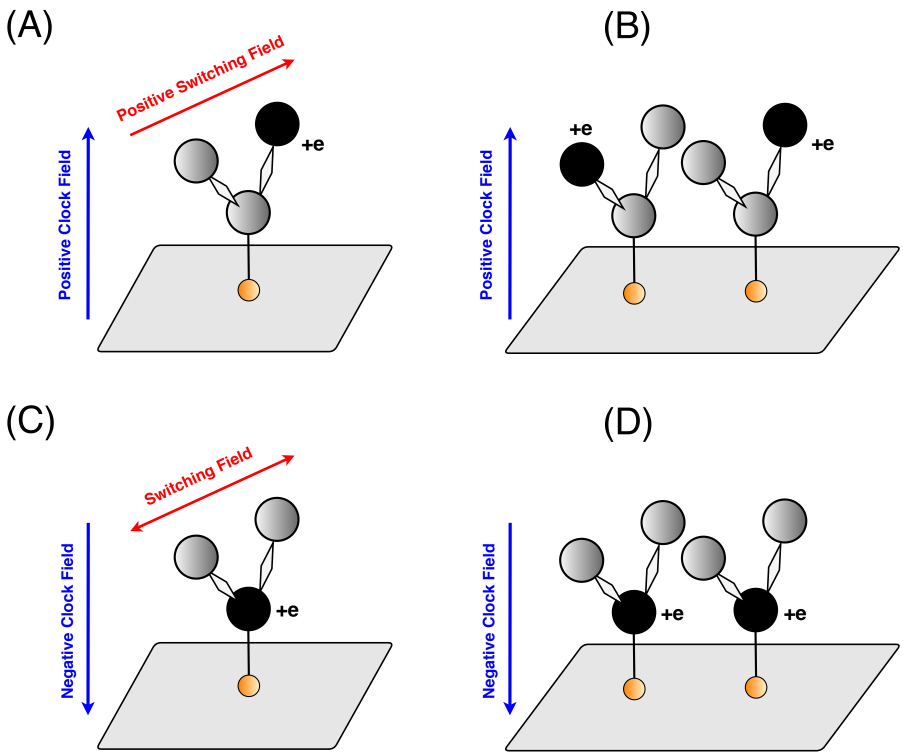

Figure 3.10. (A) Charge localization example with positive Clock Field and positive Switching Field; (B) Charge configuration deriving from molecular coupling achievable thanks positive clock field; (C) Charge localization with negative Clock Field and Positive/Negative Switching Field and (D) Charge localization with negative Clock Field depicting the molecular interaction suppression.

3.3.2 Driver-Molecule and Molecule-Molecule Interactions

Following the molecular analysis methodology in [18, 43, 41, 22], in order to study the interaction between molecules, and consequently the binary transmission, an entire MQCA il cell is considered. To analyse *Driver-Molecule Interaction*, in this single cell, one molecule is replaced by an ideal *Polarized Charge Driver* formed by two point charges (D_1 and D_2) placed at one inter-molecular distance from the bis-ferrocene molecule, emulating a MQCA device input (Figure 3.11).
The case of oxidized molecule is analysed, thus the ideal driver presents only one positive charge $+e$ (elementary charge) located on one of the two points. In particular, for defined driver logical state the resulting polarization on the *Molecule Under Test* (MUT) is expected to have the opposite logic state due to the electrostatic interaction [18, 43].

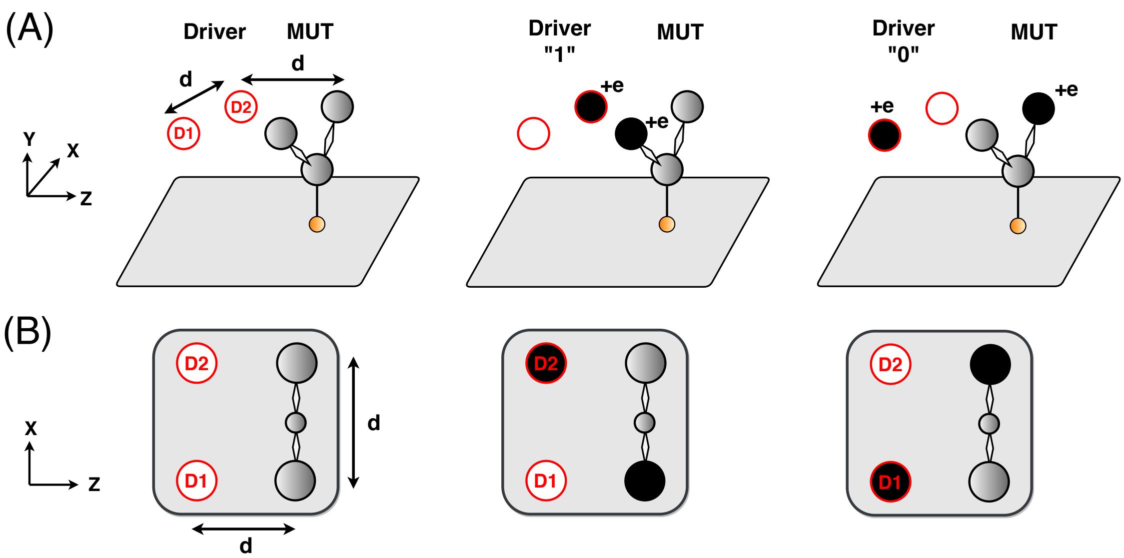

Figure 3.11. Driver-molecule interactions model: (A) 3D view and (B) top view.

Concerning *Molecule-Molecule Interaction*, three *Aggregated Charges* (Q_1, Q_2 and Q_3) are estimated (Figure 3.12). This new quantity arises from the sum of the *atomic charges* corresponding to the three redox sites (two ferrocenes groups and carbazole+thiol group), whose values are obtained by means ab-initio simulations using ESP approximation [36]. The Aggregated charge defines a new figure of merit more suitable with an electronic engineering point of view, rather than considering HOMO of the molecule like in Figure 3.6, since simplifying the molecular system in a reliable way [4, 18]. Therefore, summing all the atomic charges included in each part of the dashed dots represented in Figure 3.13, it is possible to obtain three aggregated charges giving the possibility to model the molecule, from a macroscopic point of view and in any working condition with 3-point charges system and to simulate molecule-molecule coupling.

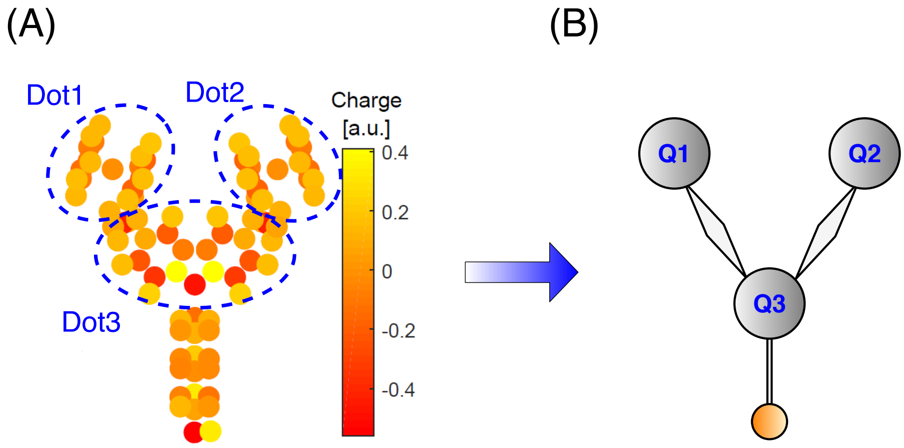

Figure 3.12. (A) Charge distributions by means of ESP computation[4] (B) Aggregated charges definition for bis-ferrocene molecule dots.

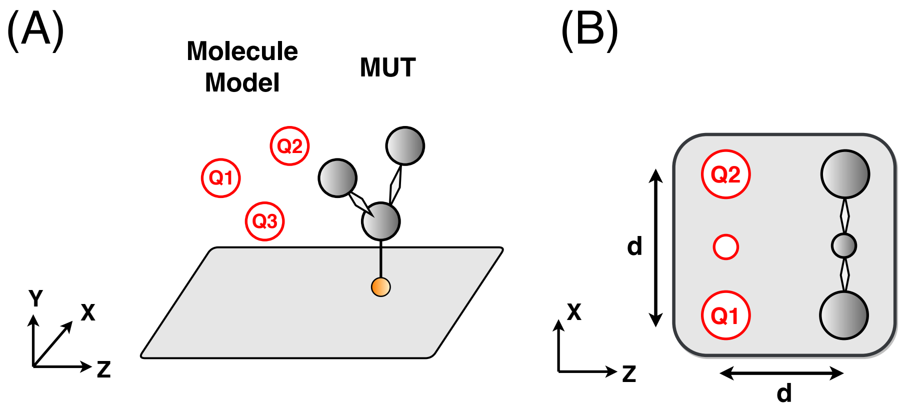

Figure 3.13. Molecule-Molecule interactions model: (A) 3D view and (B) top view.

Consequently, evaluation of the electric field generated by the Polarized Charge Driver, at any points in the space all around it, is done following the mathematical formulation in [18]. Then, placing a fictitious molecule at inter-molecular distance d from it, the so-called *Input Voltage* (V_{IN}) is measured, considering the component of the electric field parallel to the MUT logic dots and integrating it along the width of the MUT itself (Figure 3.14.A). Similarly, once the three aggregated charges concerning the molecule are evaluated, whose values depend on bias conditions (i.e point charge based driver, switching field and clock signal configurations), the electric field generated by 3-aggregated charges system and V_{IN} are computed (Figure 3.14.B).

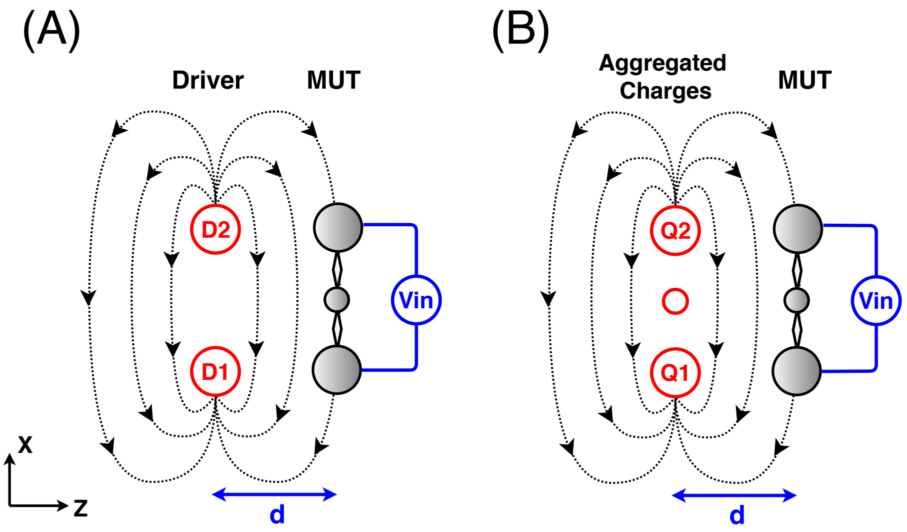

Figure 3.14. Electric field generated by the distribution of: (A) Point charges of ideal driver (B) Aggregated charge of a bis-ferrocene molecule and the corresponding V_{IN}.

The importance of this new figure of merit V_{IN} consists of the fact that it quantifies and describes the external influence of the write-in system to the molecules or the interaction that takes place inside the MQCA cell, depending on whether the voltage is generated by charges representing a Driver or a molecule, respectively.

To complete the characterization of molecular interaction, the two interaction models are joint together to model *Driver-QCA cell Interaction* or *QCA cell-cell Interaction* in order to describe the interaction among Polarized Charge Driver and the first whole MQCA cell of the device or the interaction between three o more molecules like in a QCA Wire.
At first, the Driver induces the charge distribution re-arrangement of the MUT, according to the V_{IN}, forming aggregated charge distribution Q_1, Q_2 and Q_3 (Figure 3.15.A). As soon as the electric field generated by MUT under the influence of a Driver configuration (D_1 and D_2), the *Output Voltage* (V_{OUT}) is evaluated at the position where the third bis-ferrocene molecule, called *Receiver*, is located (Figure 3.15.B) [41, 22].
Obviously, substituting the point charges of the Driver with Aggregated charges the

characterization interaction between different molecules is achieved (Figure 3.15.C and Figure 3.15.D). As V_{IN} also the voltage at the Receiver V_{OUT} is evaluated by integrating the electric field generated by the MUT, computed using the Aggregated Charges, on the segment that connects the Receiver logic dots (Dot 1 and Dot 2).

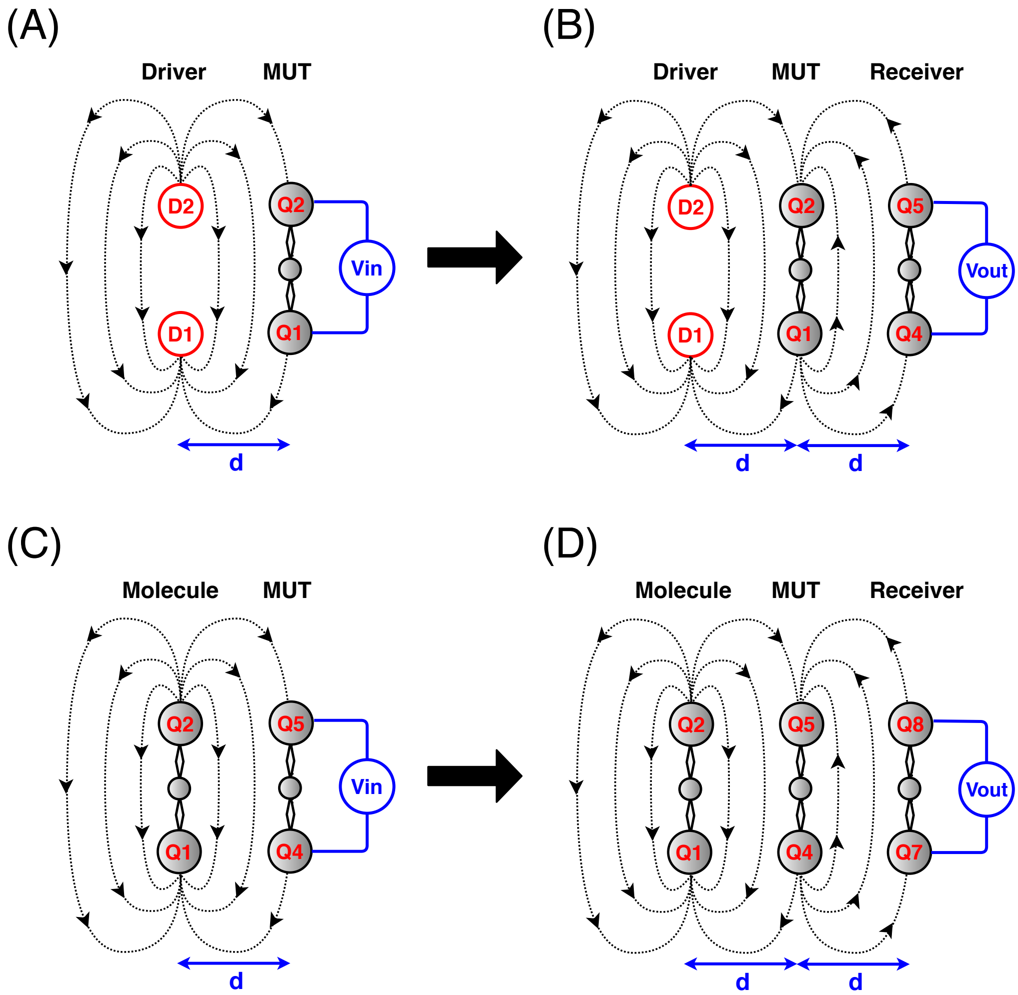

Figure 3.15. V_{IN}–V_{OUT} schematic representation: (A) Point charges of ideal driver (B) Aggregated charge of a bis-ferrocene molecule and the corresponding V_{IN} (for the sake of clarity the left part of generated electric field by the MUT is not reported).

The V_{IN}–V_{OUT} *Trans-characteristics*, consisting in the relation between V_{IN} and V_{OUT} voltages, is therefore obtained providing fully molecule's characterization [41, 22]. Such relationship is clock-dependent because of the clock signal defines the total charge quantity on molecule active dots that participates in the interaction [43].

3.3.3 Write-In and Read-Out Systems

An experimental setup to model real write-in system in order to apply the Switching Field, and to force a status at the input molecule or at several molecules, has been demonstrated in [15].
According to [15], a uniform electric field equal to $\pm 10\,V/nm$ generated by two electrodes placed near molecule is simulated, demonstrating the correct writing of a Bis-ferrocene molecule validated by the computation of the charge distribution of the molecule. The proposed and feasible experimental scheme in [17, 15], to simulate the write-in system with consequent information propagation into MQCA Wire, consists in a gold nanowire in which an aligned array of oxidized bis-ferrocene molecules are anchored through the thiol binding group; plus two gold nanoelectrodes placed close the input molecule, as illustrated in Figure 3.16.

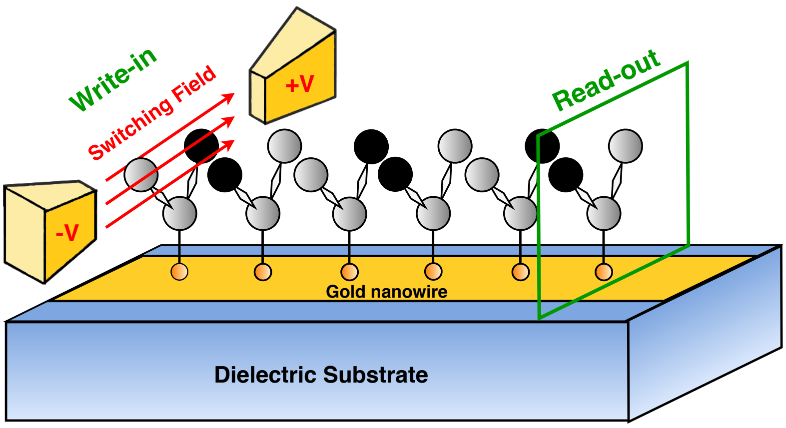

Figure 3.16. Write-in and Read-out system for a MQCA wire.

As soon as the two electrodes generate the switching field the first molecule trapped in the nanogap is forced into defined logic state, then due to the Coulomb interaction, the second molecule assume opposite polarization with respect to the input molecule, as well as the third molecule compared to the second one and so on and so forth, propagating the information along the molecular wire [15].
Figure 3.17 displays the experimental results obtained in [15] from Aggregated charge analysis on the three dots of molecule as a function of Switching Field. With electric field equal to $10\,V/nm$ one Dot has a negative charge value and the other has a positive one. On the contrary, with electric field equal to $-10\,V/nm$ the charge values of the Dots are reversed. The constant charge values concerning the carbazole (Dot3) and thiol confirms the writing possibility in the molecule by means of electric fields.

The usage of aggregated charge is based to the fact that could better represent

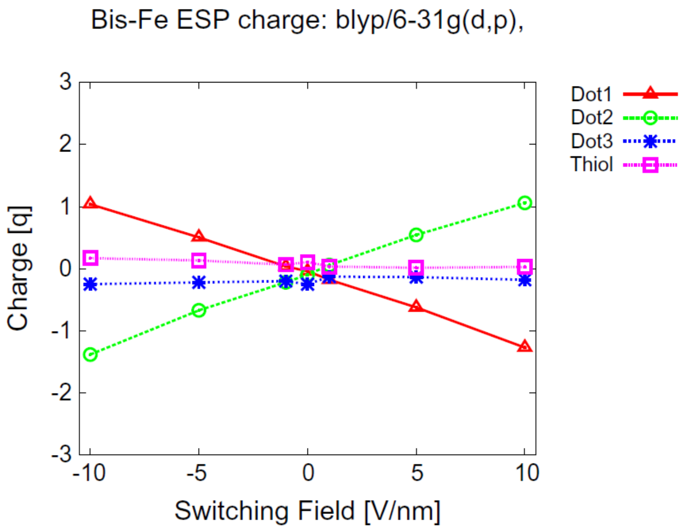

Figure 3.17. Aggregated charge analysis on the three dots vs. the Switching Field [15].

the effective charge distribution inside a molecule and could be a suitable quantity to read with possible read-out system applications [15, 18, 43]. Although not yet experimentally proven, according to literature two are the possible methods [15]:

1. The use of a structure similar to the *floating-gate MOSFET* [1]. This possibility consists in measuring the variation of the current in a MOS transistor as a function of the charges trapped in the redox sites of the molecule, placing it as a floating gate in a MOS structure. In the case in question, the charge localization within the last Bis-ferrocene molecule of the MQCA Wire, that acts as the floating gate, generates different measurable threshold voltages.

2. The use of a *Single Electron Transistor* (SET) [21]. In this solution, the molecular charge confinement could affect the electrostatic potential of the island in a SET. The charge displacement that occurs inside the last Bis-ferrocene molecule leads to a variation in the SET current, due to the capacitive coupling among this molecule and the island.

The read-out state is still not fully demonstrated because of the charge variation inside the molecule involves one or few electrons, leading to the need to fabricate a deeply nanoscale device with single-electron sensitivity.

3.3.4 MQCA Clock System: Three-Phase Clock

According to the clock system explained in section 1.2.4, also in the case of large MQCA Bis-ferrocene based devices the division into clock zones is essential to ensure the proper information flow, as demonstrated in [22]. The possible physical implementation for MQCA structures analysed and studied in [16, 38, 2] is illustrated in Figure 3.18.A. This implementation consists in placing two nanoelectrodes positioned at the top, beyond the molecule, in which the same voltage is applied and a third electrode under the molecule itself constantly grounded. The reason behind this choice derives from the requirement to have a vertical controlled field that crosses the molecules (Figure 3.18.B).

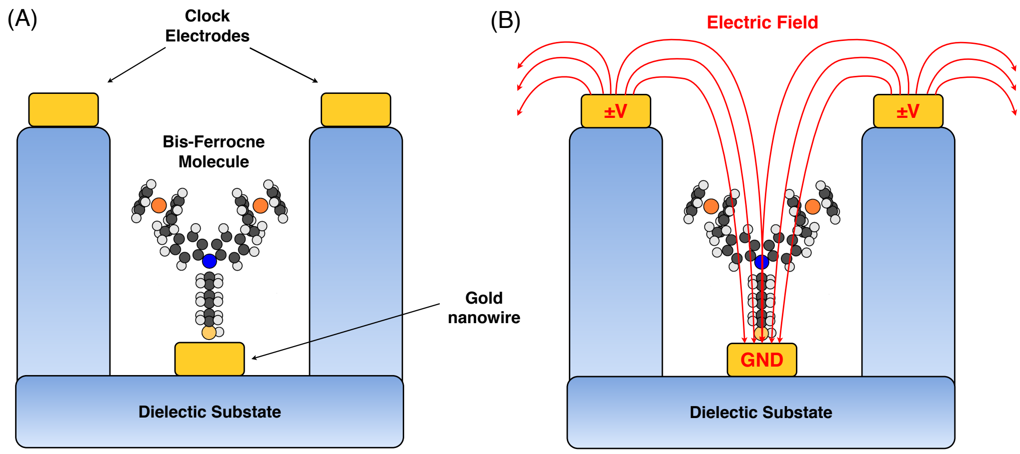

Figure 3.18. (A) Scheme of physical implementation of MQCA clock system (B) Almost vertical Clock field generated by the designed clock system.

Following the implementation in Figure 3.18 to generate adiabatic propagation of information the MQCA device, for example, a MQCA Wire is divided into three clock zones as illustrated in Figure 3.19. The reason why three electrodes are used, instead of four, is that a movement towards a zone-less configuration is accomplished. Reflecting the clock zones three gold clock electrodes for each side are patterned and in each of these electrodes the same time varying trapezoidal clock signal, but with different phase, is applied.

According to the *Finite Element Method* (FEM) simulations performed in [2] with COMSOL Multiphysics® program, the maximum and minimum values that the clock signal reaches are $+8.5\,V$ and $-8.5\,V$, respectively, because they ensure to have a clock field equal to $\pm 2\,V/nm$ necessary to optimally enhance/inhibit the molecular interaction between oxidized Bis-ferrocene molecules, as demonstrated in [22]. Higher voltage values generate clock signals greater than $\pm 2\,V/nm$, giving the possibility to increase the amount of charge in the active dots, however, this leads

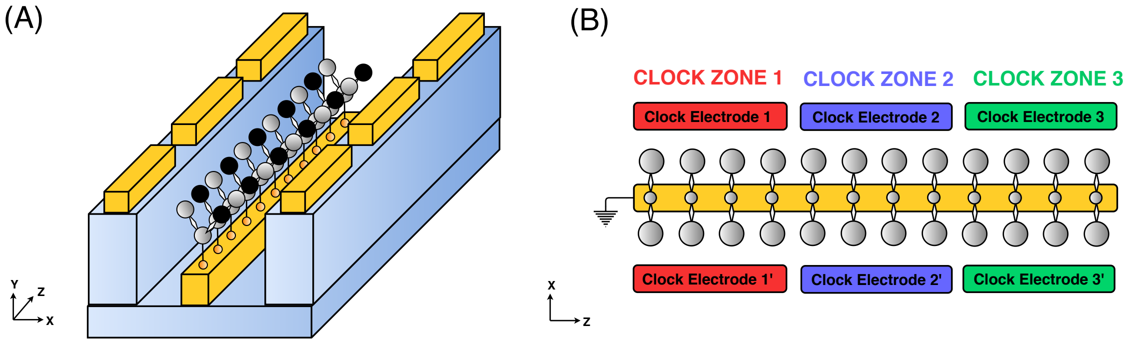

Figure 3.19. Scheme representation of MQCA physical implementation: (A) 3D view (B) Top view with Clock Zone partition.

a higher power consumption and at an extra amount of charge that is unnecessary for logic switching. To explain how propagation occurs, four time instants involved on MQCA Wire propagation are described and sketched in Figure 3.20.A.

- **Time 1:** The set of three values ($+8.5\,V$, $-8.5\,V$, $-8.5\,V$) is applied to the *Clock Zone 1*, *Clock Zone 2* and *Clock Zone 3*, respectively. In the meantime, at the input molecule is assigned externally the desired logic state by means write-in system. Since the clock signal applied in Zone 1 allows the molecules to electrostatically change their polarization according to the logic state of the input molecule, the binary information propagates, while the molecules in Zone 2 and Zone 3 are forcibly induced in the NULL state prohibiting any form of molecular communication with the molecules in Zone 1 (Figure 3.20.B).

- **Time 2:** When all molecules in Zone 1 complete their logic states switching, the set of three values ($+8.5\,V$, $+8.5\,V$, $-8.5\,V$) is applied to the three Clock Zones. In this way the polarization of the molecules in Zone 1 maintain their previous configuration, while those belonging to Zone 2 are able to assume the proper polarity according to the new Zone 2 input (which in turn depends on the molecules' polarization of Zone 1), continuing the transmission of information. Concerning the Zone 3 the molecules are frozen in the NULL state (Figure 3.20.C).

- **Time 3:** Keeping going with the same mechanism, the applied set of three voltage values is ($-8.5\,V$, $+8.5\,V$, $+8.5\,V$). The molecules in Zone 2 maintain their previous polarization and molecular communication among Clock Zone 2 and Clock Zone 3 is possible allowing information flow in Zone 3. Regarding the Zone 1 molecules, they undergo a *Reset* operation setting them in the NULL state (Figure 3.20.D).

- **Time 4:** With the set $(-8.5\,V,\,-8.5\,V,\,+8.5\,V)$ fully propagation occurs in Zone 3 and Zone 2 is reset together with the Zone 1, in order to be ready for the transmission of a new binary data (Figure 3.20.E). Whereupon, the process starts again with another imposed logic state to the input molecule in the Clock Zone 1.

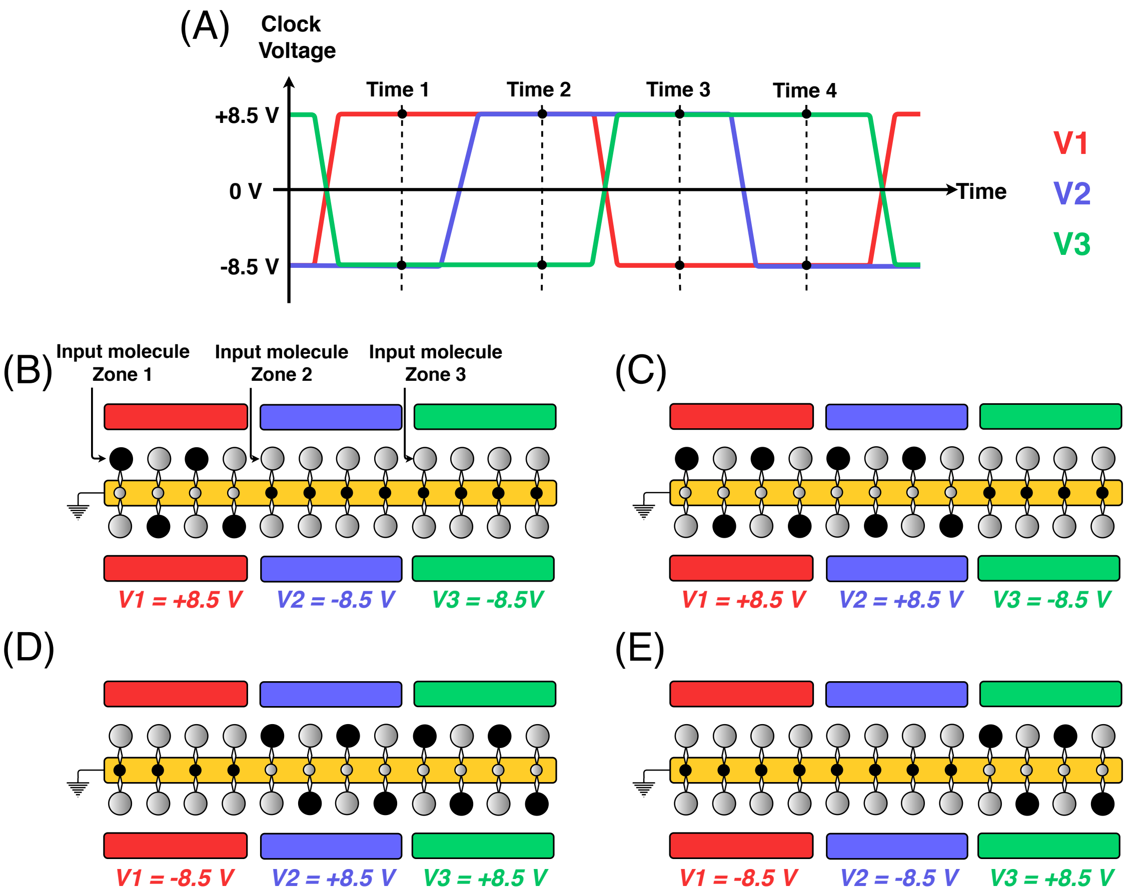

Figure 3.20. Schematic example of information propagation in MQCA Wire.

In particular, using this implementation, in each clock zone three working conditions are involved. Taking as reference the Time 2 depicted in Figure 3.20.C, it is possible to identify that in the first Clock Zone all molecule are in *Hold State*, in the Clock Zone 2, the information propagates until all molecules assume proper polarization (*Switch State*), while in Clock Zone 3 all molecules are in *Reset State*. For this reason, this clock mechanism is called *Three-Phase Clocking*. Therefore, alternating the phases of the clock signal applied to the electrodes along the Molecular QCA Wire, the correct information flow is ensured, as demonstrated in [22, 23].

Chapter 4

Sinusoidal Clocking Mechanism

A possible zone-less clocking configuration is the so-called *Sinusoidal Clocking*. This configuration is based on the idea to have a single electrode in which a high-frequency signal is applied. Therefore, instead of dividing the QCA Wire into clock regions, the electrode is made continuous and it is treated as a transmission line where the signal is supposed to propagate as electromagnetic wave, generating an electric field which changes with respect to the position and to the time.
Making a comparison among the Sinusoidal Clocking and Three-Phase Clocking, illustrated in Figure 4.1.A, in the former one electrode is present and only one signal propagates in the space, in the latter three electrodes and as many signals, with annexed interconnects to provide them, are needed.

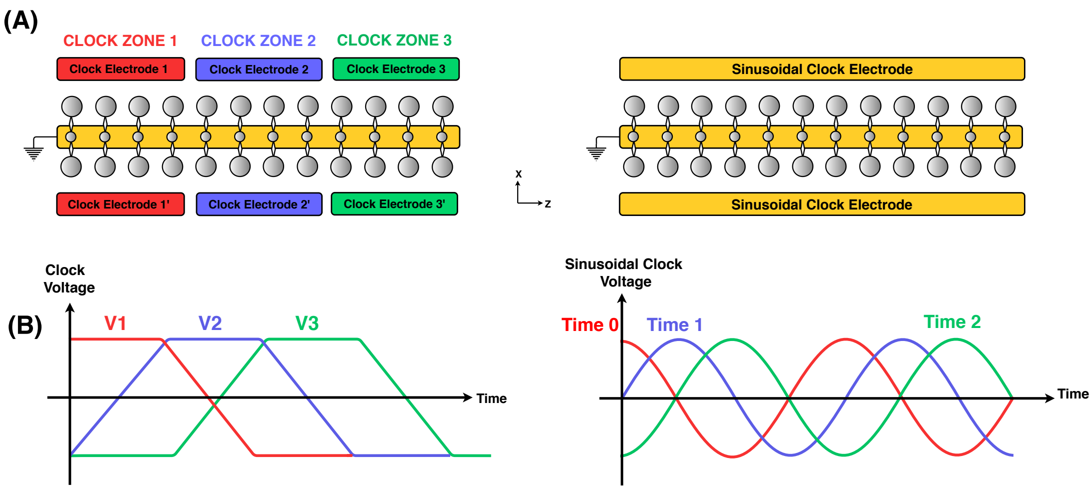

Figure 4.1. (A) Clock systems comparison: Three-Phase Clock schematic (left) Sinusoidal Clock schematic (right), (B) corresponding Clock voltages.

The Sinusoidal Clocking principle consists of inducing the pipeline mechanism similar to the one in the Three-phase clock, exploiting the time-space varying electromagnetic wave in the electrode/transmission line, as depicted in Figure 4.1.B.

In particular, in Three-phase clocking the propagation performances are influenced by the inter-electrode space in which there is a sudden change of applied electric field into the Wire. This criticality is removed with Sinusoidal Clocking configuration, and in addition, it may be very interesting from a technological point of view because a single electrode fabrication could be easier to obtain.
One physical implementation of this novel clocking mechanism has been reported in [24] and illustrated in Figure 4.2.A, where the MQCA circuit (in this case a simple Wire) has been placed in between a ground plane and an array of nanoelectrodes. In each electrode is applied the same periodic multi-phase clock signal, shown in Figure 1.16, with a $\pi/2$ phase shift between one and another, so that in the $i-th$ electrode, where $i = 1,5,9...$, the same trapezoidal signal is present.

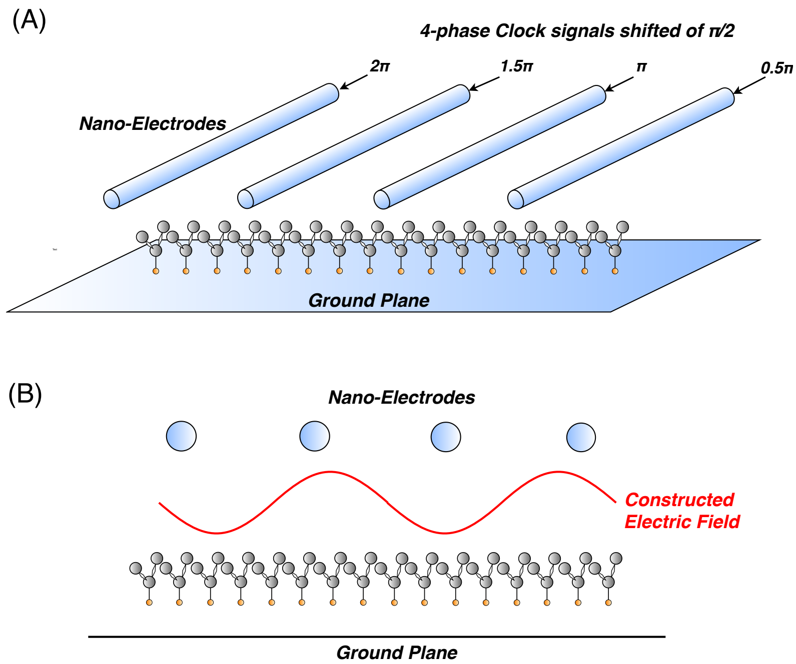

Figure 4.2. Sinusoidal Clock physical implementation proposed in [24]: (A) 3D view, (B) Transversal view with schematic representation of induced sinusoidal clock field.

As result of this $\pi/2$ shifting and the coupling of electric fields generated by the nanoelectrodes' array, an almost sinusoidal clock field is induced in the molecules, as depicted in Figure 4.2.B. Moreover, FEM simulation with COMSOL Multiphysics® program has been executed to verify the theoretical concepts discussed in [24], obtaining a result, illustrated in Figure 4.3, in line with what was expected and demonstrating the possibility to implement this kind of Clock.

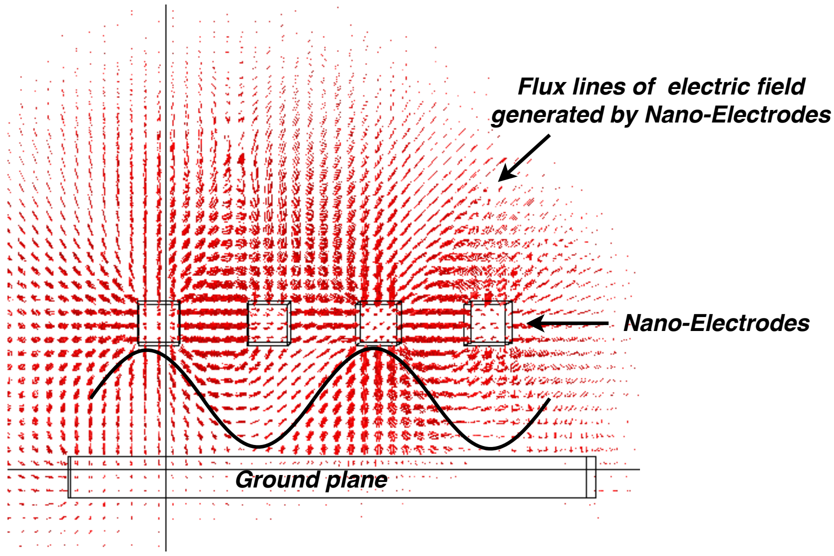

Figure 4.3. Flux lines of electric field generated by nanoelectrodes obtained through COMSOL program

4.1 Sinusoidal Clock Simulation with SCERPA

To study the concept of Sinusoidal Clocking from a theoretical point of view, and analyse the effectiveness of this clocking mechanism on MQCA structures the MATLAB® program *Self Consistent Electrostatic Potential Algorithm* (SCERPA) is used. It is not possible to implement the sinusoidal signal as a continuous function since the algorithm can deal only with discrete voltages, for this reason a discretization of Sinusoidal Clock Voltage and extraction of corresponding samples is performed as depicted in Figure 4.4.

The SCERPA program is divided into two main sections:

1. **Algorithm section**;

2. **Layout section**.

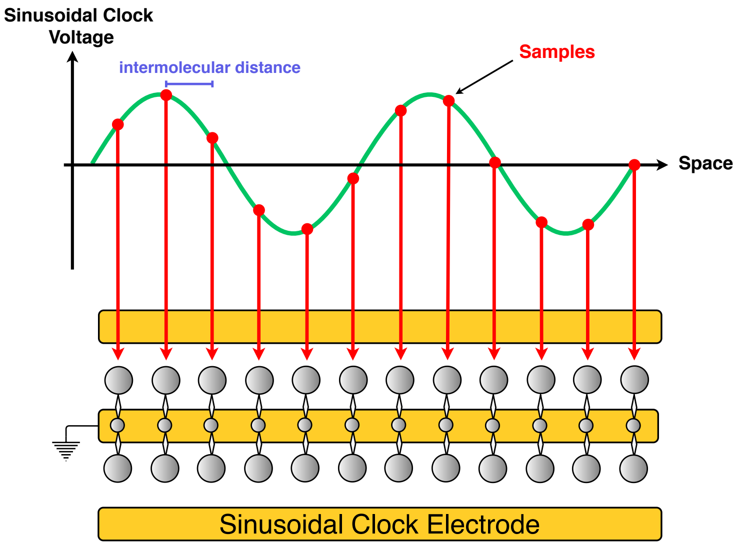

Figure 4.4. Discretization of the Sinusoidal Clock to the QCA Wire.

4.2 Algorithm section

This section uses a deterministic algorithm proposed in [43] and improved in [4], computing the aggregated charge distribution in all molecules of the MQCA system. The flow of algorithm operations is represented by the flow chart in Figure 4.5.

First of all, it is performed an evaluation of the potential produced by the driver on all molecules of the circuit. Whereupon, considering the molecules one-by-one, it is calculated the potential generated by the other molecules. Finally, the procedure is iteratively applied to each molecule in a self-consistent procedure to find the final stable solution.

4.3 Layout section

In this section, it is possible to define the MQCA structure or MQCA circuit properly setting its main parts:

- **Molecule Settings**;
- **Sinusoidal Clock Settings**;
- **Driver Definition**;
- **Process Variation**;
- **Layout QCA Circuit**;
- **"Fake" Clock Sinusoidal Phases**.

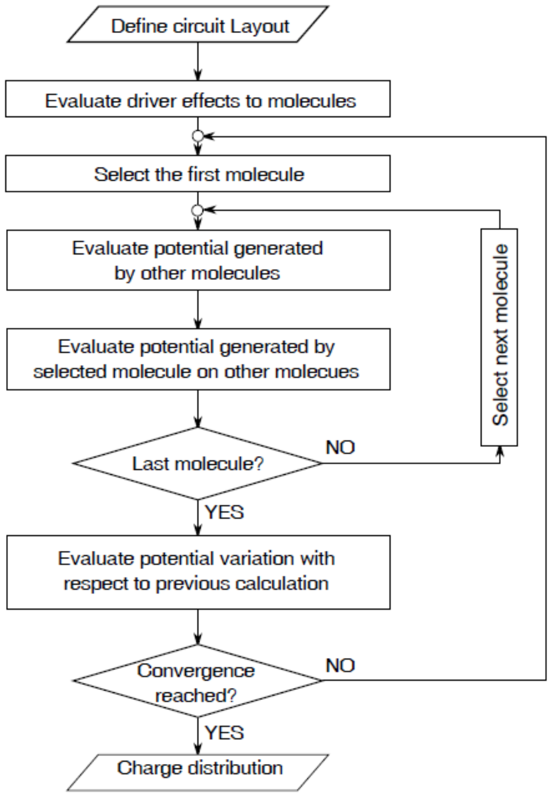

Figure 4.5. Flow chart of SCERPA for MQCA simulations.

4.3.1 Molecule Settings

This part regards the settings used for the reference molecule and the relative instructions are shown in `Layout_Molecule_Setting` box:

Listing 4.1. `Layout_Molecule_Settings`

```
clc;
close all;
clear ;
%======================= SETTINGS =====================
% initial_charge   = [0.475, 0.471, -0.223, 0.277];  % charge ck=+2V
initial_charge   = [0.370, 0.352, -0.023, 0.307];  % charge ck=+0V
% initial_charge   = [0.027, 0.026,  0.141, 0.806];  % charge ck=-2V

molecule_type='bisfe4';
```

With the `initial_charge` instruction arbitrarily setting of the initial amount of charge is accomplished, according to three standard configurations:

CK	DOT1	DOT2	DOT3	DOT4
+2 V	0.475	0.471	-0.223	0.277
0 V	0.370	0.352	-0.023	0.307
-2 V	0.027	0.026	0.141	0.806

Table 4.1. Possible initial charge configurations of Bis-ferrocene molecule.

In all simulations, the uncommented instruction concerning the clock at 0 Volt has been used. The `molecule_type = 'bisfe4'` instruction definition allows simulating the Bis-ferrocene molecule.

4.3.2 Sinusoidal Clock Settings

The following designed section regards Sinusoidal Clock parameters definition, in particular:

- `lambda`: is the wavelength of Sinusoidal Clock;
- `sin_ck.num_mol`: is the number of molecules that are used to create the MQCA Wire (this parameter is defined only for the Wire, not for the other structures);
- `mol_dist`: is the intermolecular distance (see Figure 4.4) and at the same time defines the spatial space between two samples;
- `sin_ck.time_step`: defines the temporal shift of Sinusoidal Clock;
- `sin_ck.time_instants`: defines the number of temporal instants to simulate;
- `period = sin_ck.time_step * sin_ck.time_instants /T`: shows in the MATLAB® Command Window the number of periods of the simulated Sinusoidal Clock.

Listing 4.2. `Sinusoidal_ck_Settings`

```
if (sin_ck.mode == 1)

    %Physical constants
    c = 2.99792458e+8; % speed of light, m/s
    mu0 = 4*pi*1.0e-7; % magnetic permeability, H/m
    eps0 = 1/(mu0*c^2); % dielectric permittivity, F/m

    % Input parameter
    sin_ck.num_mol = 300; % number of molecules in the WIRE only
    lambda = 50e-9; % wavelength
    A = 2; % wave amplitude
    n = 1; %refractive index air
    mol_dist = 1e-9; % distance between molecules
    v = c / n; % propagation velocity
    T = lambda / v; % wave period

    sin_ck.time_step = 0.025*T; % time shift of the wave
    sin_ck.time_instants = 10; % In the first instant the whole
                        % structure is in Reset state

    period = sin_ck.time_step * sin_ck.time_instants / T; % simulated clock period
    X = ['It is simulating ',num2str(period), ' periods.'];
    disp(X)

end
```

4.3.3 Driver Definition

This section regards naming definition of one or more Drivers inside the QCA structure and their possible configurations during the simulation. As reported in `Driver_definition` box, the Driver naming occurs in the first column of `Values_Dr` matrix with `'Dri'` parameter.

Listing 4.3. `Driver_Definition`

```
%                     time1  |   time 2->9    |
Values_Dr = { 'Dr1'  '1'   '1' '1' '1' '1' '1' '1' '1'  '1' '1'  'end';
              'Dr2'  '0'   '0' '0' '0' '0' '0' '0' '0'  '0' '0'  'end';
              'Dr3'  '1'   '1' '1' '1' '1' '1' '1' '1'  '1' '1'  'end';
              'Dr4'  nan   '0' '0' '0' '0' '0' '0' '0'  '0' '0'  'end';
              'Dr5'  '0'    Not_Enabled{:}   'end'};
```

In the remaining columns, using the concept of time slicing, Driver charge configuration at different time instants is imposed:

- `'1'`: the driver is activated with logic charge localized in Dot1 at that given time slice (Figure 3.6.E);
- `'0'`: the driver is activated with logic charge localized in Dot2 at that given time slice (Figure 3.6.F);
- `Not_Enabled:`: The driver is disabled for a set of seven time instants;
- `nan`: the driver is deactivated for a specific time instant.

4.3.4 Process Variation

In this section, enabling or disabling of the process variation of the MCQA circuit by means of `process_variation`, `auto_variations` and `electrode_variations` instructions is possible. Three possibilities are available regarding the kind of process variation:

1. **Uniform Distribution**: to apply the same distribution for all molecules of mQCA circuit;
2. **Gaussian Distribution**: setting the mean value `mu` and the variance `sigma` shift and rotation application is possible.
3. **Deterministic Distribution**: the causality variability of the input data is not taken into account, which means that fixed the driver configuration and MQCA structure the simulation result will be always the same.

Listing 4.4. `Process_Variation`

```
%||*||*||*||*||*||*||*||*||*||*||*||*||*||*||*||*||*||*||*||*||
process_variation='on';
%||*||*||*||*||*||*||*||*||*||*||*||*||*||*||*||*||*||*||*||*||
%\./.\./.\./.\./.\./.\./.\./.\./.\./.\./.\./.\./.\./.\./.\./.\./.\./.\%
%----------------------------auto variation--------------------------%
auto_variations='off';
%\./.\./.\./.\./.\./.\./.\./.\./.\./.\./.\./.\./.\./.\./.\./.\./.\./.\%
%|.|.|.|.|.|.|.|.|.|.|.|.|.|.|.|.|.|.|.|.|.|.|.|.|.|.|.|.|.|.|.|.|.|.|%
%-------------------------electrode variaiton------------------------%
electrode_variation='off';
%|.|.|.|.|.|.|.|.|.|.|.|.|.|.|.|.|.|.|.|.|.|.|.|.|.|.|.|.|.|.|.|.|.|.|%
% Number of Process Variations
kind_proc_variation = 'Deterministic';
num_processor = 1;


% With 'map' the values of rotation are taken from the
%  text file in process variation folder.
% If we set this function to 'yes' the values
```

```
% are calculated from normal distribution MU and
% standard deviation SIGMA.
% Other value set the rotations to zero;
% mu and sigma value for x,y,z rotation and shift.
rotation_selection='yes';

% x rotation y rotation z rotation [degree]
% x shift y shift z shift [A]
mu   =[0, 0, 0, 0, 0, 0];
sigma=[0, 0, 0, 0, 0, 0];
pv=variation_selection(process_variation,auto_variations,
electrode_variation, rotation_selection,mu,sigma);
```

4.3.5 Layout QCA Circuit

Concerning this part, the placement of molecules at given inter-molecular distance, their rotation and shifting definition is performed, filling properly the matrices `QCA_circuit.structure` and `QCA_circuit.rotation` (the shift matrix is not considered in this thesis) present in *select_structure.m* and *select_structure_sin_ck.m* files. An QCA wire example layout in the case of Three-phase clocking is visible in the `Qca_wire` box hereinafter:

Listing 4.5. `Qca_wire`

```
dist_z = 10;
dist_y = (dist_z + abs(dot_position(1,2) - dot_position(2,2)));

QCA_circuit.structure={'Dr1' '1' '1' '1' '1' '2' '2' '2' '2'  '3' '3' '3' '3'};

QCA_circuit.rotation = {'0' '0' '0' '0' '0' '0' '0' '0' '0' '0' '0' '0' '0'};
```

Where:

- `dist_z`: it is the distance between two adjacent columns of the `QCA_circuit.structure` matrix and represents the intermolecular distance between two molecules in Å placed side by side. Its schematic representation is illustrated in Figure 4.6;

- `dist_y`: it is the distance between two adjacent rows of the `QCA_circuit.structure` matrix and represents the intermolecular distance between two molecules in Å placed one above, or underneath, the other. Its schematic representation is illustrated in Figure 4.6;

- `dist_x`: it is not considered because only 2D structures are analysed, not 3D;

- `QCA_circuit.structure`: it is the matrix which defines the position of the drivers, molecules and electrodes. Driver placement occurs inserting `'Dr#'`, while molecules placement and electrodes definition (that reflect the wanted clock zones) occurs with `'1' '2' '3'` parameters, as shown in Figure 4.7. Subsequently, the association between the clock zones and the *"Fake" Clock Phases* is performed, as explained in the next section;

- `QCA_circuit.rotation`: it is the matrix which defines the rotation in degrees of the drivers and molecules collocated during `QCA_circuit.structure` matrix design. This matrix is fundamental for structures like the Majority Voter, where rotation's molecules is necessary to create two of the three device's branches, as illustrated in Figure 4.8. Rotation operation is available by setting the `'90'` values in the corresponding molecule positions of `QCA_circuit.structure`, as reported in `Qca_majority_voter` box.

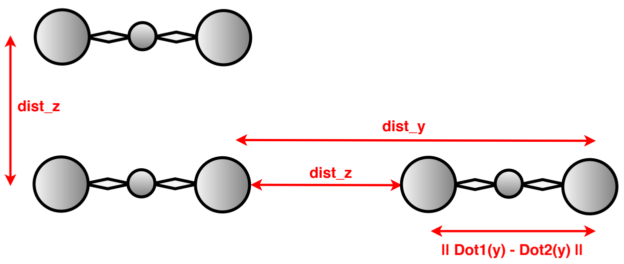

Figure 4.6. Schematic representation of `dist_z` and `dist_y` (top view)

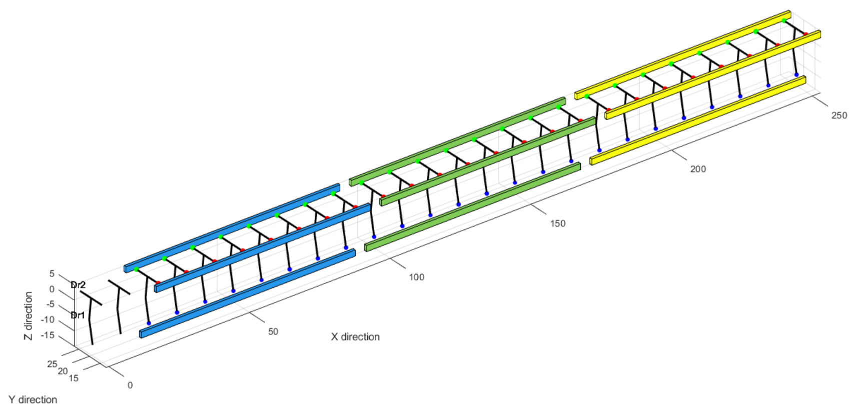

Figure 4.7. Layout of the MQCA Wire obtained with the instructions in `Qca_wire` box.

Listing 4.6. `Qca_majority_voter`

```
dist_z = 5;
dist_y = 5;

QCA_circuit.structure = {
  0   0   0   0  0  0  0  0  0  0  0  0  0 'Dr1' 0  0  0  0  0  0  0  0  0
  0   0   0   0  0  0  0  0  0  0  0  0  0   0   0  0  0  0  0  0  0  0  0
  0   0   0   0  0  0  0  0  0  0  0  0  0 'Dr2' 0  0  0  0  0  0  0  0  0
  0   0   0   0  0  0  0  0  0  0  0  0  0   0   0  0  0  0  0  0  0  0  0
  0   0   0   0  0  0  0  0  0  0  0  0  0  '1'  0  0  0  0  0  0  0  0  0
  0   0   0   0  0  0  0  0  0  0  0  0  0   0   0  0  0  0  0  0  0  0  0
  0   0   0   0  0  0  0  0  0  0  0  0  0  '1'  0  0  0  0  0  0  0  0  0
  0   0   0   0  0  0  0  0  0  0  0  0  0   0   0  0  0  0  0  0  0  0  0
  0   0   0   0  0  0  0  0  0  0  0  0  0  '1'  0  0  0  0  0  0  0  0  0
  0   0   0   0  0  0  0  0  0  0  0  0  0   0   0  0  0  0  0  0  0  0  0
  0   0   0   0  0  0  0  0  0  0  0  0  0  '1'  0  0  0  0  0  0  0  0  0
  0   0   0   0  0  0  0  0  0  0  0  0  0   0   0  0  0  0  0  0  0  0  0
  0   0   0   0  0  0  0  0  0  0  0  0  0   0   0  0  0  0  0  0  0  0  0
'Dr1' 0 'Dr2' 0 '1' 0 '1' 0 '1' 0 '1' 0 '2'  0  '2' 0 '2' 0 '2' 0 '2' 0 '2'
  0   0   0   0  0  0  0  0  0  0  0  0  0   0   0  0  0  0  0  0  0  0  0
  0   0   0   0  0  0  0  0  0  0  0  0  0   0   0  0  0  0  0  0  0  0  0
  0   0   0   0  0  0  0  0  0  0  0  0  0  '1'  0  0  0  0  0  0  0  0  0
  0   0   0   0  0  0  0  0  0  0  0  0  0   0   0  0  0  0  0  0  0  0  0
  0   0   0   0  0  0  0  0  0  0  0  0  0  '1'  0  0  0  0  0  0  0  0  0
  0   0   0   0  0  0  0  0  0  0  0  0  0   0   0  0  0  0  0  0  0  0  0
  0   0   0   0  0  0  0  0  0  0  0  0  0  '1'  0  0  0  0  0  0  0  0  0
  0   0   0   0  0  0  0  0  0  0  0  0  0   0   0  0  0  0  0  0  0  0  0
  0   0   0   0  0  0  0  0  0  0  0  0  0  '1'  0  0  0  0  0  0  0  0  0
  0   0   0   0  0  0  0  0  0  0  0  0  0   0   0  0  0  0  0  0  0  0  0
  0   0   0   0  0  0  0  0  0  0  0  0  0 'Dr1' 0  0  0  0  0  0  0  0  0
  0   0   0   0  0  0  0  0  0  0  0  0  0   0   0  0  0  0  0  0  0  0  0
  0   0   0   0  0  0  0  0  0  0  0  0  0 'Dr2' 0  0  0  0  0  0  0  0  0 };

  QCA_circuit.rotation =  {
 '0''0''0''0''0''0''0''0''0''0''0''0''0''90''0''0''0''0''0''0''0''0''0'
 '0''0''0''0''0''0''0''0''0''0''0''0''0' '0''0''0''0''0''0''0''0''0''0'
 '0''0''0''0''0''0''0''0''0''0''0''0''0''90''0''0''0''0''0''0''0''0''0'
 '0''0''0''0''0''0''0''0''0''0''0''0''0' '0''0''0''0''0''0''0''0''0''0'
 '0''0''0''0''0''0''0''0''0''0''0''0''0''90''0''0''0''0''0''0''0''0''0'
 '0''0''0''0''0''0''0''0''0''0''0''0''0' '0''0''0''0''0''0''0''0''0''0'
 '0''0''0''0''0''0''0''0''0''0''0''0''0''90''0''0''0''0''0''0''0''0''0'
 '0''0''0''0''0''0''0''0''0''0''0''0''0' '0''0''0''0''0''0''0''0''0''0'
 '0''0''0''0''0''0''0''0''0''0''0''0''0''90''0''0''0''0''0''0''0''0''0'
 '0''0''0''0''0''0''0''0''0''0''0''0''0' '0''0''0''0''0''0''0''0''0''0'
 '0''0''0''0''0''0''0''0''0''0''0''0''0''90''0''0''0''0''0''0''0''0''0'
 '0''0''0''0''0''0''0''0''0''0''0''0''0' '0''0''0''0''0''0''0''0''0''0'
 '0''0''0''0''0''0''0''0''0''0''0''0''0' '0''0''0''0''0''0''0''0''0''0'
 '0''0''0''0''0''0''0''0''0''0''0''0''0' '0''0''0''0''0''0''0''0''0''0'
 '0''0''0''0''0''0''0''0''0''0''0''0''0' '0''0''0''0''0''0''0''0''0''0'
```

```
'0''0''0''0''0''0''0''0''0''0''0''0''0' '0''0''0''0''0''0''0''0''0''0'
'0''0''0''0''0''0''0''0''0''0''0''0''0''90''0''0''0''0''0''0''0''0''0'
'0''0''0''0''0''0''0''0''0''0''0''0''0' '0''0''0''0''0''0''0''0''0''0'
'0''0''0''0''0''0''0''0''0''0''0''0''0''90''0''0''0''0''0''0''0''0''0'
'0''0''0''0''0''0''0''0''0''0''0''0''0' '0''0''0''0''0''0''0''0''0''0'
'0''0''0''0''0''0''0''0''0''0''0''0''0''90''0''0''0''0''0''0''0''0''0'
'0''0''0''0''0''0''0''0''0''0''0''0''0' '0''0''0''0''0''0''0''0''0''0'
'0''0''0''0''0''0''0''0''0''0''0''0''0''90''0''0''0''0''0''0''0''0''0'
'0''0''0''0''0''0''0''0''0''0''0''0''0' '0''0''0''0''0''0''0''0''0''0'
'0''0''0''0''0''0''0''0''0''0''0''0''0''90''0''0''0''0''0''0''0''0''0'
'0''0''0''0''0''0''0''0''0''0''0''0''0' '0''0''0''0''0''0''0''0''0''0'
'0''0''0''0''0''0''0''0''0''0''0''0''0''90''0''0''0''0''0''0''0''0''0' };
```

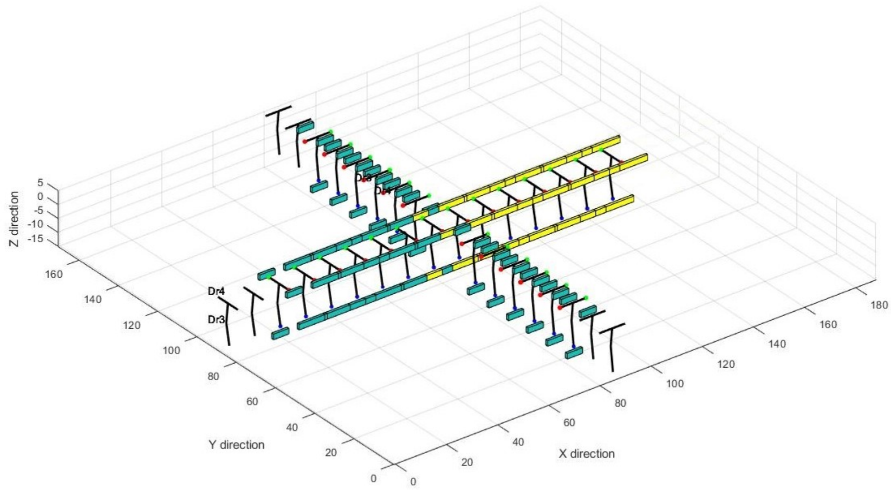

Figure 4.8. Layout of the MQCA Majority Voter obtained with the instructions in `Qca_majority_voter` box (two Clock Zone are enough).

To accomplish the Sinusoidal Clock implementation, in the previous described structures a new variant of the code has been designed for the Wire and the Majority Voter, as reported in `Qca_wire_sinusoidal_ck` box and `Qca_majority_voter_sinusoidal_ck` box, respectively.

Listing 4.7. `Qca_wire_sinusoidal_ck`

```
dist_z = 10;
dist_y = (dist_z + abs(dot_position(1,2) - dot_position(2,2)));

QCA_circuit.structure={'Dr1' '1' '2' '3' '4' '5' '6' '7' '8'  '9' '10' '11' '12'};

QCA_circuit.rotation = {'0' '0' '0' '0' '0' '0' '0' '0' '0' '0' '0' '0' '0'};
```

Listing 4.8. `Qca_majority_voter_sinusoidal_ck`

```
dist_z = 5;
dist_y = 5;

QCA_circuit.structure = {
  0    0    0    0  0  0  0  0  0  0  0  0  0 'Dr1' 0  0  0  0  0  0  0  0  0
  0    0    0    0  0  0  0  0  0  0  0  0  0   0   0  0  0  0  0  0  0  0  0
  0    0    0    0  0  0  0  0  0  0  0  0  0 'Dr2' 0  0  0  0  0  0  0  0  0
  0    0    0    0  0  0  0  0  0  0  0  0  0   0   0  0  0  0  0  0  0  0  0
  0    0    0    0  0  0  0  0  0  0  0  0  0  '1'  0  0  0  0  0  0  0  0  0
  0    0    0    0  0  0  0  0  0  0  0  0  0   0   0  0  0  0  0  0  0  0  0
  0    0    0    0  0  0  0  0  0  0  0  0  0  '2'  0  0  0  0  0  0  0  0  0
  0    0    0    0  0  0  0  0  0  0  0  0  0   0   0  0  0  0  0  0  0  0  0
  0    0    0    0  0  0  0  0  0  0  0  0  0  '3'  0  0  0  0  0  0  0  0  0
  0    0    0    0  0  0  0  0  0  0  0  0  0   0   0  0  0  0  0  0  0  0  0
  0    0    0    0  0  0  0  0  0  0  0  0  0  '4'  0  0  0  0  0  0  0  0  0
  0    0    0    0  0  0  0  0  0  0  0  0  0   0   0  0  0  0  0  0  0  0  0
  0    0    0    0  0  0  0  0  0  0  0  0  0   0   0  0  0  0  0  0  0  0  0
'Dr1'  0  'Dr2'  0 '1' 0 '2' 0 '3' 0 '4' 0 '5'  0  '6' 0 '7' 0 '8' 0 '9' 0 '10'
  0    0    0    0  0  0  0  0  0  0  0  0  0   0   0  0  0  0  0  0  0  0  0
  0    0    0    0  0  0  0  0  0  0  0  0  0   0   0  0  0  0  0  0  0  0  0
  0    0    0    0  0  0  0  0  0  0  0  0  0  '4'  0  0  0  0  0  0  0  0  0
  0    0    0    0  0  0  0  0  0  0  0  0  0   0   0  0  0  0  0  0  0  0  0
  0    0    0    0  0  0  0  0  0  0  0  0  0  '3'  0  0  0  0  0  0  0  0  0
  0    0    0    0  0  0  0  0  0  0  0  0  0   0   0  0  0  0  0  0  0  0  0
  0    0    0    0  0  0  0  0  0  0  0  0  0  '2'  0  0  0  0  0  0  0  0  0
  0    0    0    0  0  0  0  0  0  0  0  0  0   0   0  0  0  0  0  0  0  0  0
  0    0    0    0  0  0  0  0  0  0  0  0  0  '1'  0  0  0  0  0  0  0  0  0
  0    0    0    0  0  0  0  0  0  0  0  0  0   0   0  0  0  0  0  0  0  0  0
  0    0    0    0  0  0  0  0  0  0  0  0  0 'Dr1' 0  0  0  0  0  0  0  0  0
  0    0    0    0  0  0  0  0  0  0  0  0  0   0   0  0  0  0  0  0  0  0  0
  0    0    0    0  0  0  0  0  0  0  0  0  0 'Dr2' 0  0  0  0  0  0  0  0  0 };

  QCA_circuit.rotation =  {
 '0''0''0''0''0''0''0''0''0''0''0''0''0''90''0''0''0''0''0''0''0''0''0'
 '0''0''0''0''0''0''0''0''0''0''0''0''0' '0''0''0''0''0''0''0''0''0''0'
 '0''0''0''0''0''0''0''0''0''0''0''0''0''90''0''0''0''0''0''0''0''0''0'
 '0''0''0''0''0''0''0''0''0''0''0''0''0' '0''0''0''0''0''0''0''0''0''0'
 '0''0''0''0''0''0''0''0''0''0''0''0''0''90''0''0''0''0''0''0''0''0''0'
 '0''0''0''0''0''0''0''0''0''0''0''0''0' '0''0''0''0''0''0''0''0''0''0'
 '0''0''0''0''0''0''0''0''0''0''0''0''0''90''0''0''0''0''0''0''0''0''0'
 '0''0''0''0''0''0''0''0''0''0''0''0''0' '0''0''0''0''0''0''0''0''0''0'
 '0''0''0''0''0''0''0''0''0''0''0''0''0''90''0''0''0''0''0''0''0''0''0'
 '0''0''0''0''0''0''0''0''0''0''0''0''0' '0''0''0''0''0''0''0''0''0''0'
 '0''0''0''0''0''0''0''0''0''0''0''0''0''90''0''0''0''0''0''0''0''0''0'
 '0''0''0''0''0''0''0''0''0''0''0''0''0' '0''0''0''0''0''0''0''0''0''0'
 '0''0''0''0''0''0''0''0''0''0''0''0''0' '0''0''0''0''0''0''0''0''0''0'
 '0''0''0''0''0''0''0''0''0''0''0''0''0' '0''0''0''0''0''0''0''0''0''0'
 '0''0''0''0''0''0''0''0''0''0''0''0''0' '0''0''0''0''0''0''0''0''0''0'
 '0''0''0''0''0''0''0''0''0''0''0''0''0' '0''0''0''0''0''0''0''0''0''0'
```

```
'0''0''0''0''0''0''0''0''0''0''0''0''0''90''0''0''0''0''0''0''0''0''0'
'0''0''0''0''0''0''0''0''0''0''0''0''0' '0''0''0''0''0''0''0''0''0'
'0''0''0''0''0''0''0''0''0''0''0''0''0''90''0''0''0''0''0''0''0''0''0'
'0''0''0''0''0''0''0''0''0''0''0''0''0' '0''0''0''0''0''0''0''0''0'
'0''0''0''0''0''0''0''0''0''0''0''0''0''90''0''0''0''0''0''0''0''0''0'
'0''0''0''0''0''0''0''0''0''0''0''0''0' '0''0''0''0''0''0''0''0''0'
'0''0''0''0''0''0''0''0''0''0''0''0''0''90''0''0''0''0''0''0''0''0''0'
'0''0''0''0''0''0''0''0''0''0''0''0''0' '0''0''0''0''0''0''0''0''0'
'0''0''0''0''0''0''0''0''0''0''0''0''0''90''0''0''0''0''0''0''0''0''0'
'0''0''0''0''0''0''0''0''0''0''0''0''0' '0''0''0''0''0''0''0''0''0'
'0''0''0''0''0''0''0''0''0''0''0''0''0''90''0''0''0''0''0''0''0''0''0' };
```

The MQCA structures created with these latest instructions are illustrated in Figure 4.9 and 4.10. Defining one different clock zone for each molecule it is possible to relate them with the *"Fake" Sinusoidal Clock Phases*, that basically are the extracted *samples*, of Sinusoidal Clock Voltage (Figure 4.4).

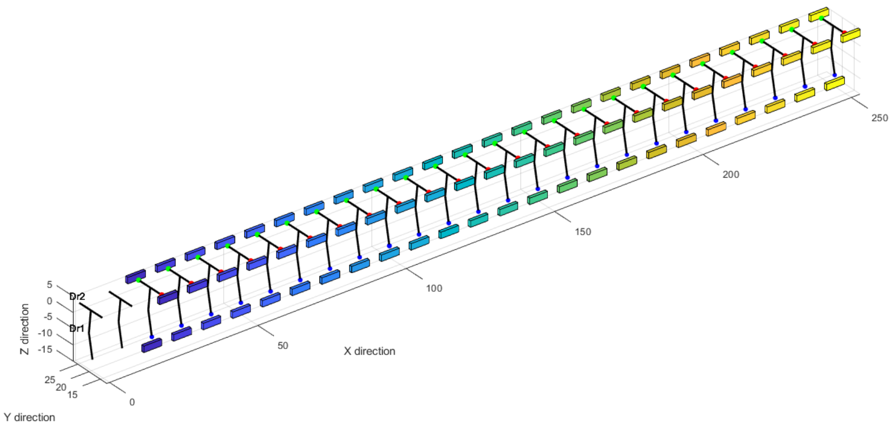

Figure 4.9. Layout of the MQCA Wire obtained with the instructions in `Qca_wire_sinusoidal_ck` box.

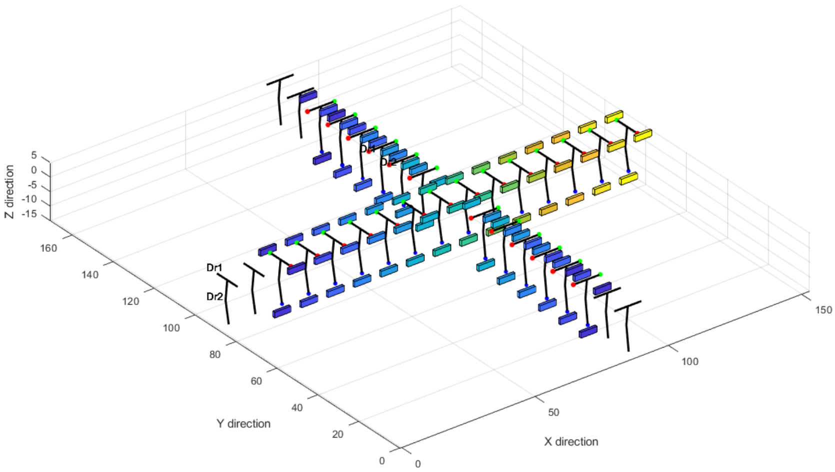

Figure 4.10. Layout of the MQCA Majority Voter obtained with the instructions in `Qca_majority_voter_sinusoidal_ck` box.

Actually, in order to gain flexibility, in the case of MQCA Wire different instructions (`Qca_wire_sinusoidal_ck2` box) has been designed to generate the layout, allowing to vary the number of molecules that compose the wire simply changing the parameter `sin_ck.num_mol` present in `Sinusoidal_ck_Settings` box.

Listing 4.9. `Qca_wire_sinusoidal_ck2`

```
   dist_z = 10;
   dist_y = (dist_z + abs(dot_position(1,2) - dot_position(2,2)));
   s0 = '0';

% generate 1 electrode for each  molecule in order to apply the sine
% values in each one in Layout.m
for k= 1:sin_ck.num_mol
     QCA_circuit.structure (1,k) = cellstr( int2str(k));
end
% Insert in the first cell the Driver
QCA_circuit.structure(1,2:end+1) = QCA_circuit.structure(1,:);
QCA_circuit.structure(1,1) = {'Dr1'};

for i=1:sin_ck.num_mol +1
          QCA_circuit.rotation(1,i)={s0};
end
```

4.3.6 "Fake" Sinusoidal Clock Phases

This section concerns "Fake" Clock Phases and "Fake" Sinusoidal Clock Phases generation, meaning the definition of the vertical voltage values applied to the molecular cluster in the former case (Three-phase clock) or in each single molecule in the latter case (Sinusoidal Clock). The reason for their usage consists of inserting reasonable values of the clock without using of FEM simulations allowing faster analysis.
To implement the "Fake" Clock Phases, regarding the Three-phase clock, the instructions reported in `Fake_ck_phases` box are used, generating the matrix in Table 4.2:

Listing 4.10. `Fake_ck_phases`

```
stack_phase(1,:) = [ 2   2  -2  -2 ];
stack_phase(2,:) = [-2   2   2  -2 ];
stack_phase(3,:) = [-2  -2   2   2 ];
```

	Clock Phases $[V]$			
	Time 0	Time 1	Time 2	Time 3
Clock Zone 1	2	2	-2	-2
Clock Zone 2	-2	2	2	-2
Clock Zone 3	-2	-2	2	2

Table 4.2. Generated matrix by the instructions in the `Fake_ck_phases` box.

Therefore, the working principle is based on the concept of time determining the temporal evolution of algorithm, in which at each time instant the given clock phase is associated and applied to the corresponding molecular cluster, as illustrated in Figure 4.11.

Moreover, it is possible to notice that the simulation result perfectly reflects the prediction made during the explanation of the Three-phase clock in Figure 3.20.

About the "Fake" Sinusoidal Clock Phases generation, more complex instructions are required to define them properly. They are listed below in the two boxes, in order to better explain the functioning principle:

- `Fake_sinusoidal_ck_phases_part1`
- `Fake_sinusoidal_ck_phases_part2`

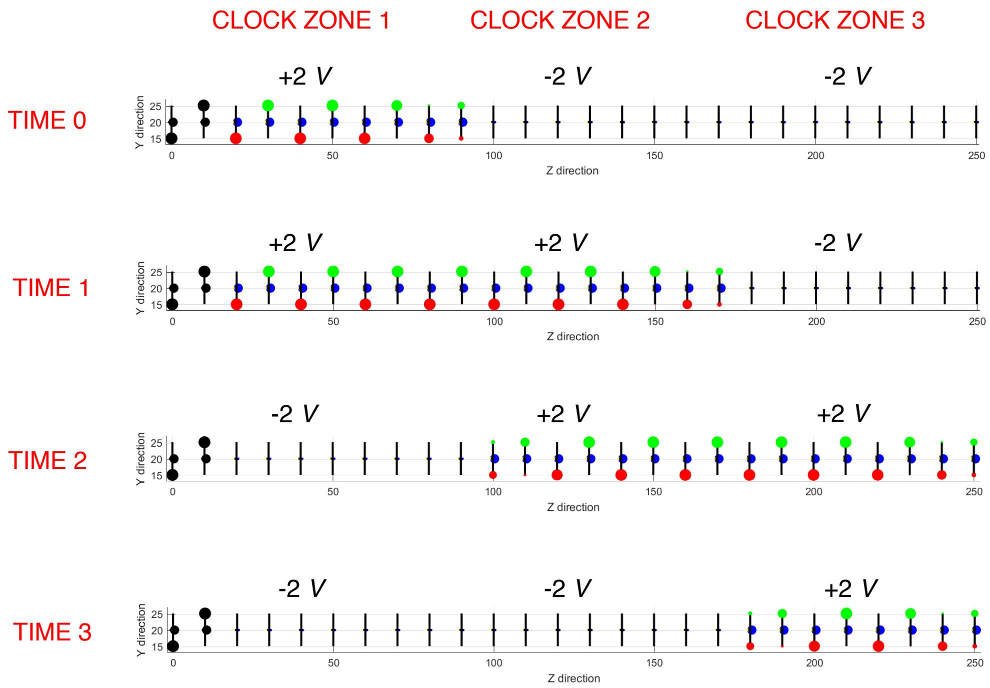

Figure 4.11. Simulation of MQCA Wire formed by 24 molecules with Three-Phase Clock.

"Fake" Sinusoidal Clock Phases generation: Part 1

Listing 4.11. `Fake_sinusoidal_ck_phases_part1`

```
k = (2*pi) / lambda; % wavenumber
freq = c / lambda; % frequency
omega = k * v; % angular frequency
%
precision = 10;
wire_length = stack_mol.num * mol_dist; % wire length
%
phi= -0.5*pi;

if lambda >= wire_length
   sin_ck.x = [0: mol_dist / precision: lambda ];
else
   z=1;
   num_samples =(lambda /  mol_dist);
   num_samples_new = num_samples;

   while num_samples_new < stack_mol.num
      num_samples_new = z*num_samples;
```

```
      z=z+1;
   end
   sin_ck.x = [0: mol_dist / precision: lambda*z ];
end

% sine wave generation at different time instants

for j = 1: sin_ck.time_instants
   sin_ck.wave(j,:) = A*sin(k*sin_ck.x - omega*((j-1)*sin_ck.time_step) + phi);

   % sampling of the wave using as distance between two sample
   % the molecular distance
   for i = 0: stack_mol.num - 1
      sample_values (j,i+1) = sin_ck.wave (j,i* precision+1);
   end

end
```

Basically, two constructs are exploited in this first portion of code:

- ***if-else***: it used to compare the sinusoidal wave defined in `Sinusoidal_ck_Settings` with the length of MQCA circuit. Taking as example the Wire, two possible situations can happen, as depicted in Figure 4.12. In the (A) case, the number of extracted samples is enough to cover the entire structure, in (B) case are not enough generating a computational error.
  Therefore, utilizing the *while* nested construct the number of periods is increased (and consequently also the number of samples) until the whole Wire is covered (dashed sine curve).

- ***for cycle***: it used to generate the harmonic wave in each cycle step, according the standard formula:

$$f(x,t) = Asin(kx - \omega t + \phi) \tag{4.1}$$

  where A is the amplitude of Sinusoidal Clock and it is set to 2 V, k is the wavenumber, x is the space (`sin_ck.x` in the code), ω is the angular frequency, t is the time (`sin_ck.time_step` in the code and it varies in each cycle), ϕ is the phase. After that, harmonic wave sampling with consequent extraction of the samples through the usage of another *for cycle* is performed.

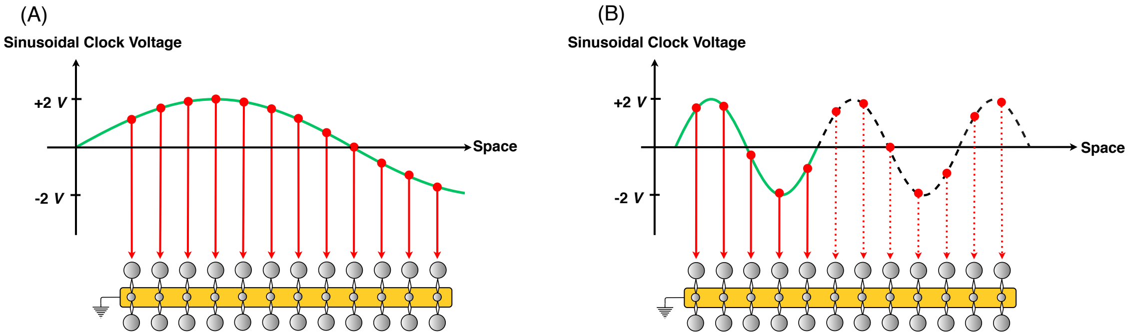

Figure 4.12. Comparison between the defined sinusoidal Clock and MQCA Wire.

"Fake" Sinusoidal Clock Phases generation: Part 2

Listing 4.12. Fake_sinusoidal_ck_phases_part2

```
% initialization of ck_table matrix with all -2 values
ck_table(1:sin_ck.time_instants,1:size(sample_values ,2)) = -2;
sin_ck.spatial_step = sin_ck.time_step * v;
num_mol_update = floor(sin_ck.spatial_step / mol_dist) ;

% generate the clock table values to associate to the electrodes
if sin_ck.spatial_step > mol_dist
   t = 1;
   q = 0;
   while (q <= stack_mol.num) && (t < sin_ck.time_instants )
      q = t * num_mol_update;

      if q > stack_mol.num
         break;
      else
         ck_table(t+1,1:q) = sample_values(t+1,1:q);
         t = t + 1;
      end
   end
   ck_table(t+1:end,:) = sample_values(t+1:end,:);
   ck_table = ck_table';
else
   num_spatial_step_update = 1;
   x = 0;
   while  x <=  mol_dist
      x = num_spatial_step_update * sin_ck.spatial_step;
      num_spatial_step_update = num_spatial_step_update + 1;
   end
   tt=1;
```

```
   ck_table(:, 1) = sample_values(:, 1);
   for cc = 2: size(sample_values ,2)-1

      ck_table((num_spatial_step_update-1)*tt:end, cc) = sample_values((
           num_spatial_step_update-1)*tt:end, cc);
      tt= tt+1;
    end
   ck_table = ck_table';
end

for jj=1:stack_mol.num
   stack_phase(jj).phase = stack_mol.stack(jj).phase;
   stack_phase(jj).ck = ck_table(jj,1:end);
end
```

The second code's portion has been designed with the aim to avoid unnatural starting point of QCA device simulation that can occur simply associating the extrapolated samples from the harmonic wave to the Bis-ferrocene molecules. Using this simple association, at Time 0 situations like in Figure 4.13 can occur, simulating a wrong starting clock configuration condition for the simulation and sometimes causing convergence errors of the algorithm. Of course, in Figure 4.13 only an example of the many possible starting configurations is depicted since it depends on how is generated the harmonic wave in the first step of *for cycle* explained before, but in any case, the concept remains unchanged.

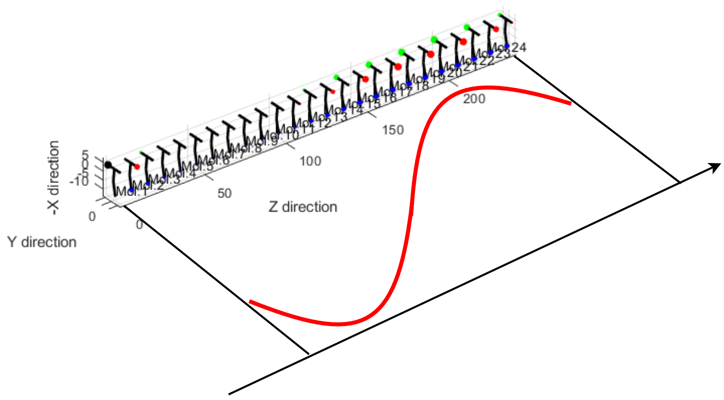

Figure 4.13. Possible initial configuration of Wire with Sinusoidal Clock.

Therefore, to simulate a more realistic Sinusoidal Clock application, in the initial configuration (at Time 0) the whole structure is forced in *Reset state* (-2 V is applied in all molecules) and the approaching of Sinusoidal Clock Field is performed, as in Figure 4.14.

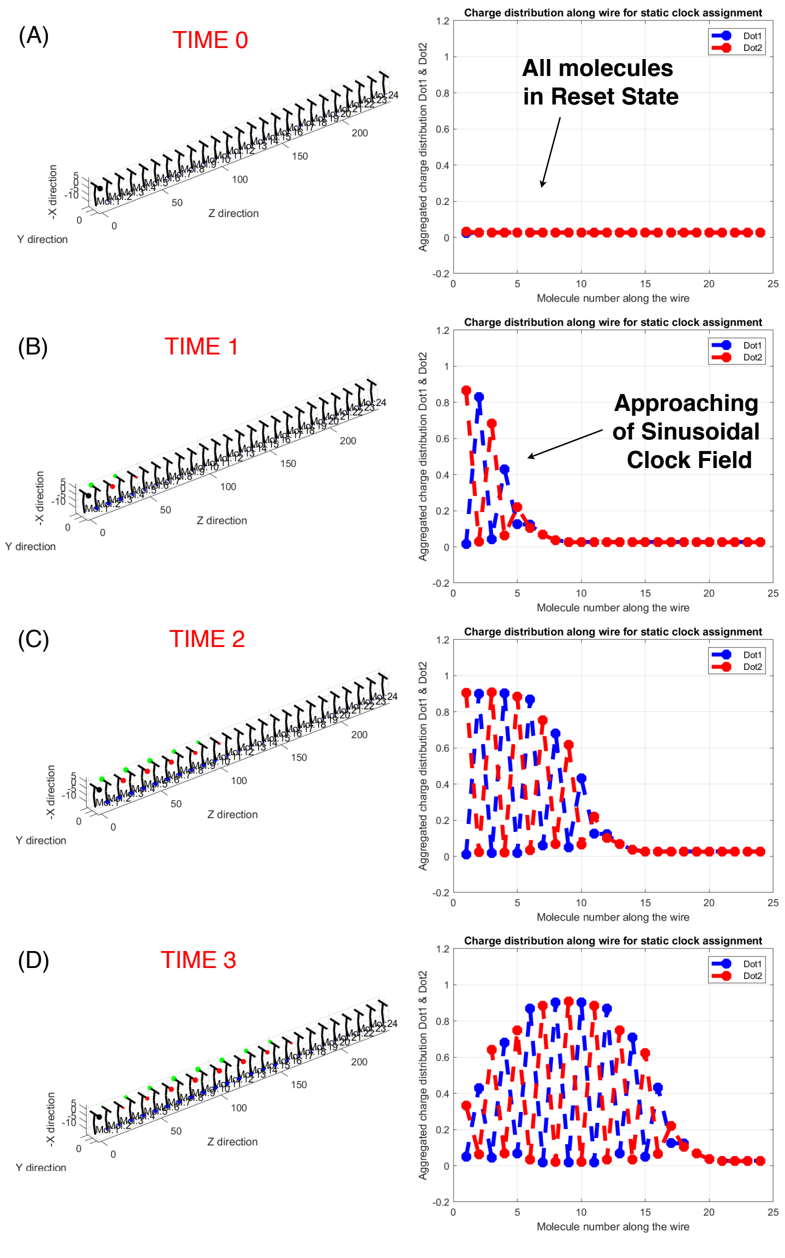

Figure 4.14. Correct initial configuration of Wire with Sinusoidal Clock, in the left the layout is present at different time instants, in the right the corresponding charge distribution along the Wire.

From the code point of view, an *if-else* construct is implemented, contemplating two possible cases that can occur during the `sin_ck.time_step` parameter definition:

1. the case in which the spatial step:

$$\Delta x = v \cdot \Delta t > intermolecular\ distance \tag{4.2}$$

where v is the propagation velocity of harmonic wave. In this case, the given `sin_ck.time_step` parameter creates a spatial step (according to the formula 4.2) greater the intermolecular distance, so through the `num_mol_update = floor(sin_ck.spatial_step/mol_dist)` instruction the number of molecules whose voltage value must be updated among two time instants is found (representation of this concept in Figure 4.15). After that, with the *while* construct usage a matrix called `ck_table`, containing the sinusoidal clock values at different time instants, is created.

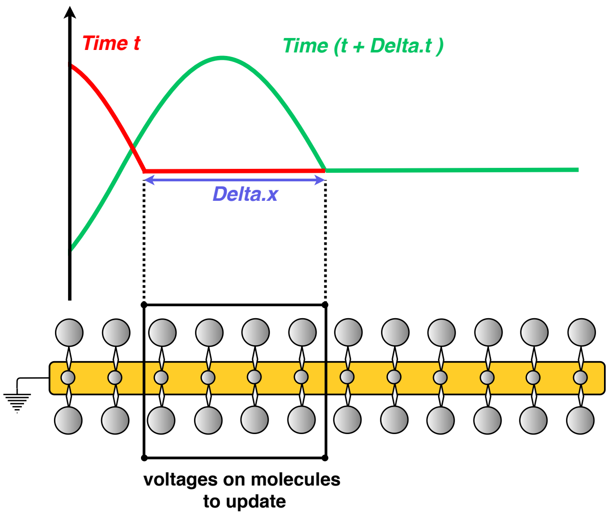

Figure 4.15. Schematic representation of voltage values updating with `num_mol_update = 4`.

2. the case in which the spatial step:

$$\Delta x < intermolecular\ distance \tag{4.3}$$

the defined temporal step generates a spatial step lower than intermolecular distance, consequently, again a *while* construct is utilized to count the number of temporal steps that the wave needs to go from molecule i to molecule $i+1$ (`num_spatial_step_update` variable in the code), see Figure 4.16 for schematic representation of this instance. Exploiting these temporal steps counter, it is possible to evaluate after how many time instants the voltage value of the next molecule needs to be updated with respect to the previous one.

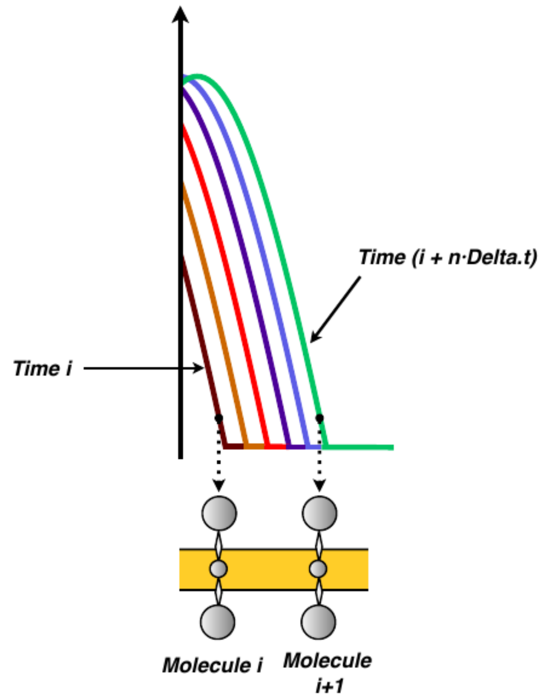

Figure 4.16. Schematic representation of voltage values updating with `num_spatial_step_update = 6` (in the picture $n = 6$).

Hereinafter, is reported the `ck_table` matrix generated in both instances: in the former matrix (Table 4.3), can be noticed that each time instant the voltage values of four molecules are updated because a simulation with `num_mol_update = 4` has been considered. In the latter matrix (Table 4.4) a simulation in which `num_spatial_step_update = 3` has been performed, where starting from the first column, representing the initial instant in which the entire structure is in Reset, it can be observed that at the third instant the voltage value on the next molecule is updated.

The `Qca_wire_sinusoidal_ck2` portion's code is mandatory to simulate in a correct way the initial approaching of Sinusoidal Clock wave when the structure is in Reset state. As soon as the voltage values on all molecules are updated, the procedure continues in a systematic way simply sampling the harmonic wave (Formula 4.1) at different time instants and relating them with the molecules, similar to what happens in the Three-phase clocking procedure.
After the generation process of Sinusoidal clock values, the `ck_table` it is copied in `stack_phase` struct variable through the final *for cycle* in order to have a similarity with the Three-phase generation process and pass the variable to the algorithm with a name that can correctly interpret.

	Time instants								
name	**0**	**1**	**2**	**3**	**4**	**5**	**6**	**7**	**8**
Mol_1	-2	-1.752	-1.071	-0.125	0.851	1.618	1.984	1.859	1.274
Mol_2	-2	-1.859	-1.274	-0.374	0.618	1.457	1.937	1.937	1.457
Mol_3	-2	-1.937	-1.457	-0.618	0.374	1.274	1.859	1.984	1.618
Mol_4	-2	-1.984	-1.618	-0.851	0.125	1.071	1.752	2	1.752
Mol_5	-2	-2	-1.752	-1.071	-0.125	0.851	1.618	1.984	1.859
Mol_6	-2	-2	-1.859	-1.274	-0.374	0.618	1.457	1.937	1.937
Mol_7	-2	-2	-1.937	-1.457	-0.618	0.374	1.274	1.859	1.984
Mol_8	-2	-2	-1.984	-1.618	-0.851	0.125	1.071	1.752	2
Mol_9	-2	-2	-2	-1.752	-1.071	-0.125	0.851	1.618	1.984
Mol_10	-2	-2	-2	-1.859	-1.274	-0.374	0.618	1.457	1.937
Mol_11	-2	-2	-2	-1.937	-1.457	-0.618	0.374	1.274	1.859
Mol_12	-2	-2	-2	-1.984	-1.618	-0.851	0.125	1.071	1.752
Mol_13	-2	-2	-2	-2	-1.752	-1.071	-0.125	0.851	1.618
Mol_14	-2	-2	-2	-2	-1.859	-1.274	-0.374	0.6189	1.457
Mol_15	-2	-2	-2	-2	-1.937	-1.457	-0.618	0.374	1.274
Mol_16	-2	-2	-2	-2	-1.984	-1.618	-0.851	0.125	1.071
Mol_17	-2	-2	-2	-2	-2	-1.752	-1.071	-0.125	0.851
Mol_18	-2	-2	-2	-2	-2	-1.859	-1.274	-0.374	0.618
Mol_19	-2	-2	-2	-2	-2	-1.937	-1.457	-0.618	0.374
Mol_20	-2	-2	-2	-2	-2	-1.984	-1.618	-0.851	0.125
Mol_21	-2	-2	-2	-2	-2	-2	-1.752	-1.071	-0.125
Mol_22	-2	-2	-2	-2	-2	-2	-1.859	-1.274	-0.374
Mol_23	-2	-2	-2	-2	-2	-2	-1.937	-1.457	-0.618
Mol_24	-2	-2	-2	-2	-2	-2	-1.984	-1.618	-0.851

Table 4.3. Generated `ck_table` matrix when $\Delta x > intermolecular\ distance$ and `num_mol_update = 4` considering a MQCA Wire formed by arrangement of 24 molecules.

	Time instants								
name	**0**	**1**	**2**	**3**	**4**	**5**	**6**	**7**	**8**
Mol_1	-2	-1.996	-1.984	-1.964	-1.937	-1.902	-1.859	-1.809	-1.752
Mol_2	-2	-2	-1.999	-1.996	-1.984	-1.9645	-1.937	-1.902	-1.859
Mol_3	-2	-2	-2	-2	-2	-1.996	-1.984	-1.964	-1.937
Mol_4	-2	-2	-2	-2	-2	-2	-2	-2	-1.984
Mol_5	-2	-2	-2	-2	-2	-2	-2	-2	-2
Mol_6	-2	-2	-2	-2	-2	-2	-2	-2	-2
Mol_7	-2	-2	-2	-2	-2	-2	-2	-2	-2
Mol_8	-2	-2	-2	-2	-2	-2	-2	-2	-2
Mol_9	-2	-2	-2	-2	-2	-2	-2	-2	-2
Mol_10	-2	-2	-2	-2	-2	-2	-2	-2	-2
Mol_11	-2	-2	-2	-2	-2	-2	-2	-2	-2
Mol_12	-2	-2	-2	-2	-2	-2	-2	-2	-2
Mol_13	-2	-2	-2	-2	-2	-2	-2	-2	-2
Mol_14	-2	-2	-2	-2	-2	-2	-2	-2	-2
Mol_15	-2	-2	-2	-2	-2	-2	-2	-2	-2
Mol_16	-2	-2	-2	-2	-2	-2	-2	-2	-2
Mol_17	-2	-2	-2	-2	-2	-2	-2	-2	-2
Mol_18	-2	-2	-2	-2	-2	-2	-2	-2	-2
Mol_19	-2	-2	-2	-2	-2	-2	-2	-2	-2
Mol_20	-2	-2	-2	-2	-2	-2	-2	-2	-2
Mol_21	-2	-2	-2	-2	-2	-2	-2	-2	-2
Mol_22	-2	-2	-2	-2	-2	-2	-2	-2	-2
Mol_23	-2	-2	-2	-2	-2	-2	-2	-2	-2
Mol_24	-2	-2	-2	-2	-2	-2	-2	-2	-2

Table 4.4. Generated `ck_table` matrix when $\Delta x < intermolecular\ distance$ and `num_spatial_step_update = 3` considering a MQCA Wire formed by arrangement of 24 molecules.

The final step to be ready for simulation consists of association of generated "Fake" Sinusoidal Clock Phases with clock zones defined in `QCA_circuit.structure` matrix. This operation is accomplished utilizing the struct variable `stack_mol.stack` in `sin_ck_phase _association` box, where through a *for cycle* the reading of the molecules' identifiers and the corresponding assigned clock zones is performed.

The evaluation of molecules' identifiers and clock zones is fundamental when structure different from Wire are simulated, in fact considering for example the Majority Voter there is a need to assign the same "Fake" Sinusoidal Clock Phases to all three input branches, in order to simulate the propagation of three identical sine waves in the respective branches.

Listing 4.13. `sin_ck_phase_association`

```
heading={'name','phase'};
tab(1,1:2)=heading;

for jj=1:size(stack_phase(1).ck,2)
    tab(1,jj+2)=num2cell(jj-1);
end

matrix_phase = tab;

% "Fake" Clock Phases - Clock zones association
for jj=1:stack_mol.num
    tab(jj+1,1:2)= [stack_mol.stack(jj).identifier cellstr(stack_mol.stack(jj).phase)];

    for kk=1:size(stack_phase(1).ck,2)
        tab(jj+1,kk+2) = num2cell(stack_phase(jj).ck(1,kk));
    end

    row_tab=cellstr(stack_mol.stack(jj).phase);
    index_row = str2double (row_tab);
    matrix_phase(jj+1,3:end) = tab(index_row +1,3:end);
    matrix_phase(:,1:2) = tab(:,1:2);
end

%         filename = sprintf('Database/Fake_Phases_tabella.xlsx');
%         xlswrite(filename,matrix_phase,1,'A1');

matrix_phase(:,2) = [ ];
matrix_phase(1,:) = [ ];

filename = 'Database/Fake_Phases.mat';
save(filename,'matrix_phase');
```

Chapter 5

Sinusoidal Clocking Simulation Analysis and Results

Results concerning Sinusoidal Clocking simulation in the different MQCA functional blocks are discussed in this chapter. In all simulated structures the distance d between two molecules, either horizontally or vertically aligned, is considered to be $d = 1\ nm$ because it is demonstrated in [37],[14] that in ideal conditions the Bis-ferrocene molecules bound at this distance through the thiol end-group element in the gold surface. Therefore, from the implementation point of view, using this intermolecular distance a more realistic configuration is simulated.

5.1 Simulation Results: Wire Structure

Obviously, the first simulated MQCA block is the most elementary one, the *MQCA Wire*. A full characterization has been performed to first establish the feasibility and correct propagation of information with this new clocking mechanism. A first attempt has been done on a Wire composed of 24 molecules, applying Sinusoidal Clock with wavelength $\lambda = 24\ nm$ to verify its functional correctness (Figure 5.1).

In order better explain the meaning of Sinusoidal Clock with wavelength $\lambda = 24\ nm$, it is useful to remember that the wavelength is the distance between two maxima or two minima of a periodic function (in this case a sinusoid). Therefore, according to this definition, taking a given time instant, the maximum number of activated molecules is the half of the applied wavelength, which means that in this case they are more or less twelve, as shown in Figure 5.2.

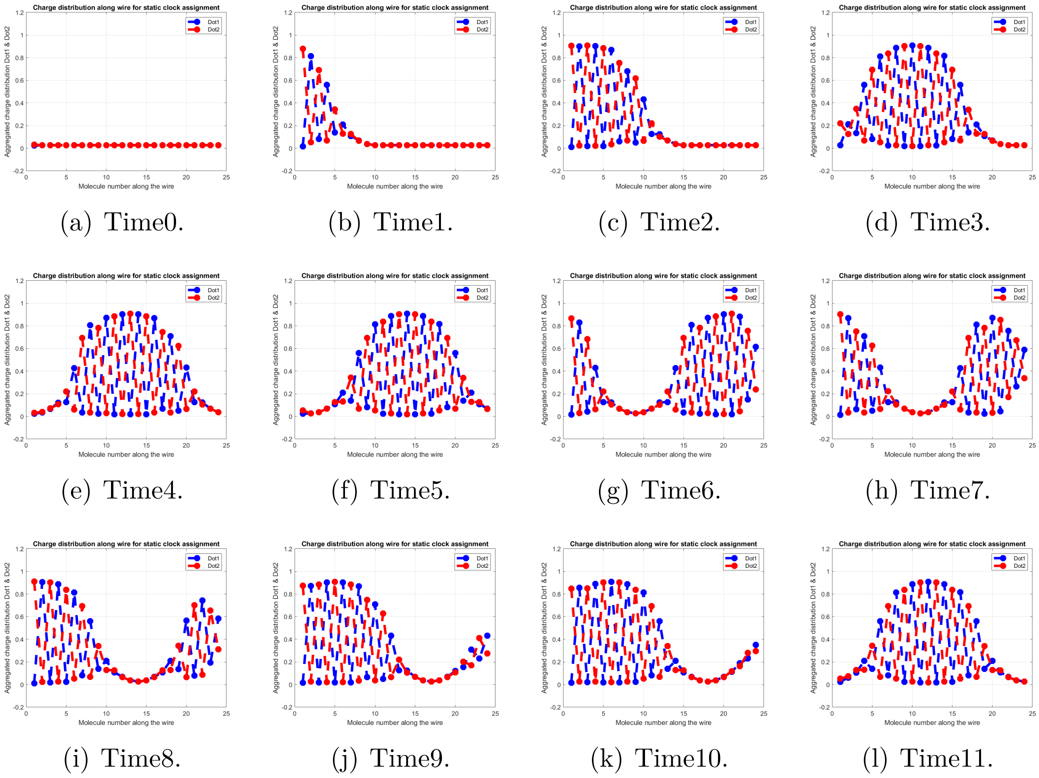

(a) Time0. (b) Time1. (c) Time2. (d) Time3.

(e) Time4. (f) Time5. (g) Time6. (h) Time7.

(i) Time8. (j) Time9. (k) Time10. (l) Time11.

Figure 5.1. Wire simulation formed by 24 molecules and Sinusoidal Clock application with a wavelength $\lambda = 24\ nm$.

A new parameter is sketched in Figure 5.2 and it is called *Transition Window*, representing the range in which the molecules have an undefined and unstable state, due to the fact that the applied clock phase on them is neither too high nor too low. This transition window, making a comparison with Four-Phase clock explained in Chapter 1, can be seen as a condition in which the cells are in Switch or Release state.

After verifying the Sinusoidal Clock applicability, to analyse and discover the limit working conditions, which means the minimum and maximum λ so that the information flow is preserved and correct, many simulations have been performed varying the number of molecules constituting the wire and the wavelength of harmonic clock.

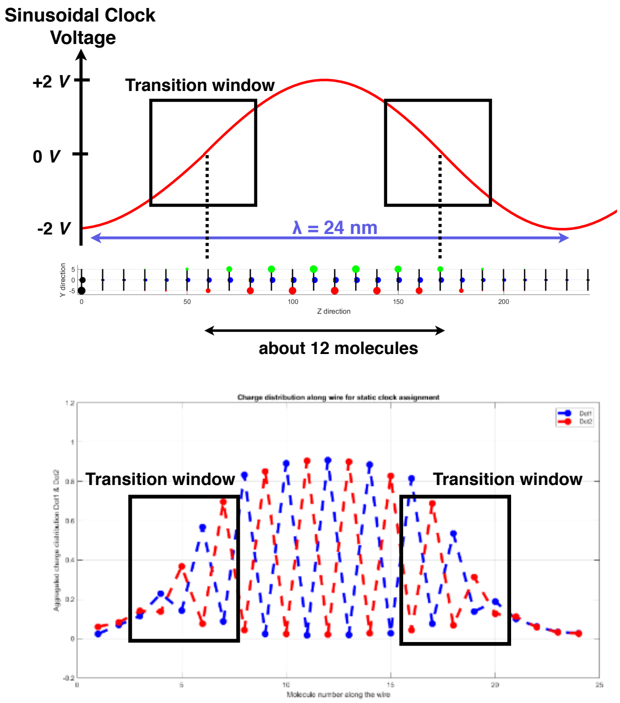

Figure 5.2. Maximum number of activated molecules in a Wire of 24 molecules with Sinusoidal Clock application at wavelength $\lambda = 24\ nm$ and at fixed time instant: Above a schematic representation, below the corresponding charge distribution.

5.1.1 Minimum Lambda of Sinusoidal Clock

This part of the analysis is conceived to understand the minimum wavelength and the corresponding number of activated QCA cells that ensure proper data transmission. To define the cluster of activated cells the name *frame* is employed.

Wire formed by 50 molecules with Sinusoidal Clock at $\lambda = 10\ nm$

Imposing the $\lambda = 10\ nm$ on Wire formed by 50 Bis-Ferrocene molecules the obtained result is shown in Figure 5.3. Analysing the charge distribution a weak polarization of cells is present, deducted from the fact that the thickness of frame charge distribution is not between 0 and 1, but narrower ($\approx 0.3 \div 0.6$). Therefore, a frame composed of two QCA cells is not enough to hold strong and reliable information.

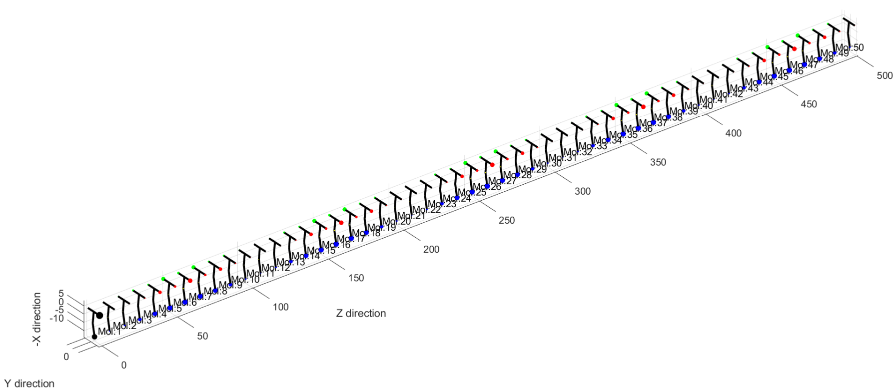

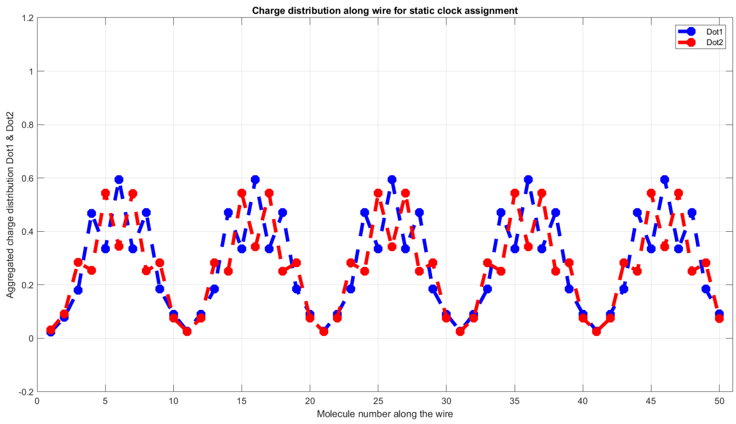

Figure 5.3. Sinusoidal Clocked behaviour of Wire with 50 molecules at wavelength $\lambda = 10\ nm$ and at fixed time instant: Above the structure layout, below the corresponding charge distribution.

Wire formed by 50 molecules with Sinusoidal Clock at $\lambda = 12\ nm$

The $\lambda = 12\ nm$ on Wire formed by 50 Bis-Ferrocene molecules has been simulated to analyse the Sinusoidal Clocked behaviour when about three QCA cells are activated (Figure 5.4). Now frames with full thickness are transmitted, denoting complete polarization of QCA cells because of the electrostatic feedback effect between them is strong enough, demonstrating the possibility to send frames in a MQCA Wire using this kind of clock at minimum $\lambda = 12\ nm$.

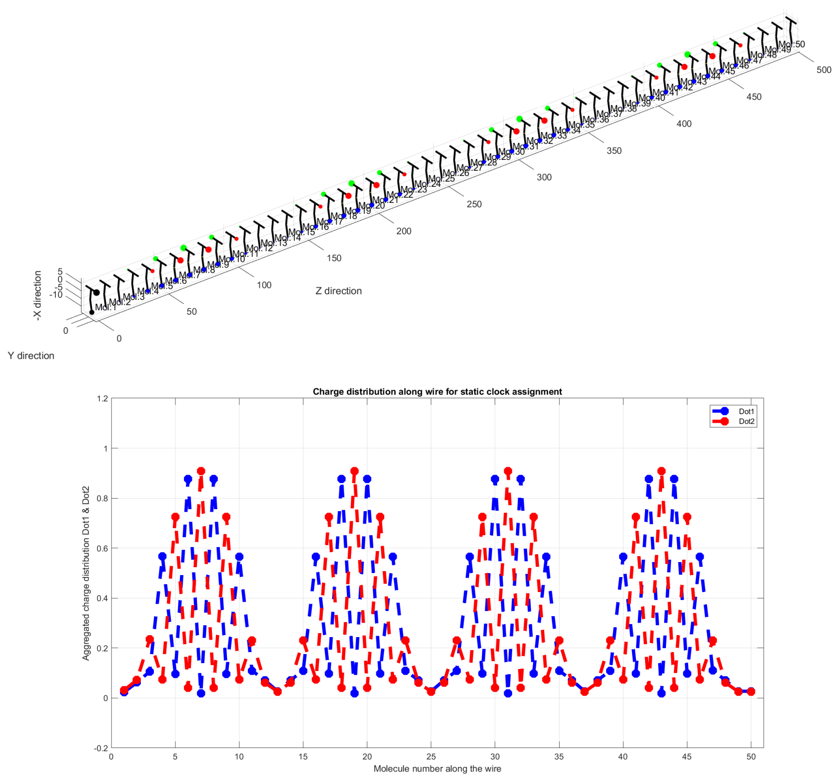

Figure 5.4. Sinusoidal Clocked behaviour of Wire with 50 molecules at wavelength $\lambda = 12\ nm$ and at fixed time instant: Above the structure layout, below the corresponding charge distribution.

Wire formed by 100 molecules with Sinusoidal Clock at $\lambda = 12\ nm$

Another test with the same operating conditions has been made but with a Wire formed by an arrangement of 100 molecules (Figure 5.5), confirming the concepts said previously.

5.1.2 Maximum Lambda of Sinusoidal Clock

Increasing the wavelength the circuit moves towards more stationary conditions, up to the limit case in which the transition window is so great that, at a fixed time instant, to all molecules the same voltage value (ranging from $-2\ V$ to $2\ V$) is applied.

Hereinafter, in Figures 5.6, 5.7, 5.8, 5.9, 5.10, 5.11 are plotted the charge distributions of Wire structures formed with different number of molecules and at different Sinusoidal Clock wavelengths, concerning the most critical instant time

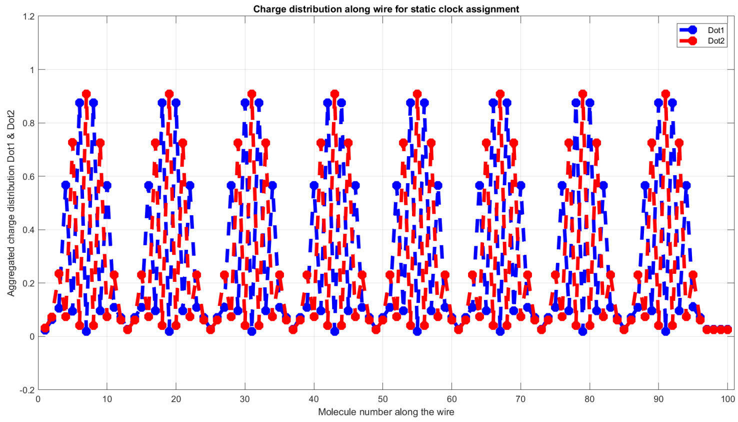

Figure 5.5. Sinusoidal Clocked behaviour of Wire with 100 molecules at wavelength $\lambda = 12\ nm$ and at fixed time instant: charge distribution.

for the transmission flow in which on the molecules is present the maximum of harmonic wave, resulting in a condition wherein all molecules the clock phase is more or less $+2\ V$.

Wire formed by 50 molecules with Sinusoidal Clock at $\lambda = 1\ \mu m$

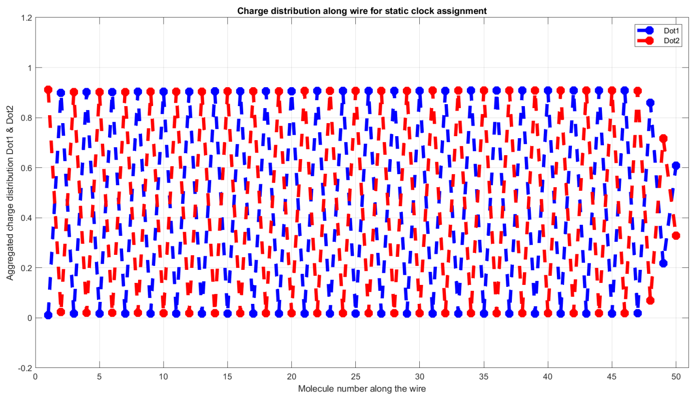

Figure 5.6. Sinusoidal Clocked behaviour of Wire with 50 molecules at wavelength $\lambda = 1\ \mu m$ and at fixed time instant (charge distribution).

Wire formed by 50 molecules with Sinusoidal Clock at $\lambda = 100\ \mu m$

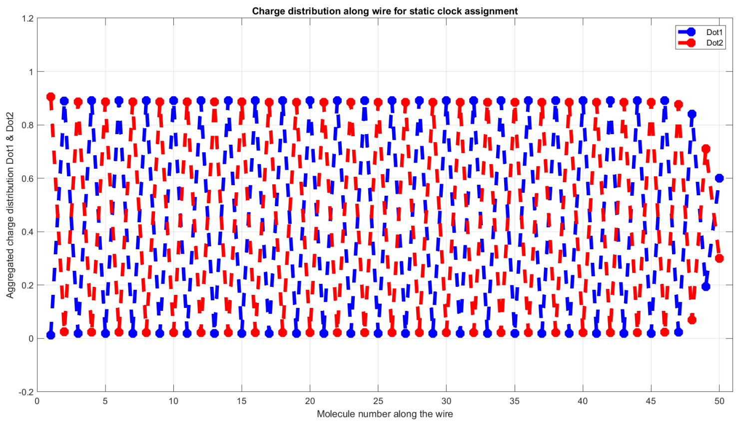

Figure 5.7. Sinusoidal Clocked behaviour of Wire with 50 molecules at wavelength $\lambda = 100\ \mu m$ and at fixed time instant (charge distribution).

Wire formed by 100 molecules with Sinusoidal Clock at $\lambda = 1\ \mu m$

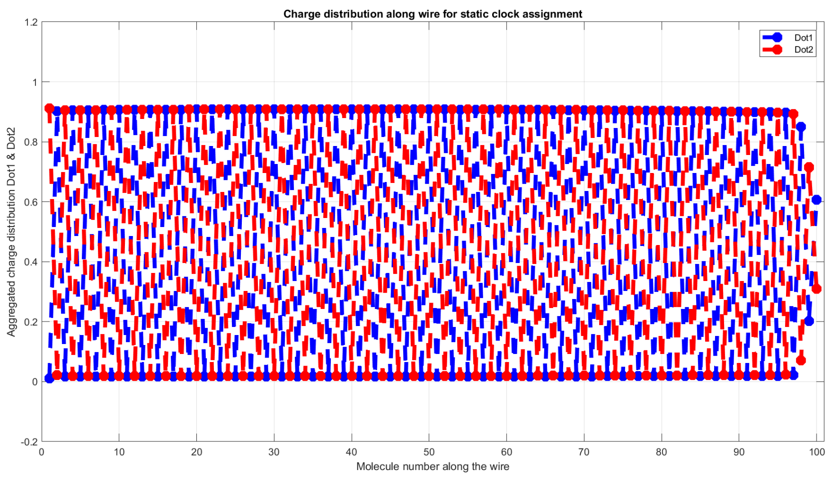

Figure 5.8. Sinusoidal Clocked behaviour of Wire with 100 molecules at wavelength $\lambda = 1\ \mu m$ and at fixed time instant (charge distribution).

Wire formed by 100 molecules with Sinusoidal Clock at $\lambda = 100\ \mu m$

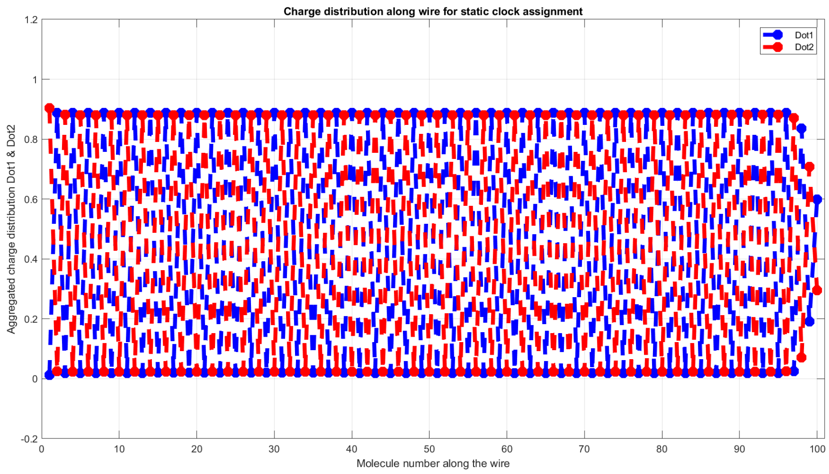

Figure 5.9. Sinusoidal Clocked behaviour of Wire with 100 molecules at wavelength $\lambda = 100\ \mu m$ and at fixed time instant (charge distribution).

Wire formed by 300 molecules with Sinusoidal Clock at $\lambda = 1\ \mu m$

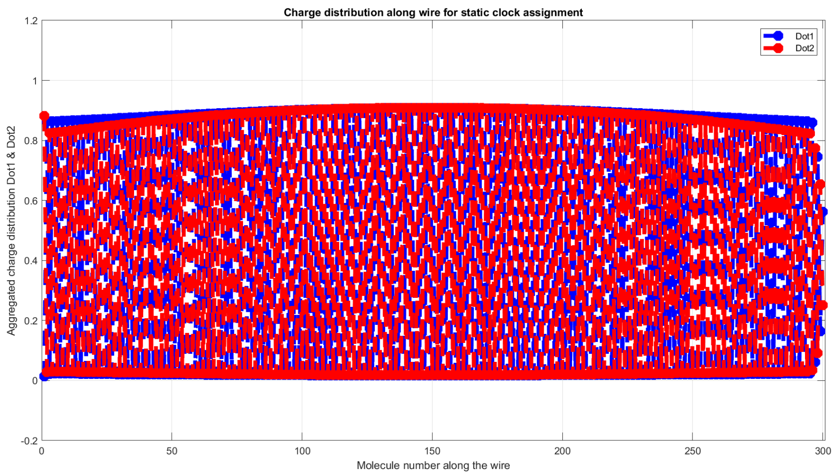

Figure 5.10. Sinusoidal Clocked behaviour of Wire with 300 molecules at wavelength $\lambda = 1\ \mu m$ and at fixed time instant (charge distribution).

Wire formed by 300 molecules with Sinusoidal Clock at $\lambda = 100\ \mu m$

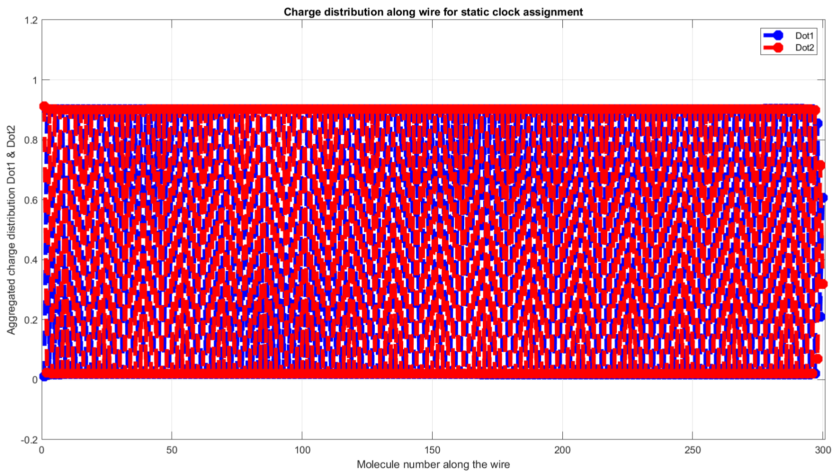

Figure 5.11. Sinusoidal Clocked behaviour of Wire with 300 molecules at wavelength $\lambda = 100\ \mu m$ and at fixed time instant (charge distribution).

According to the studies concerning the quantum phenomena involved in QCA cell interactions, there is a maximum number of cells that can be activated at the same time without having meta-stability problem, from which it derives the need to use a clock system. However, in all analysed simulations no propagation corruption is present, due to the fact that the transition window is so large to have as a final result the slow turning on of the device.
This effect provides the possibility, at least in ideal conditions, to preserve the integrity of information with arbitrarily large wavelengths.
Therefore, becomes fundamental to introduce noise sources in the QCA circuits and perform noise analysis to discover the limit on maximum Sinusoidal Clock wavelength and, at the same time, to obtain more realistic results.

To continue the MQCA components characterization from this point on a method of analysis is adopted, consisting of applying a Sinusoidal Clock with:

1. $\boldsymbol{\lambda <}$ ***structure dimensions***: $\lambda_{min} = 12\ nm$ is adopted;
2. $\boldsymbol{\lambda \approx}$ ***structure dimensions***: $\lambda = 50\ nm$ are adopted;
3. $\boldsymbol{\lambda >>}$ ***structure dimensions***: $\lambda = 1\ \mu m$ is adopted;

Moreover, the *wavefront* concept (Figure 5.12), defined as the surfaces on which the phase ϕ of the wave is constant, can be useful to better understand the direction of propagation of Sinusoidal Field and consequently of the information one.

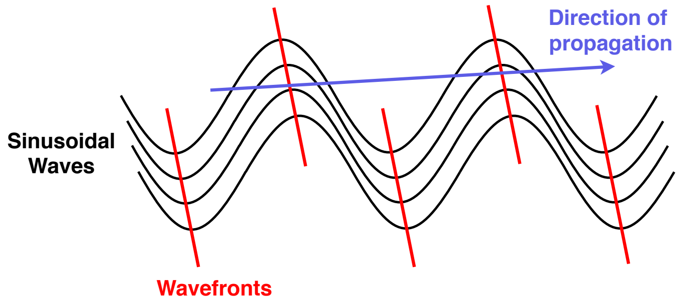

Figure 5.12. Wavefronts schematic representation.

5.2 Simulation Results: Angle Structure

The *Angle* structure is created placing an orthogonal segment of wire at the end of another one, giving the possibility to route the information flow in two-dimensional direction. The layout designed inside SCERPA is depicted in Figure 5.13 (it is not the standard angle shape because one more cell, called *stub* is inserted to improve its Three-phase clocking functioning, according to the study in [2]).

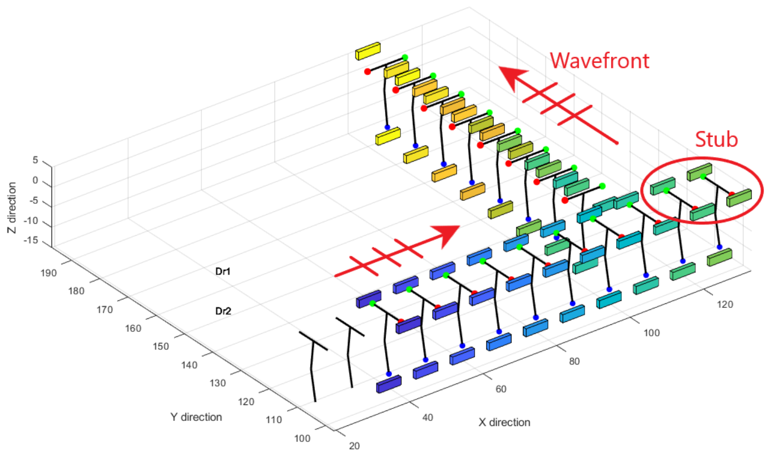

Figure 5.13. Schematic layout of Angle structure and direction propagation of wavefronts.

Angle structure with Sinusoidal Clock at $\lambda = 12$ nm

The aforementioned structure has been initially tested with the minimum wavelength $\lambda_{min} = 12$ nm deriving from the Wire's analysis, in order to establish its behaviour when a frame of minimal dimension runs in this structure. Observing the results in Figures 5.14, six time instants are plotted, it is important to point out that the simulated instants of time are much more, but only a few of them are reported to explain concisely the concepts and the various cases found (this is also true for the other structures).

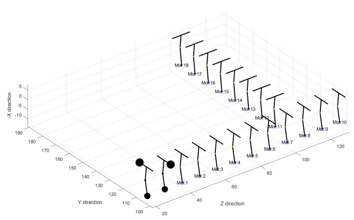

(a) Time0.

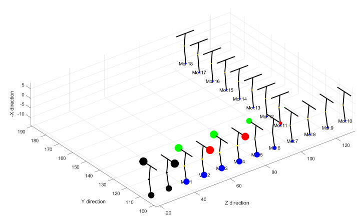

(b) Time1.

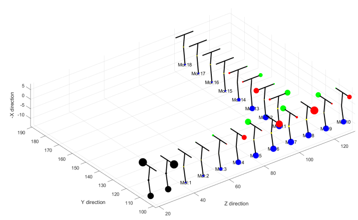

(c) Time2.

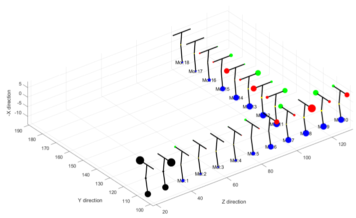

(d) Time3.

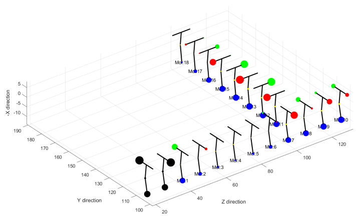

(e) Time4.

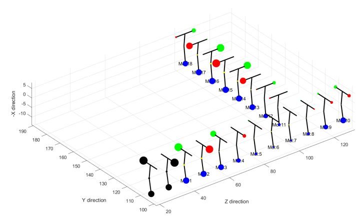

(f) Time4.

Figure 5.14. Sinusoidal Clocked behaviour of Angle at wavelength $\lambda = 12$ nm with logic input state "0".

In particular, considering the top view of Figure 5.14 at Time 3 and Time 4, propagation corruption occurs due to the *corner electrostatic interaction* (highlighted in Figure 5.15.A) that generates a repulsion strong enough to lead a state inversion of the cell above another cell defined as *intersection cell* (Figure 5.15.B). This derives from almost completely unpolarization of horizontal wire's part near the driver and by the presence of total polarization in its final part.

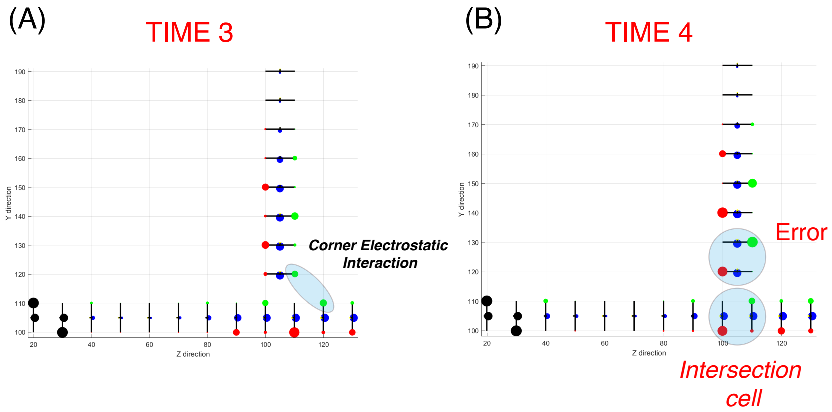

Figure 5.15. Top view of Sinusoidal Clocked behaviour of Angle at wavelength $\lambda = 12\ nm$, with logic input state "0": (A) Before information corruption, (B) After information corruption.

Angle structure with Sinusoidal Clock at $\lambda = 50\ nm$

The Angle structure performance with Sinusoidal Field at $\lambda = 50\ nm$ is illustrated in Figure 5.16.

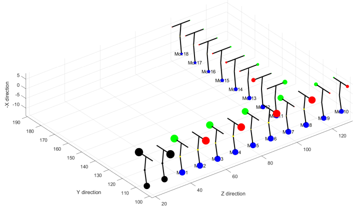

(a) Time0.

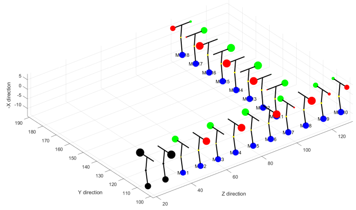

(b) Time1.

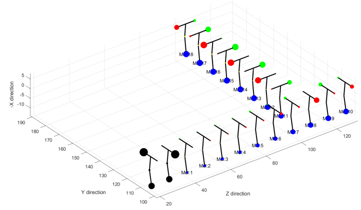

(c) Time2.

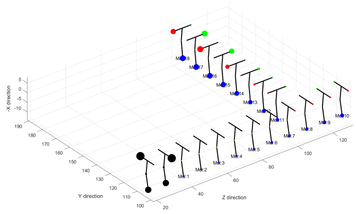

(d) Time3.

Figure 5.16. Sinusoidal Clocked behaviour of Angle at wavelength $\lambda = 50\ nm$ with logic input state "0".

In this condition, the first segment of wire remains well polarized during the data transfer in the second vertical segment and the transition window is not so large with respect to the circuit dimension, ensuring information integrity.

Angle structure with Sinusoidal Clock at $\lambda = 1\ \mu m$

The Angle structure performance with Sinusoidal Field at $\lambda = 1\ \mu m$ is illustrated in Figure 5.17.

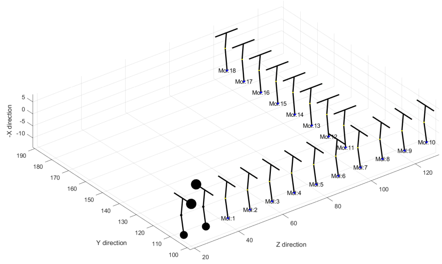

(a) Time0.

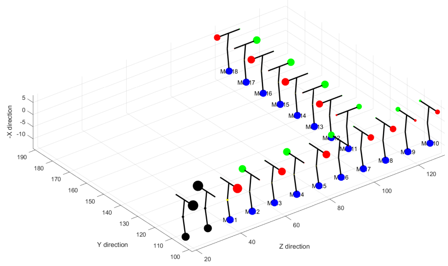

(b) Time1.

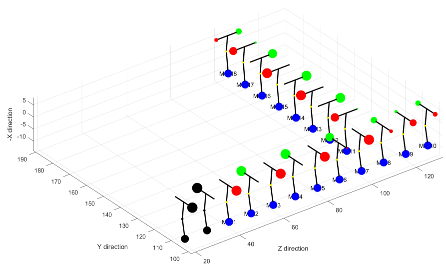

(c) Time2.

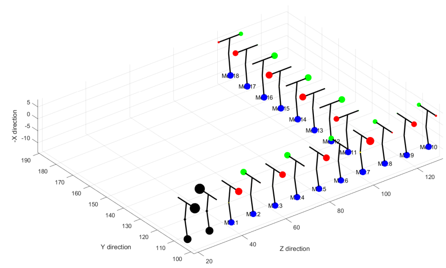

(d) Time3.

Figure 5.17. Sinusoidal Clocked behaviour of Angle at wavelength $\lambda = 1\ \mu m$ with logic input state “1”.

Again considering the top view of Time 1, inside the transition window, an error occurs deriving from the voltage values imposed on the molecules, that are not strong enough to full polarize the cells of the horizontal wire. This condition leads to the wrong cell configuration highlighted in Figure 5.18.A. As soon as the voltage values on horizontal wire increase, the MQCA cells polarize completely imposing their polarization also in the vertical wire (Time 2 reported in Figure 5.18.B).

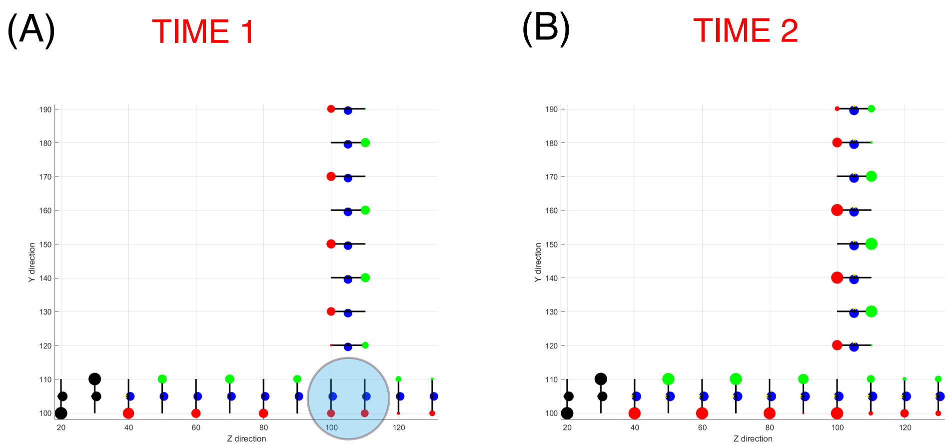

Figure 5.18. Top view of Sinusoidal Clocked behaviour of Angle at wavelength $\lambda = 1$ μm, with logic input state "1": (A) inside transition window, (B) outside transition window.

To overcome these limitations an additional stub has been inserted to strengthen properly the polarization of intersection cell during the transition phase, as shown in Figure 5.19, guaranteeing correct behaviour of Angle device for both input configurations and for each λ examined before. In particular, in Figure 5.19 are shown at the same time instants of previous cases in which the error propagation occurs.

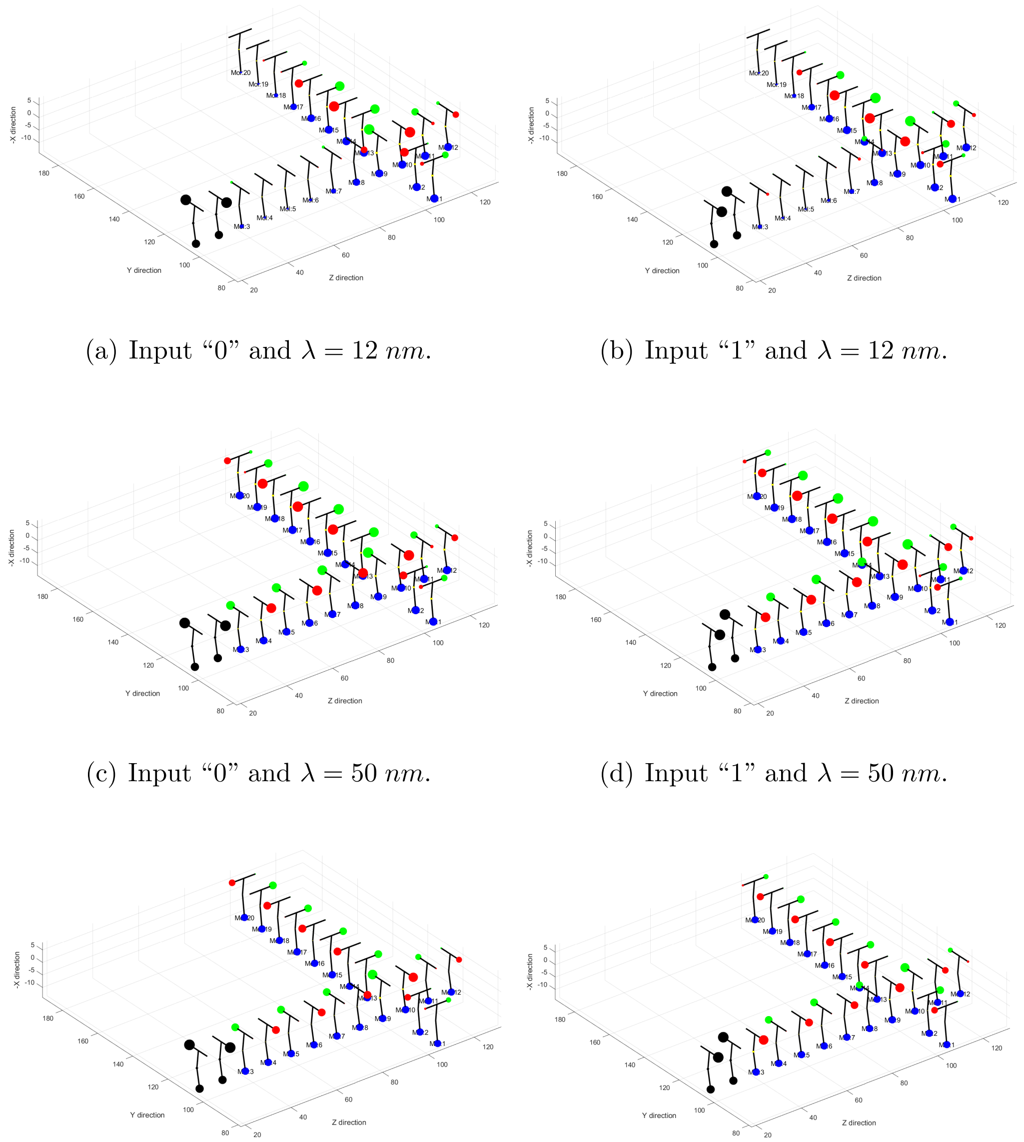

(a) Input "0" and $\lambda = 12\ nm$.

(b) Input "1" and $\lambda = 12\ nm$.

(c) Input "0" and $\lambda = 50\ nm$.

(d) Input "1" and $\lambda = 50\ nm$.

(e) Input "0" and $\lambda = 1\ \mu m$.

(f) Input "1" and $\lambda = 1\ \mu m$.

Figure 5.19. Sinusoidal Clocked behaviour of Angle at wavelengths $\lambda = 12\ nm$, $\lambda = 50\ nm$, $\lambda = 1\ \mu m$, at fixed time instants and with logic input state "0" (left column) and "1" (right column).

5.3 Simulation Results: T-shape Structure

The *T-shape* structure is created placing an orthogonal segment of wire in the centre of another one, giving the possibility to split the information flow in two specular directions. The layout designed inside SCERPA is depicted in Figure 5.20.

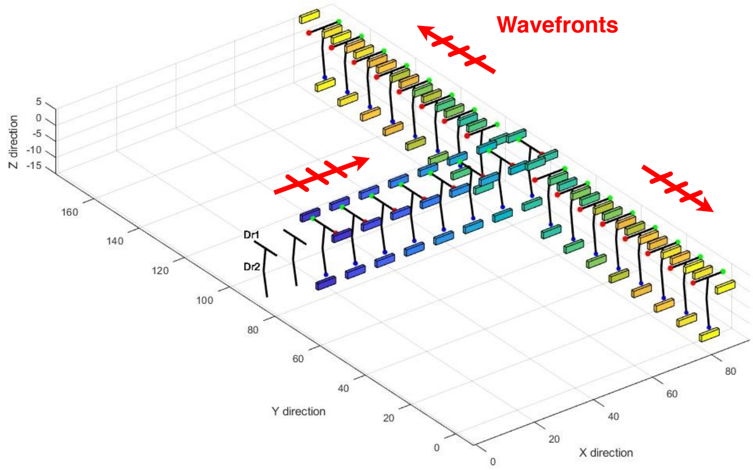

Figure 5.20. Schematic layout of T-shape structure and direction propagation of wavefronts.

T-shape structure with Sinusoidal Clock at $\lambda = 12\ nm$

Following the same procedure performed for Angle structure, the aforementioned structure has been initially tested with the minimum wavelength $\lambda_{min} = 12\ nm$, obtaining the right behaviour (also with driver configuration set to “1”) plotted in Figure 5.21.

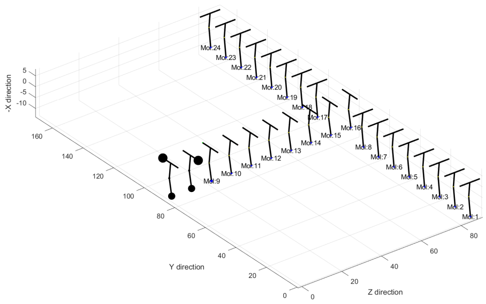

(a) Time0.

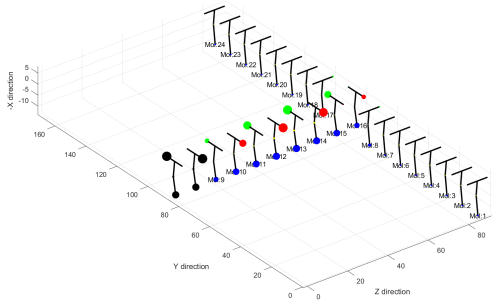

(b) Time1.

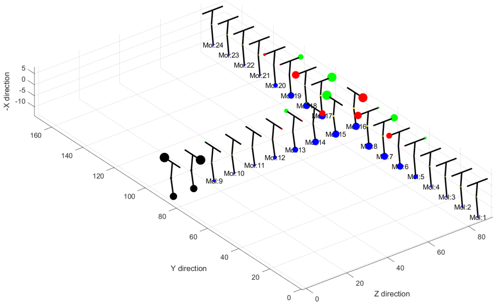

(c) Time2.

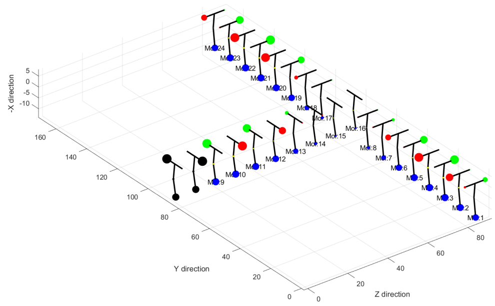

(d) Time3.

Figure 5.21. Sinusoidal Clocked behaviour of T-shape structure at wavelength $\lambda = 12\ nm$ with logic input state “0”.

T-shape structure with Sinusoidal Clock at $\boldsymbol{\lambda = 50\ nm}$

The T-shape structure performance with Sinusoidal Field at $\lambda = 50\ nm$ is illustrated in Figure 5.22 manifesting good results (also with driver configuration set to “1”).

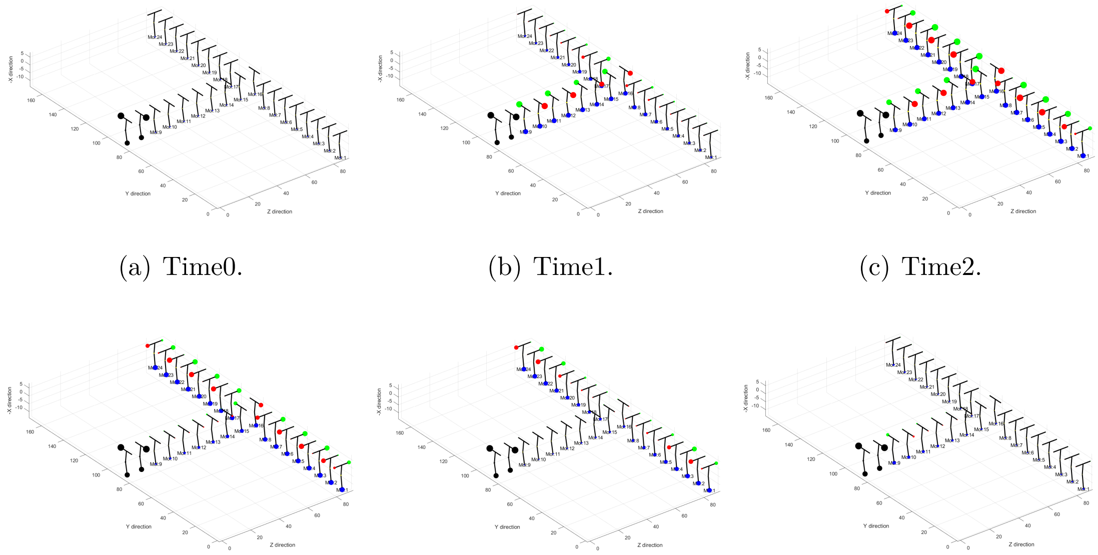

(a) Time0. (b) Time1. (c) Time2.

(d) Time3. (e) Time4. (f) Time5.

Figure 5.22. Sinusoidal Clocked behaviour of T-shape structure at wavelength $\lambda = 50\ nm$ with logic input state “0”.

T-shape structure with Sinusoidal Clock at $\lambda = 1\ \mu m$

The T-shape structure performance with Sinusoidal Field at $\lambda = 1\ um$ is illustrated in Figure 5.23, highlighting an information fault at Time 1 generated by the diagonal interaction between molecules during the transition window. As soon as the cells in the wire segment connected to Driver are full polarized, the circled cell polarizes in the right way (Time 3).

To overcome the problem, also in this QCA block a stub has been inserted to enforce the polarization of intersection cell avoiding the failure during the transition window. Figure 5.24 shows a comparison of the standard version with the enhanced one at the same time instant.

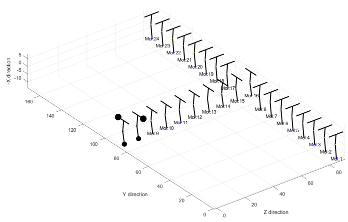

(a) Time0.

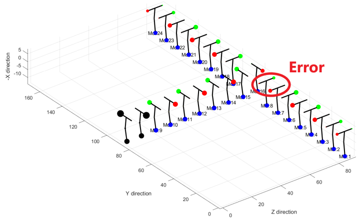

(b) Time1.

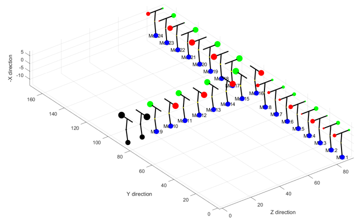

(c) Time2.

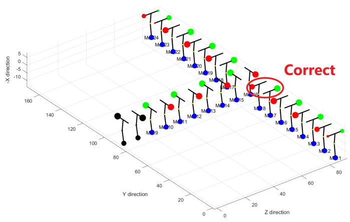

(d) Time3.

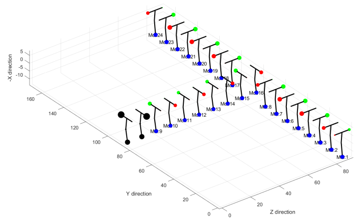

(e) Time4.

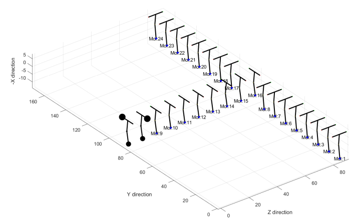

(f) Time5.

Figure 5.23. Sinusoidal Clocked behaviour of T-shape structure at wavelength $\lambda = 1\ \mu m$ with logic input state "0".

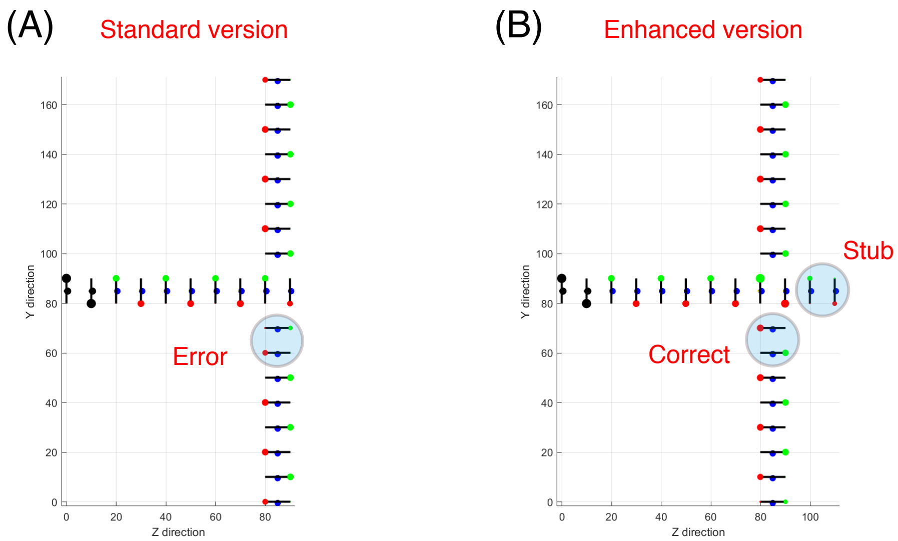

Figure 5.24. Comparison between the standard T-shape structure and the enhanced one at the same time instant (inside the transition window).

The enhanced version has been tested also for the previous cases demonstrating proper behaviour for both input states (Figure 5.25).

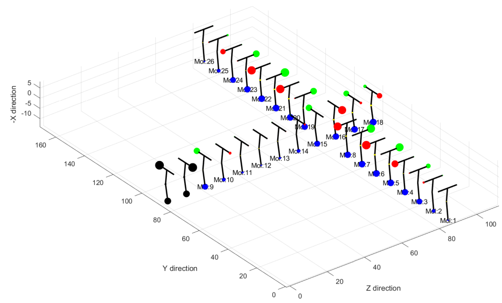

(a) Input "0" and $\lambda = 12\ nm$.

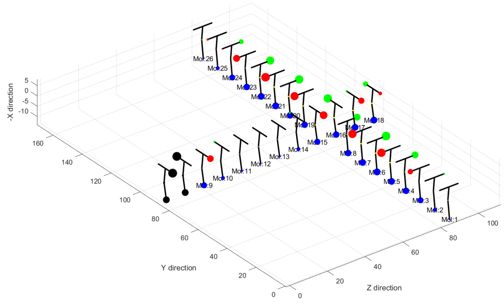

(b) Input "1" and $\lambda = 12\ nm$.

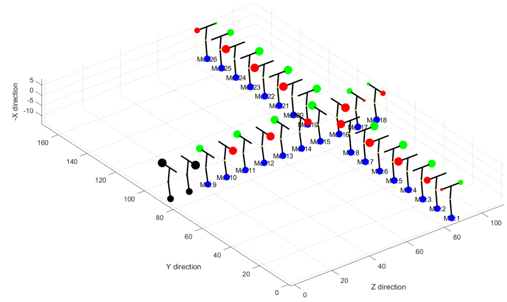

(c) Input "0" and $\lambda = 50\ nm$.

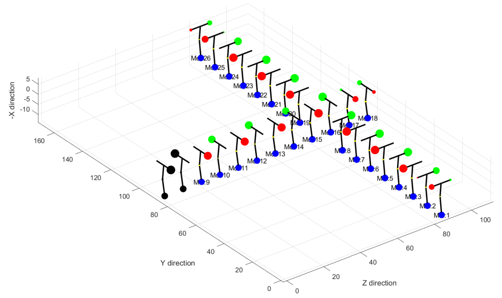

(d) Input "1" and $\lambda = 50\ nm$.

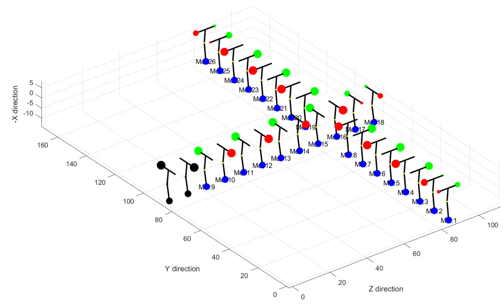

(e) Input "0" and $\lambda = 1\ \mu m$.

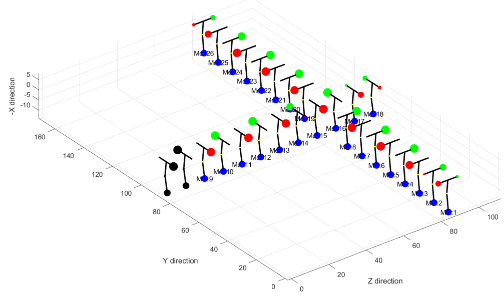

(f) Input "1" and $\lambda = 1\ \mu m$.

Figure 5.25. Sinusoidal Clocked behaviour of T-shape structure at wavelengths $\lambda = 12\ nm$, $\lambda = 50\ nm$, $\lambda = 1\ \mu m$, at fixed time instants and with logic input state "0" (left column) and "1" (right column).

5.4 Simulation Results: Majority Voter

The three-input *Majority Voter* is obtained by placing three wires that merge into a single intersection cell, whose logic state depends on the polarization of three segments according to majority rule. The layout designed inside SCERPA is depicted in Figure 5.26 and its functioning is based on the truth Table 5.1.

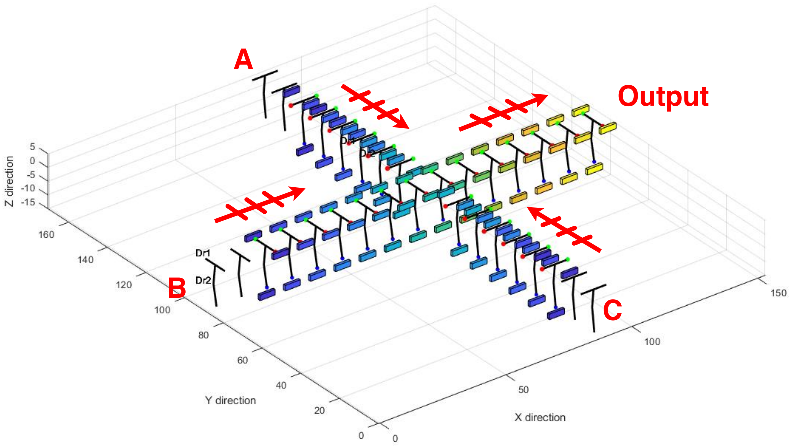

Figure 5.26. Schematic layout of Majority Voter and direction propagation of wavefronts.

Inputs			**Output**
A	**B**	**C**	
0	0	0	0
0	0	1	0
0	1	0	0
0	1	1	1
1	0	0	0
1	0	1	1
1	1	0	1
1	1	1	1

Table 5.1. Truth table of Majority Voter.

Majority Voter with Sinusoidal Clock at $\lambda = 12\ nm$

The Majority Voter performance with Sinusoidal Field at $\lambda = 12\ nm$ is illustrated in Figure 5.27 demonstrating good results, apart from the case where the input pattern is $A = 0$, $B = 1$, $C = 0$.
In particular, in Figures 5.27, 5.29, 5.30 are depicted the eight input configurations at the time instant in which a frame arrives into intersection cell, in order to show the occurrence of majority rule (the input configurations $A = 1$, $B = 1$, $C = 1$ and $A = 0$, $B = 0$, $C = 0$ are not plotted because their correct functioning is obvious since all three inputs are identical).

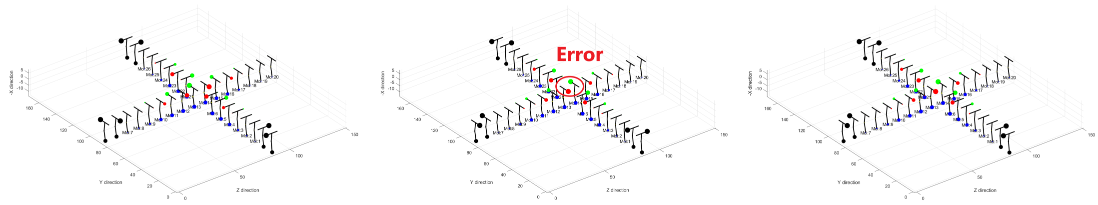

(a) $A = 0$, $B = 0$, $C = 1$. (b) $A = 0$, $B = 1$, $C = 0$. (c) $A = 0$, $B = 1$, $C = 1$.

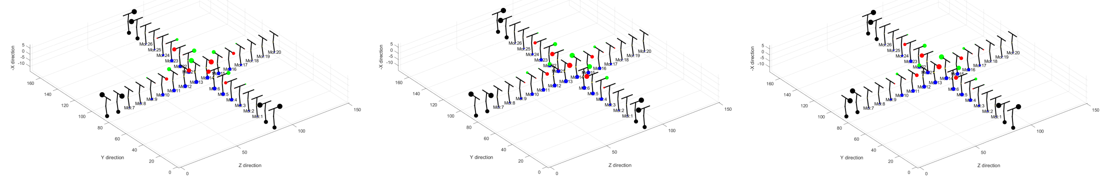

(d) $A = 1$, $B = 0$, $C = 0$. (e) $A = 1$, $B = 0$, $C = 1$. (f) $A = 1$, $B = 1$, $C = 0$.

Figure 5.27. Sinusoidal Clocked behaviour of Majority Voter at wavelength $\lambda = 12\ nm$, at fixed time instants and with the eight logic input states reported in Table 5.1.

Although the very small $\lambda = 12\ nm$ is able to activate more or less three MQCA cells, which correspond to the entire length of the majority voter's branch, an error occurs in Figure 5.27.b, corresponding to the case whose input pattern is $A = 0$, $B = 1$, $C = 0$ (in Figure 5.28.A the top view of the same time instant is reported). Considering the situation in Figure 5.28.B, only the central cell is completely polarized, while the two peripheral cells are slightly less polarized leading to a possible error state configuration of the intersection cell. This statement is verified since simply by slightly widening the wavelength (for example $\lambda = 20\ nm$) the majority voter always works since it makes possible to fully polarize the three-input branches of the device (see Section 5.6).

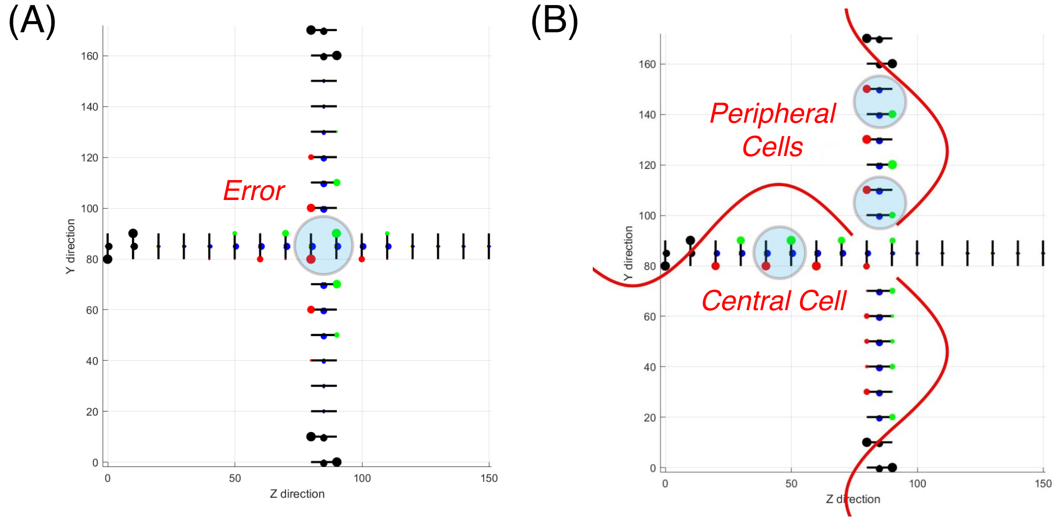

Figure 5.28. Polarization error of intersection cell with input pattern $A = 0$, $B = 1$, $C = 0$ at $\lambda = 12\ nm$: (A) Top view of Figure 5.27.b, (B) Central and peripheral cells definition.

Majority Voter with Sinusoidal Clock at $\lambda = 50\ nm$

The Majority Voter performance with Sinusoidal Field at $\lambda = 50\ nm$ is illustrated in Figure 5.29 demonstrating good results in all cases.

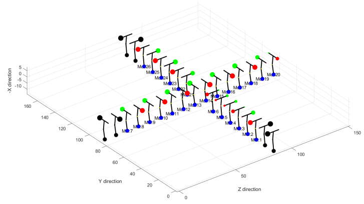

(a) $A = 0,\ B = 0,\ C = 1.$

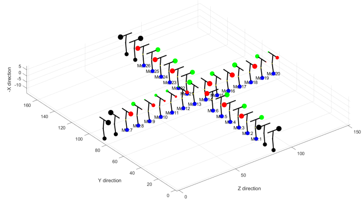

(b) $A = 0,\ B = 1,\ C = 0.$

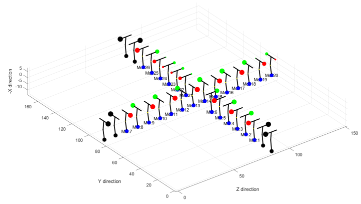

(c) $A = 0,\ B = 1,\ C = 1.$

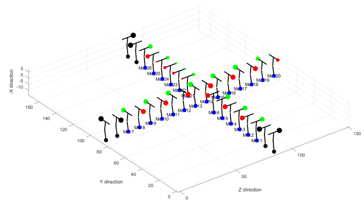

(d) $A = 1,\ B = 0,\ C = 0.$

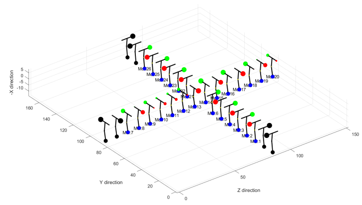

(e) $A = 1,\ B = 0,\ C = 1.$

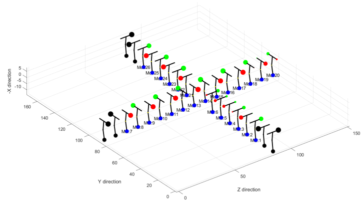

(f) $A = 1,\ B = 1,\ C = 0.$

Figure 5.29. Sinusoidal Clocked behaviour of Majority Voter at wavelength $\lambda = 50\ nm$, at fixed time instants and with the eight logic input states reported in Table 5.1.

Majority Voter with Sinusoidal Clock at $\lambda = 1\ \mu m$

The Majority Voter performance with Sinusoidal Field at $\lambda = 1\ \mu m$ is illustrated in Figure 5.30 behaving well in all cases.

Therefore, this component is the only one that works correctly in all three lambda conditions seen previously for the other devices (except only the case discussed before), without any need for modifications compared to the standard version.

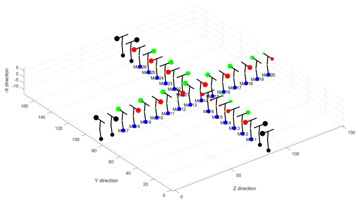

(a) $A = 0$, $B = 0$, $C = 1$.

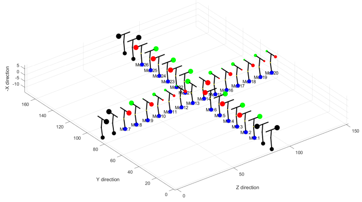

(b) $A = 0$, $B = 1$, $C = 0$.

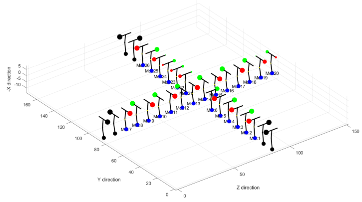

(c) $A = 0$, $B = 1$, $C = 1$.

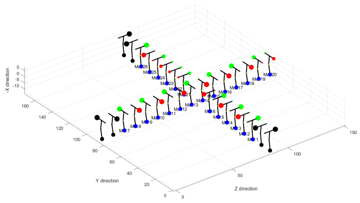

(d) $A = 1$, $B = 0$, $C = 0$.

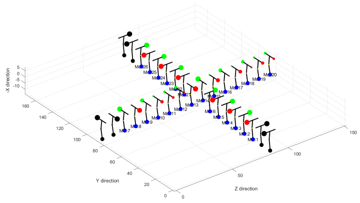

(e) $A = 1$, $B = 0$, $C = 1$.

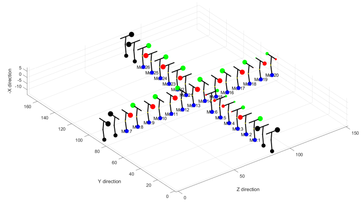

(f) $A = 1$, $B = 1$, $C = 0$.

Figure 5.30. Sinusoidal Clocked behaviour of Majority Voter at wavelength $\lambda = 1\ \mu m$, at fixed time instants and with the eight logic input states reported in Table 5.1.

5.5 Simulation Results: Inverter

The MQCA Inverter is a device that exploits the diagonal electrostatic interaction to induce an information inversion in the final part of the circuit, as explained in Chapter 1. Its operation is based on the copy of information arriving from the initial part of the device on the two branches, which in turn induce the negation of it on its final part. The Three-phase behaviour is not analysed in [2], therefore, initially this type of study and analysis has been done to verify its correct functioning.

5.5.1 Inverter behaviour with Three-Phase Clock

The layout designed inside SCERPA is shown in Figure 5.31, while Figure 5.32 and Figure 5.33 illustrate its Three-phase clocked behaviour with both logic input states. In both cases, using an intermolecular distance $d = 1\ nm$ the two branches are slightly polarized and the device completely loses the polarization in the final moments of propagation, leading to incorrect behaviour of the device and to a failed transmission and inversion of information.

With the aim to overcome this propagation restriction, a new device structure has been designed and its layout is shown in Figure 5.34. The alterations made to the standard structure regard all three parts of the device: the initial part

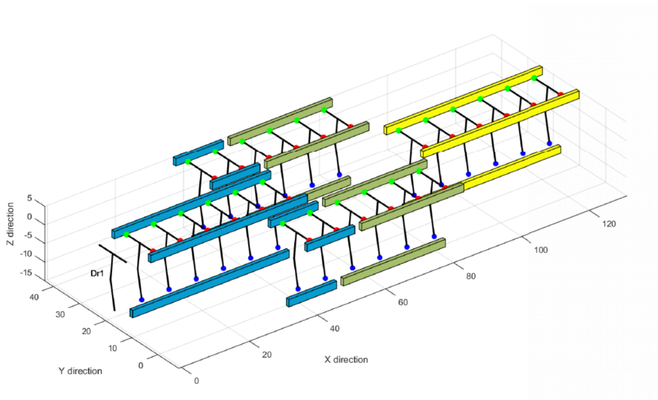

Figure 5.31. Schematic layout of Inverter structure used for Three-phase Clock analysis.

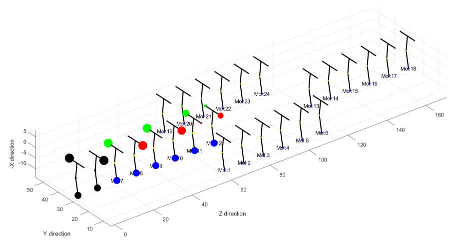

(a) Time0.

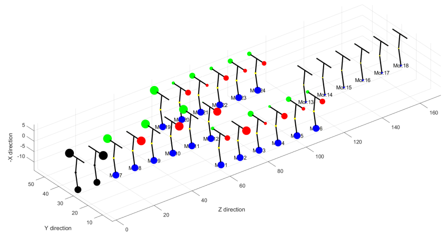

(b) Time1.

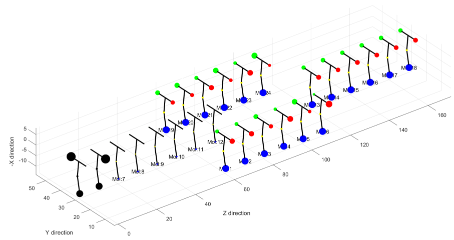

(c) Time2.

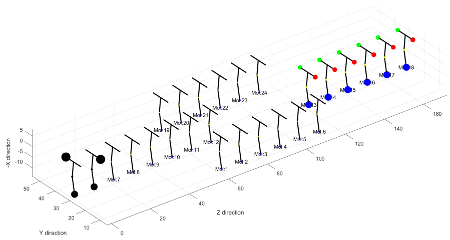

(d) Time3.

Figure 5.32. Three-Phase Clocked behaviour of Inverter with logic input state “0”.

reinforcement plus the doubled branches are required to bring the information from the input to the two branches avoiding data corruption, while the reinforcement of final part it is essential to have reversed information.

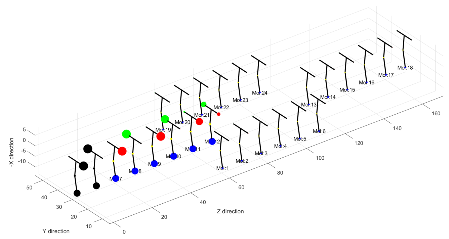

(a) Time0.

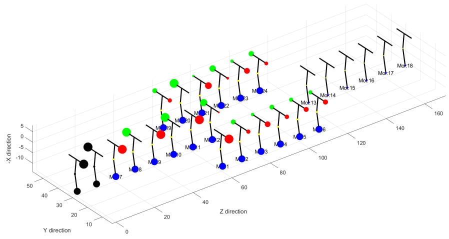

(b) Time1.

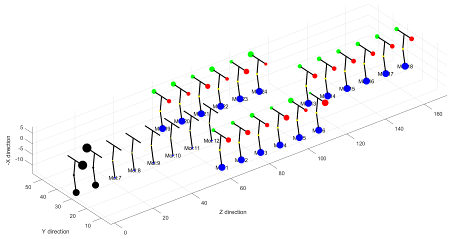

(c) Time2.

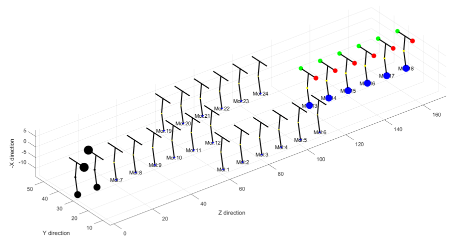

(d) Time3.

Figure 5.33. Three-Phase Clocked behaviour of Inverter with logic input state “1”.

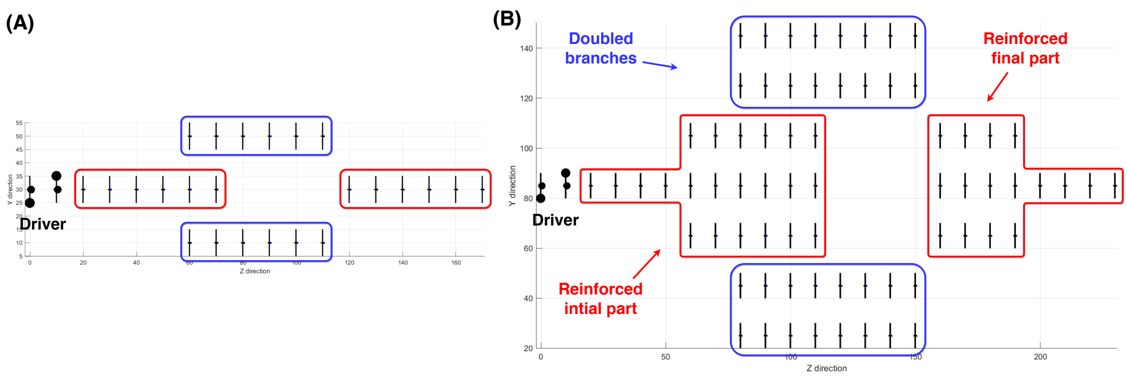

Figure 5.34. Structures’ comparison: (A) Standard Inverter, (B) new Enhanced Inverter structure, highlighting the corresponding modifications with respect standard structure.

The correct behaviour reported in Figure 5.35 and Figure 5.36, validates the all modifications described before and demonstrates the possibility to invert the information with Three-phase clock.

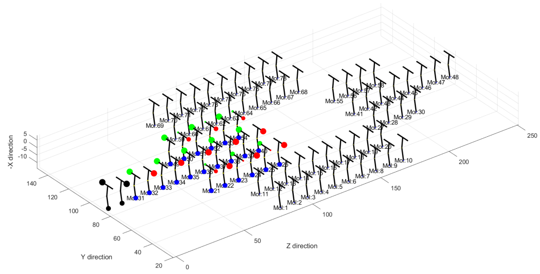

(a) Time0.

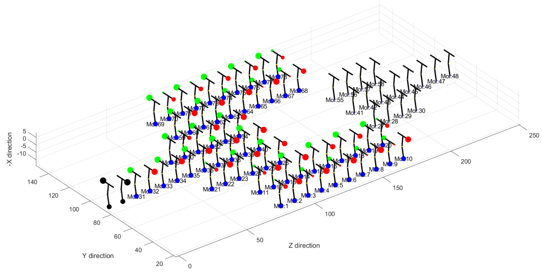

(b) Time1.

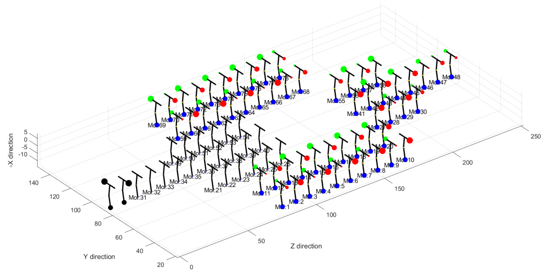

(c) Time2.

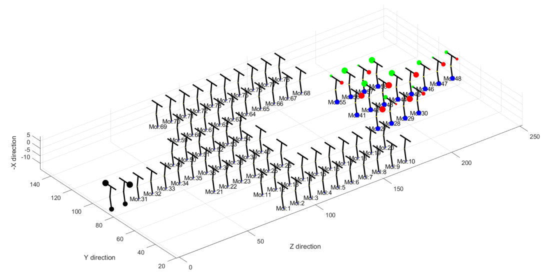

(d) Time3.

Figure 5.35. Three-Phase Clocked behaviour of new Enhanced Inverter with logic input state “0”.

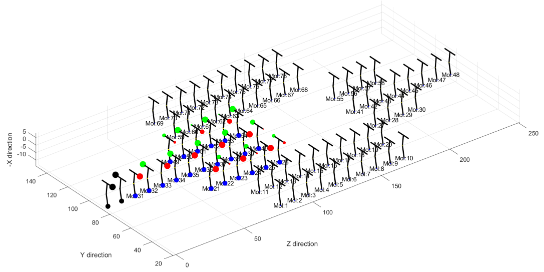

(a) Time0.

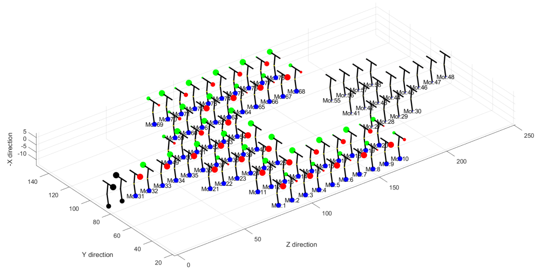

(b) Time1.

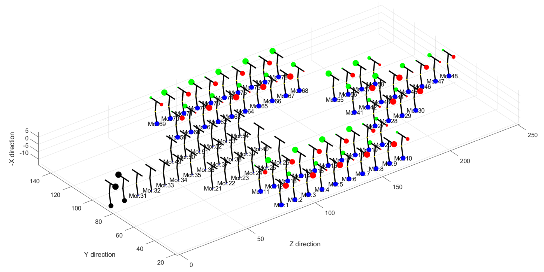

(c) Time2.

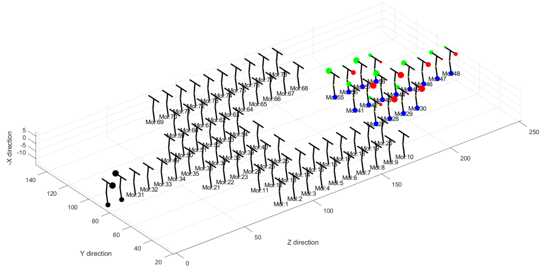

(d) Time3.

Figure 5.36. Three-Phase Clocked behaviour of new Enhanced Inverter with logic input state “1”.

5.5.2 Inverter behaviour with Sinusoidal Clock

After Three-phase Clock performance analysis, the translation to Sinusoidal Clock of new Enhanced Inverter has been carried out. The layout designed inside SCERPA is depicted in Figure 5.37.

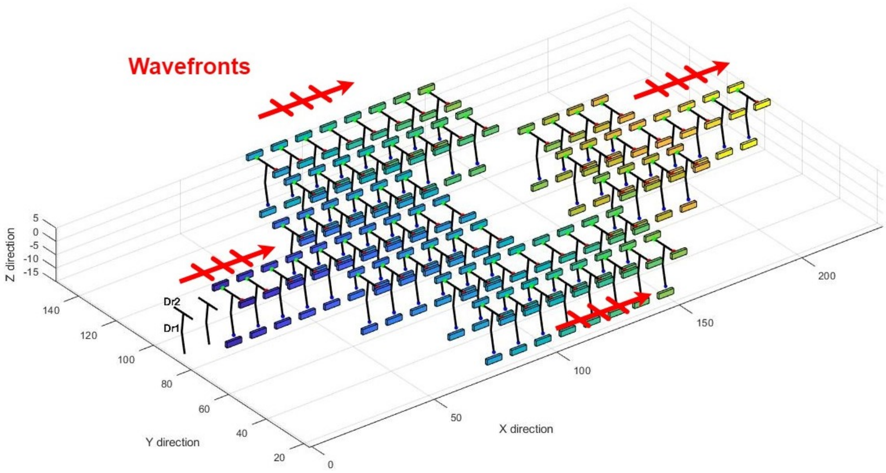

Figure 5.37. Schematic layout of Enhanced Inverter structure used for Sinusoidal Clock analysis and direction propagation of wavefronts.

Enhanced Inverter with Sinusoidal Clock at $\lambda = 12\ nm$

The Enhanced Inverter performance with Sinusoidal Field at $\lambda_{min} = 12\ nm$ is illustrated in Figure 5.38 demonstrating correct behaviour for both logic input configurations (for brevity's sake the only simulation with "0" input state is reported).

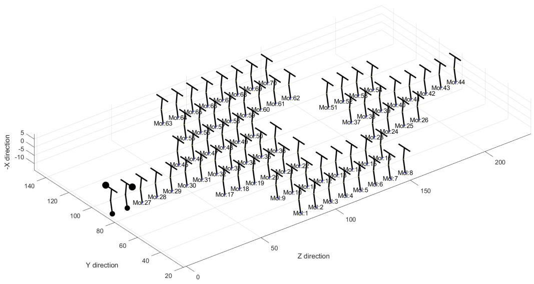

(a) Time0.

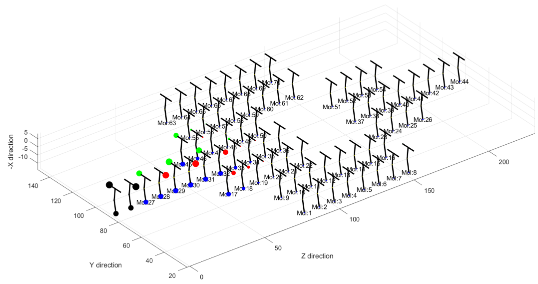

(b) Time1.

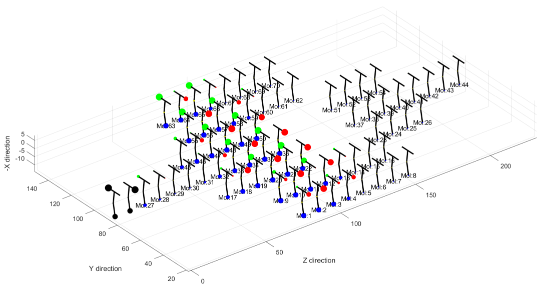

(c) Time2.

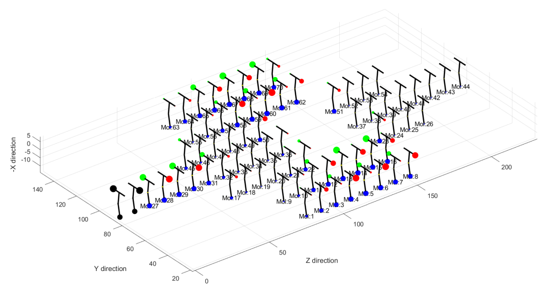

(d) Time3.

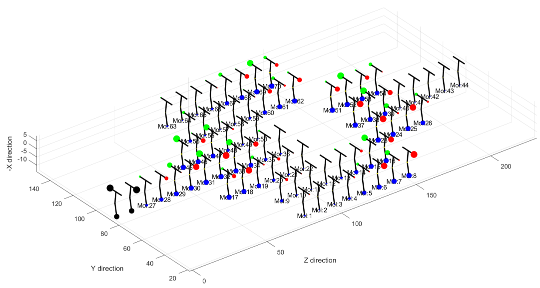

(e) Time4.

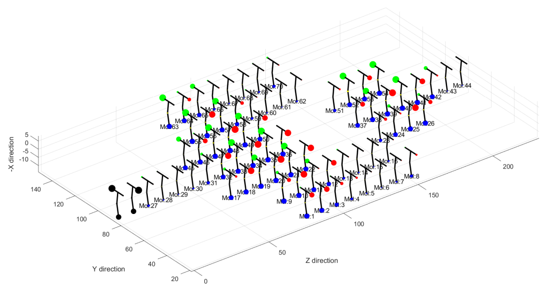

(f) Time5.

Figure 5.38. Sinusoidal Clocked behaviour of Enhanced Inverter at wavelength $\lambda = 12\ nm$ with the logic input state “0”.

Enhanced Inverter with Sinusoidal Clock at $\lambda = 50\ nm$

The Enhanced Inverter performance with Sinusoidal Field at $\lambda = 50\ nm$ is illustrated in Figure 5.39 demonstrating correct behaviour for both logic input configurations (for brevity’s sake the only simulation with “1” input state is reported).

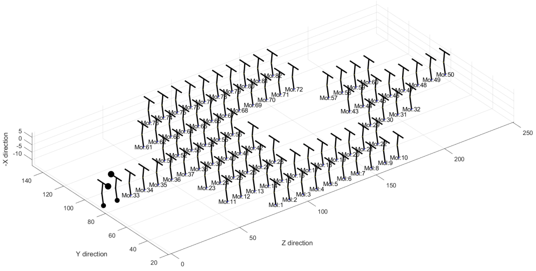

(a) Time0.

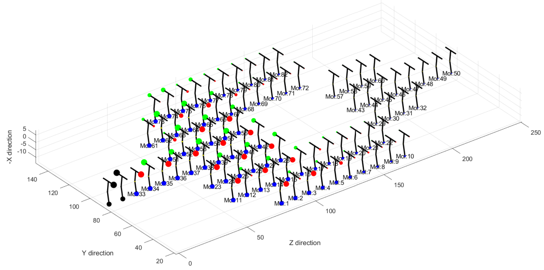

(b) Time1.

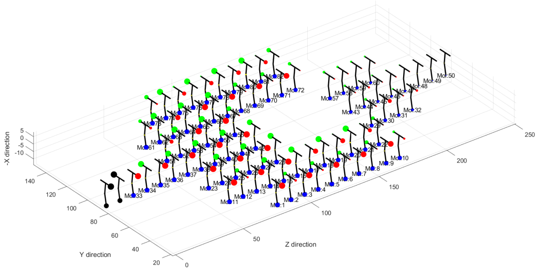

(c) Time2.

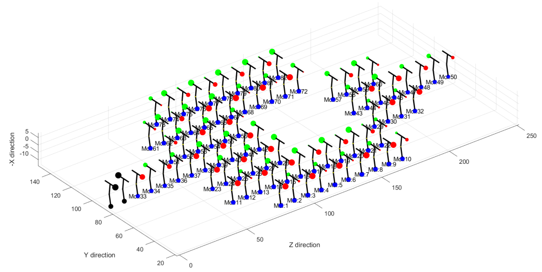

(d) Time3.

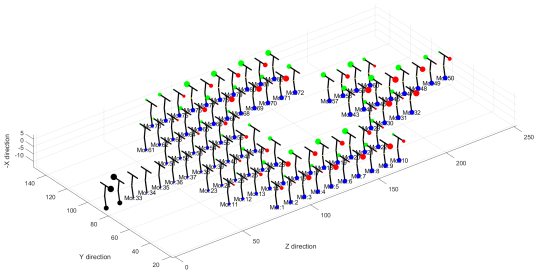

(e) Time4.

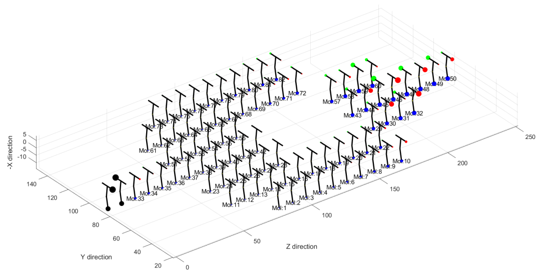

(f) Time5.

Figure 5.39. Sinusoidal Clocked behaviour of Enhanced Inverter at wavelength $\lambda = 50\ nm$ with the logic input state "1".

Enhanced Inverter with Sinusoidal Clock at $\lambda = 1\ \mu m$

Concerning the Enhanced Inverter performance with Sinusoidal Field at $\lambda = 1\ \mu m$, it demonstrates correct behaviour only with logic input "1", in the opposite case information fault occurs, as depicted in Figure 5.40.

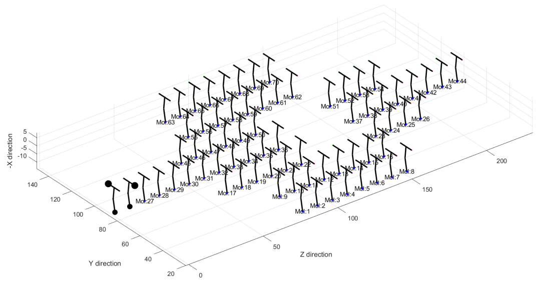

(a) Time0.

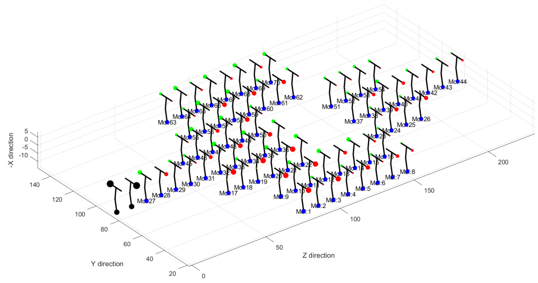

(b) Time1.

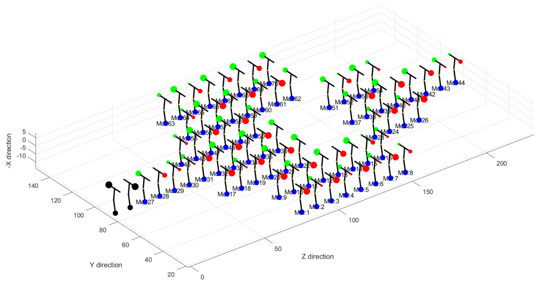

(c) Time2.

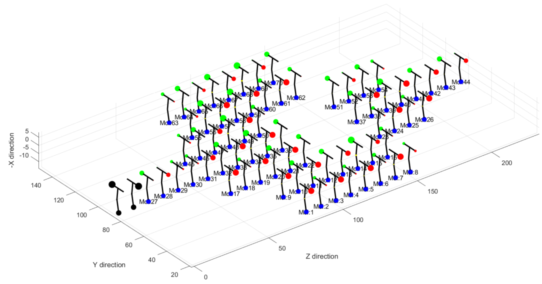

(d) Time3.

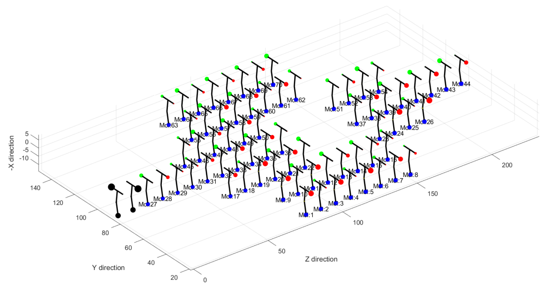

(e) Time4.

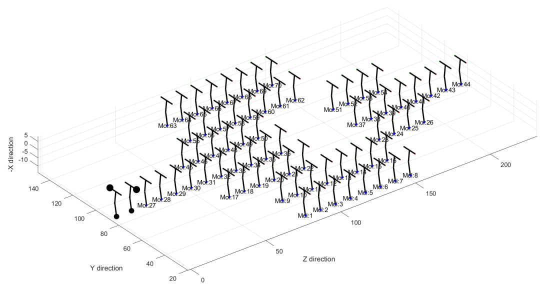

(f) Time5.

Figure 5.40. Sinusoidal Clocked behaviour of Enhanced Inverter at wavelength $\lambda = 1\ \mu m$ with the logic input state "0".

Plotting the top view of Time 2 of Figure 5.40, an information fault in the second cell of the structure is visible. This always happens because of the large transition window that generates the situation shown in Figure 5.41. Looking this Figure, during the transition phase from $-2\ V$ to $+2\ V$ the corner repulsion is predominant inducing the logic state "1" in the *cell y*, as a result, the larger portion of the inverter's initial part assumes wrong polarization which in turn creates the error in the *cell x* due to the feedback interactions among molecules.

The error does not take place in two previous cases ($\lambda = 12\ nm$, $\lambda = 50\ nm$) because the part underlined in Figure 5.41.C is quite inhibited when the cell x is full polarized, therefore during propagation the cells' column, where the cell y is located, is influenced only by the cell x and not by the remaining circuit. But now, with $\lambda = 1\ \mu m$ both cells are influenced by all other cells since at the entire circuit, at given time instant, is applied about the same clock phase value.

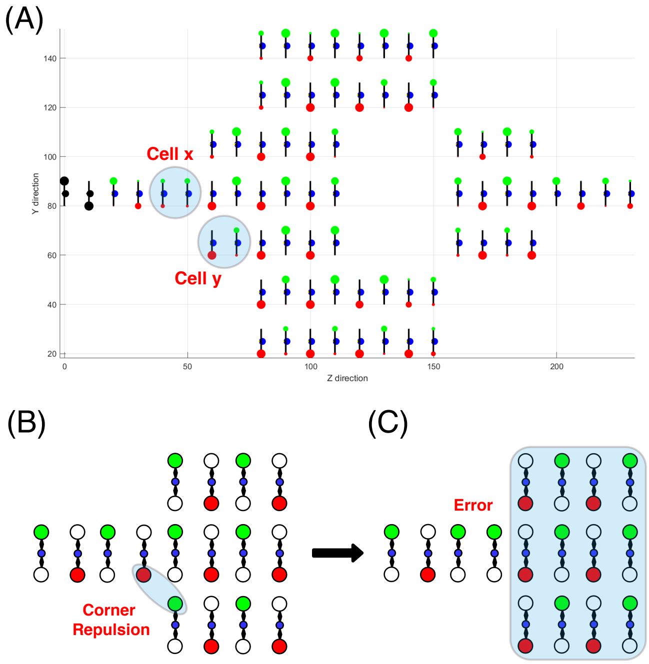

Figure 5.41. Error corruption in Enhanced Inverter with Sinusoidal Clock at wavelength $\lambda = 1\ \mu m$: (A) Top view and cell x, cell y definition, (B) and (C) Schematic representation of the parties responsible for the error.

5.6 Lower Bound of Sinusoidal Clock Wavelength

Therefore, all MQCA functional blocks work correctly with the minimal lambda $\lambda = 12\ nm$, except the majority voter whose minimum limit found, from the wavelength point of view, is $\lambda = 20\ nm$, as illustrated in Figure 5.45. For this reason all structures have been tested with $\lambda = 20\ nm$ proving proper behaviour in any cases and for both logic inputs, as depicted in Figures 5.42, 5.43, 5.44,5.45, 5.46, 5.47.
Consequently, the lower bound of Sinusoidal Clock wavelength that ensures integrity of information in all basic MQCA gates is $\boldsymbol{\lambda = 20\ nm}$.

Moreover, a linear relationship between the number of activated cells and wavelength of Sinusoidal Clock has been demonstrated permitting to control, simply changing the λ, the length of the frames as well as the information flow in terms of frequency.

Wire formed by 50 molecules with Sinusoidal Clock at $\lambda = 20\ nm$

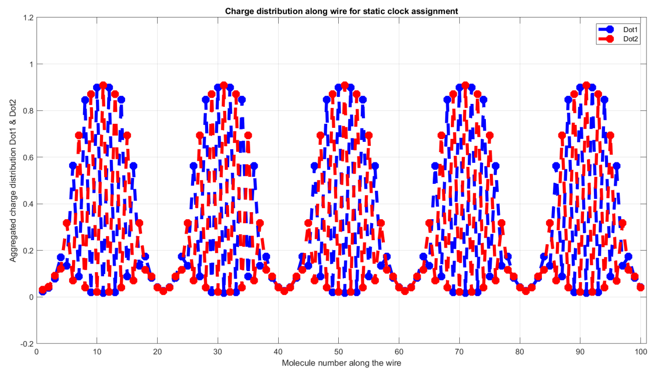

Figure 5.42. Sinusoidal Clocked behaviour of Wire with 100 molecules at wavelength $\lambda = 20\ nm$ and at fixed time instant: charge distribution.

Angle structure with Sinusoidal Clock at $\lambda = 20\ nm$

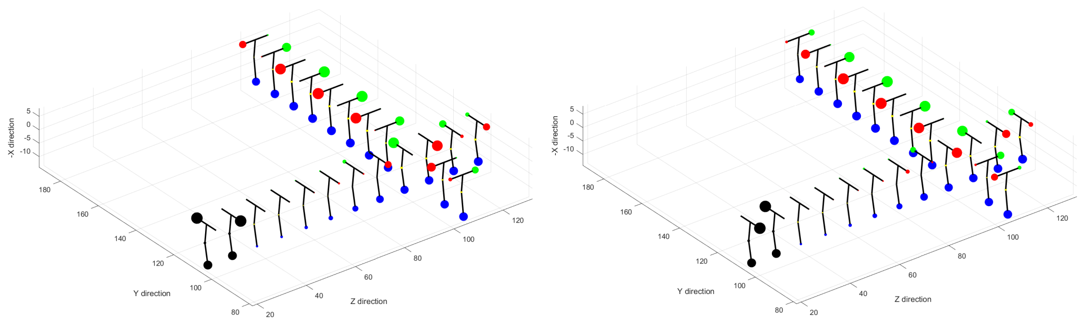

(a) Input "0" and $\lambda = 20\ nm$.

(b) Input "1" and $\lambda = 20\ nm$.

Figure 5.43. Sinusoidal Clocked behaviour of Angle at wavelength $\lambda = 20\ nm$, at fixed time instant and with both logic input states.

T-shape structure with Sinusoidal Clock at $\boldsymbol{\lambda = 20}$ $\boldsymbol{nm}$

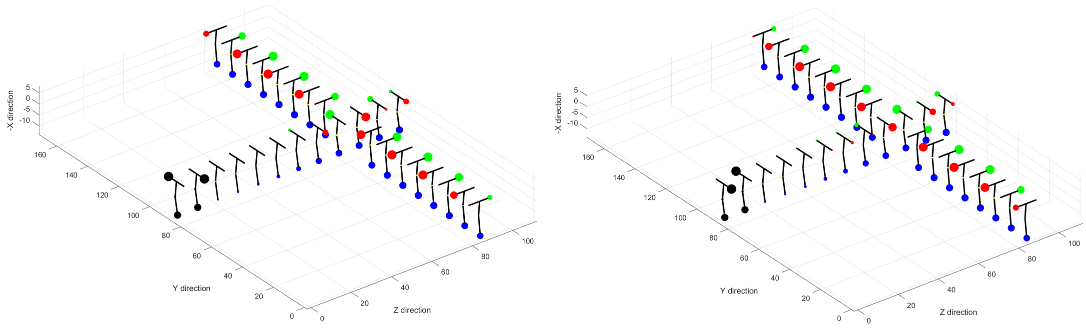

(a) Input "0" and $\lambda = 20$ nm. (b) Input "1" and $\lambda = 20$ nm.

Figure 5.44. Sinusoidal Clocked behaviour of T-shape structure at wavelength $\lambda = 20$ nm, at fixed time instant and with both logic input states.

Majority Voter with Sinusoidal Clock at $\boldsymbol{\lambda = 20}$ $\boldsymbol{nm}$

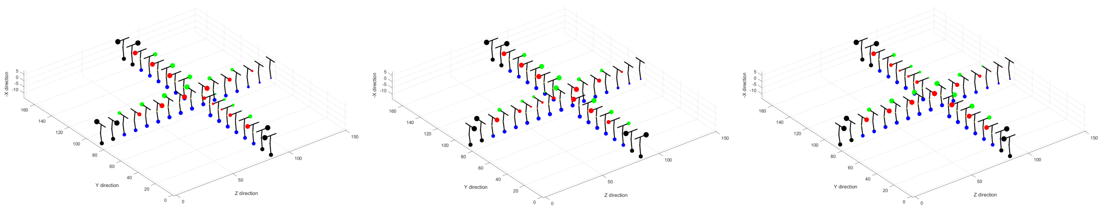

(a) $A = 0$, $B = 0$, $C = 1$. (b) $A = 0$, $B = 1$, $C = 0$. (c) $A = 0$, $B = 1$, $C = 1$.

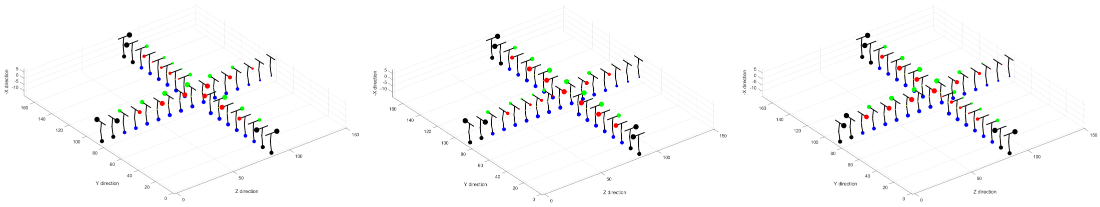

(d) $A = 1$, $B = 0$, $C = 0$. (e) $A = 1$, $B = 0$, $C = 1$. (f) $A = 1$, $B = 1$, $C = 0$.

Figure 5.45. Sinusoidal Clocked behaviour of Majority Voter at wavelength $\lambda = 20$ nm, at fixed time instant and with the eight logic input states reported in Table 5.1.

Enhanced Inverter with Sinusoidal Clock at $\lambda = 20\ nm$

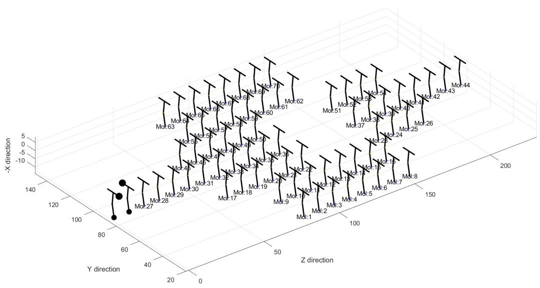

(a) Time0.

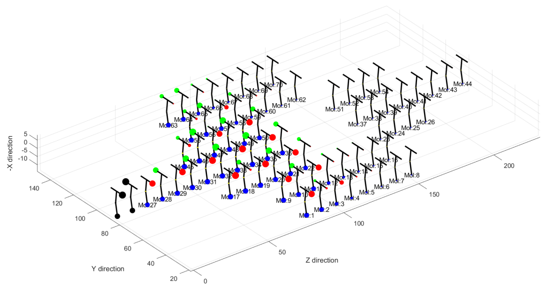

(b) Time1.

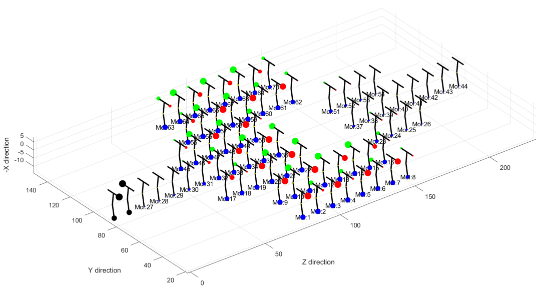

(c) Time2.

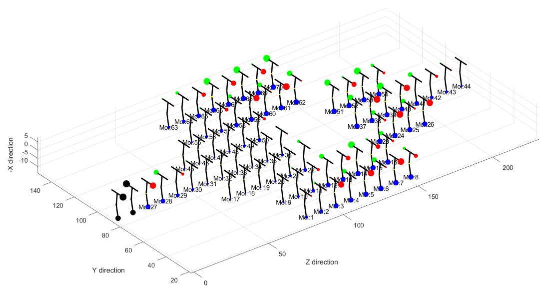

(d) Time3.

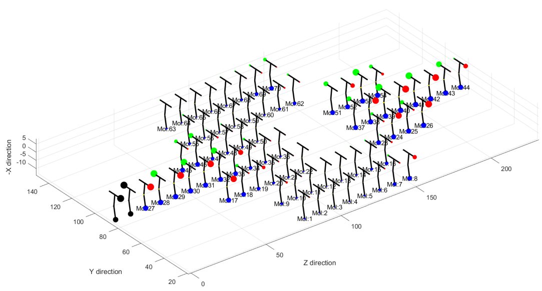

(e) Time4.

Figure 5.46. Sinusoidal Clocked behaviour of Enhanced Inverter at wavelength $\lambda = 20\ nm$ with the logic input "1".

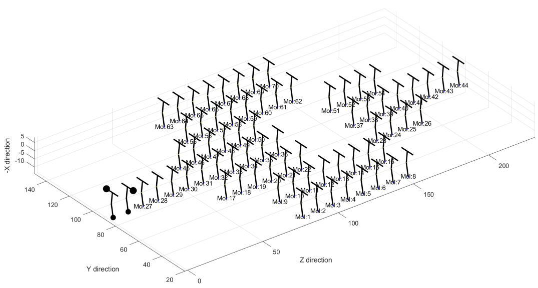

(a) Time0.

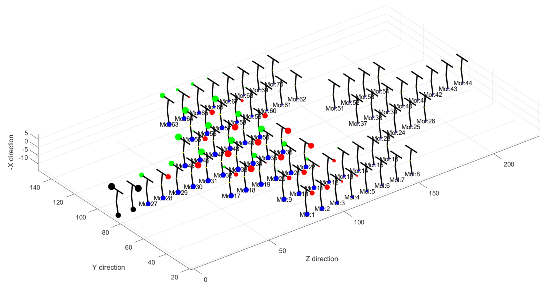

(b) Time1.

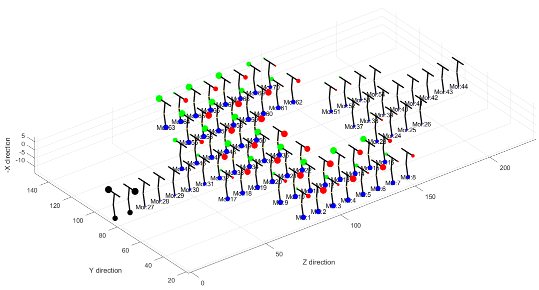

(c) Time2.

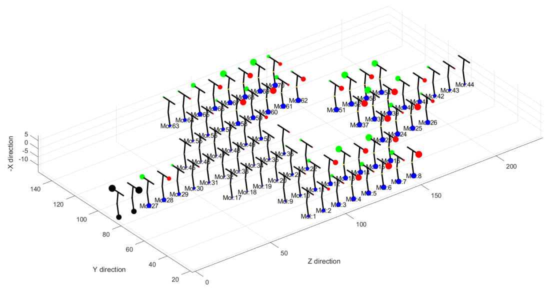

(d) Time3.

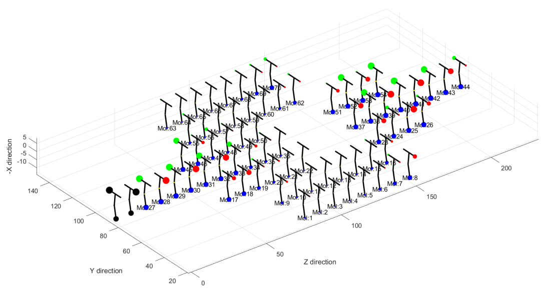

(e) Time4.

Figure 5.47. Sinusoidal Clocked behaviour of Enhanced Inverter at wavelength $\lambda = 20\ nm$ with the logic input “0”.

Chapter 6

Sinusoidal Clocking Simulation of MQCA Circuit: Half Adder

After Sinusoidal Clock characterization, design and improvement of all basic MQCA devices, a combination of them has been performed in order to create the *MQCA Half Adder* according to the schematic diagram in Figure 6.1.

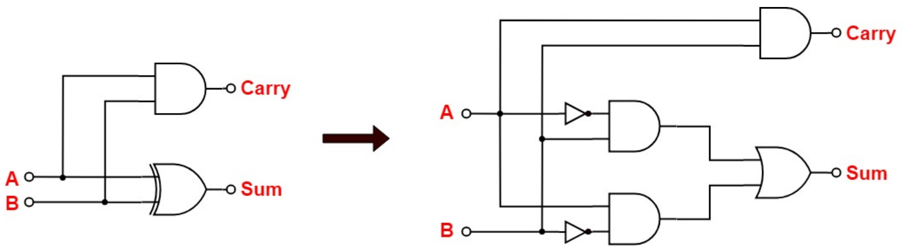

Figure 6.1. Left: Schematic diagram of Half Adder, Right: The Schematic diagram of Half Adder used to design the MCQA Half Adder, where is visible the schematic of XOR gate.

6.1 Sub-Circuit of Half Adder

Before designing the entire circuit, a preliminary step has been carried out, consisting in the simulation of the Half Adder's section formed by the union of Inverter, AND (Majority Voter with one input fixed to "0") and Angle structure, as illustrated in Figure 6.2.

After layout definition, the four logic possible configurations of A and B inputs have been simulated in order to completely characterize the structure under test according to the truth Table 6.1.

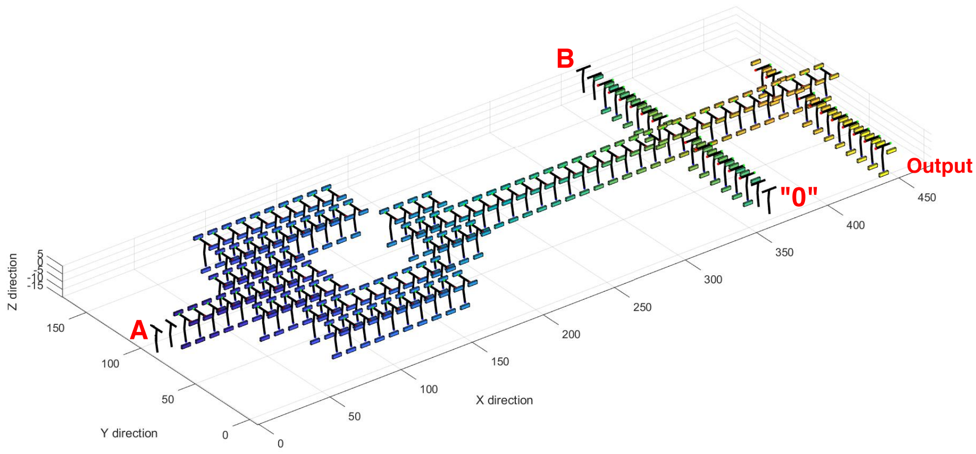

Figure 6.2. Schematic layout of Half Adder Sub-Circuit.

Inputs		Output
A	B	
0	0	0
0	1	1
1	0	0
1	1	0

Table 6.1. Truth table of Half Adder Sub-Circuit.

The simulation of Half Adder and its Sub-Circuit has been performed with Sinusoidal Clock at $\lambda = 50\ nm$ because it is the wavelength at which no device has generated information corruption. The obtained results simulation indicate that the Sub-circuit behaves correctly for all input configurations, as depicted in Figures 6.3, 6.4, 6.5, 6.6.

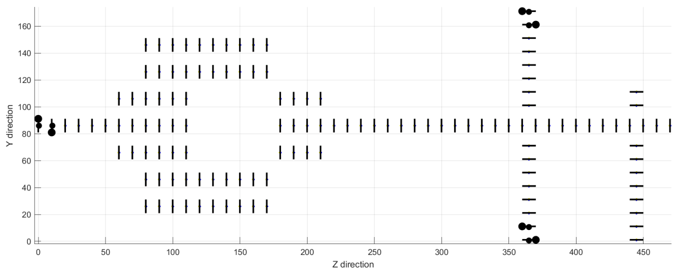

(a) Time0.

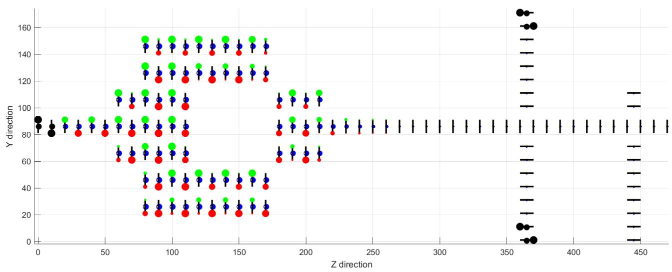

(b) Time1.

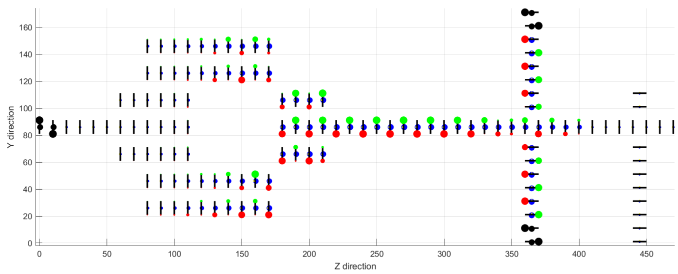

(c) Time2.

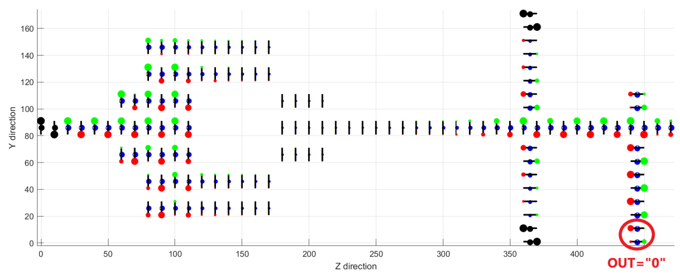

(d) Time3.

Figure 6.3. Sinusoidal Clocked behaviour of Half Adder Sub-Circuit at wavelength $\lambda = 50\ nm$ with the logic input configurations $A = 0$, $B = 0$ and and $Output = 0$.

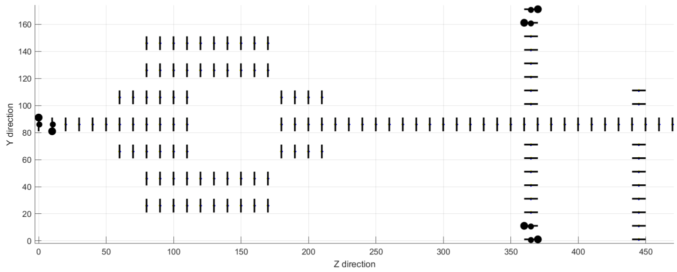

(a) Time0.

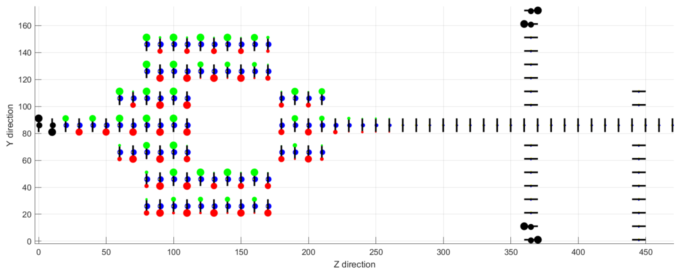

(b) Time1.

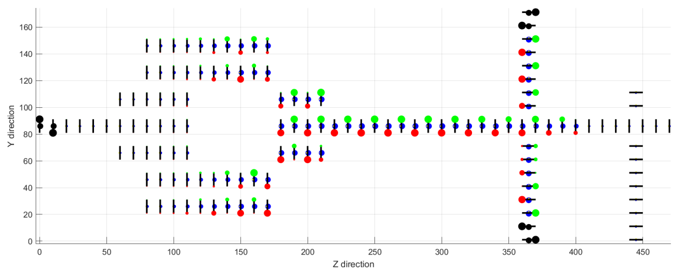

(c) Time2.

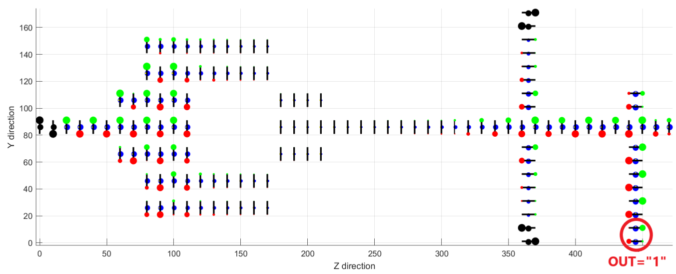

(d) Time3.

Figure 6.4. Sinusoidal Clocked behaviour of Half Adder Sub-Circuit at wavelength $\lambda = 50\ nm$ with the logic input configurations $A = 0$, $B = 1$ and $Output = 1$.

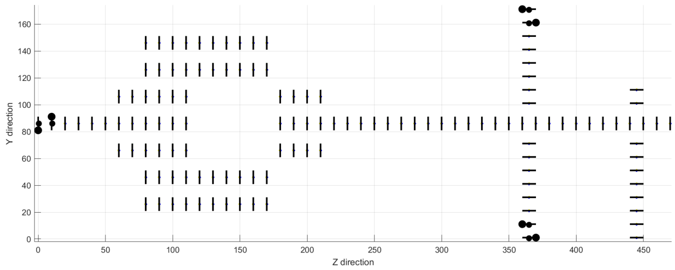

(a) Time0.

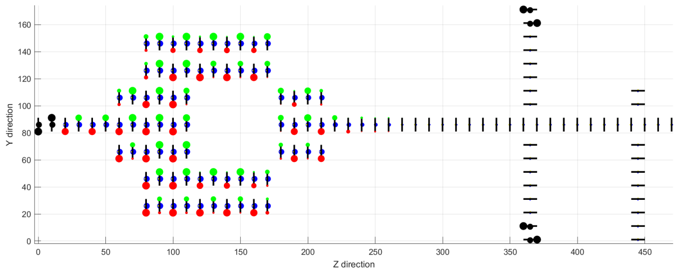

(b) Time1.

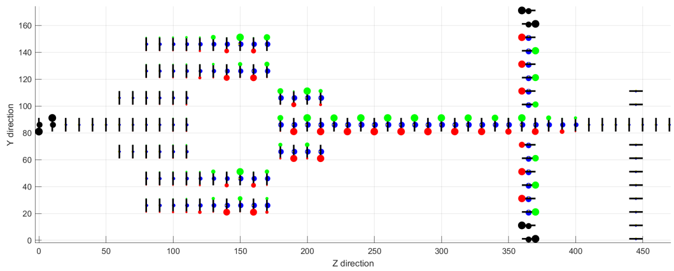

(c) Time2.

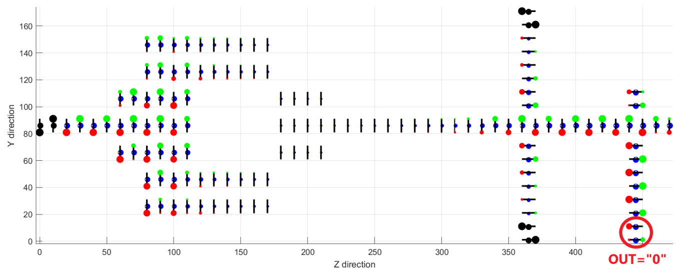

(d) Time3.

Figure 6.5. Sinusoidal Clocked behaviour of Half Adder Sub-Circuit at wavelength $\lambda = 50\ nm$ with the logic input configurations $A = 1$, $B = 0$ and $Output = 0$.

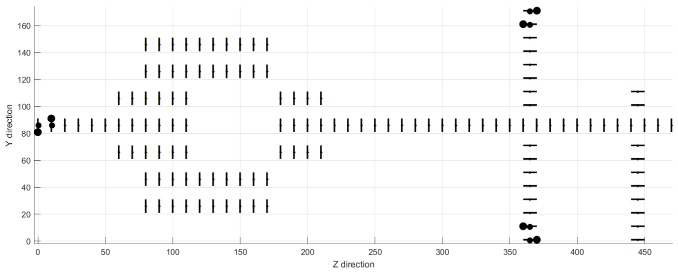

(a) Time0.

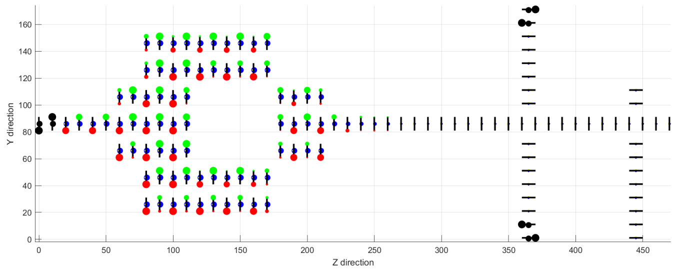

(b) Time1.

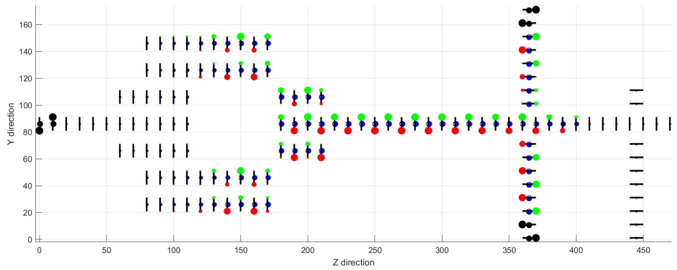

(c) Time2.

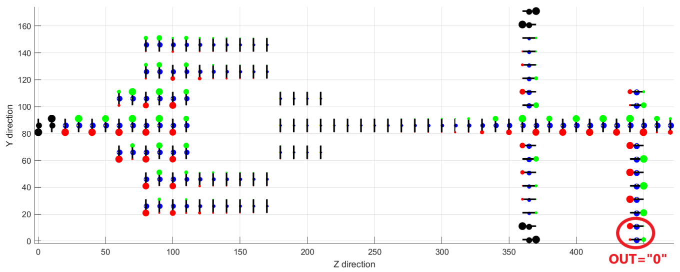

(d) Time3.

Figure 6.6. Sinusoidal Clocked behaviour of Half Adder Sub-Circuit at wavelength $\lambda = 50\ nm$ with the logic input configurations $A = 1$, $B = 1$ and $Output = 0$.

To verify the reliability and robustness of the new designed Enhanced Inverter when connected with other components (implying a verification also of the inverter itself) a new type of test has been performed. This verification test consists in simulating the Half Adder Sub-Circuit always in the same operating conditions ($\lambda = 50\ nm$) with unchanged input configuration, by varying the distance between the two branches of the inverter and its final part in which the information is reversed.

In particular, as Figure 6.7 shows three different distances have been simulated and tested.

- $distance\_branches\_finalpart = 1\ nm$: it is the standard one, already simulated in all previous cases;
- $distance\_branches\_finalpart = 1.5\ nm$: it is simulated according to the deposition feasibility reported in [37];
- $distance\_branches\_finalpart = 2\ nm$: the standard distance is doubled.

Results demonstrate certain robustness of the device due to its capability to invert the data up to a distance of 1.5 nm, giving the possibility to partially relax the constraints on molecules deposition.

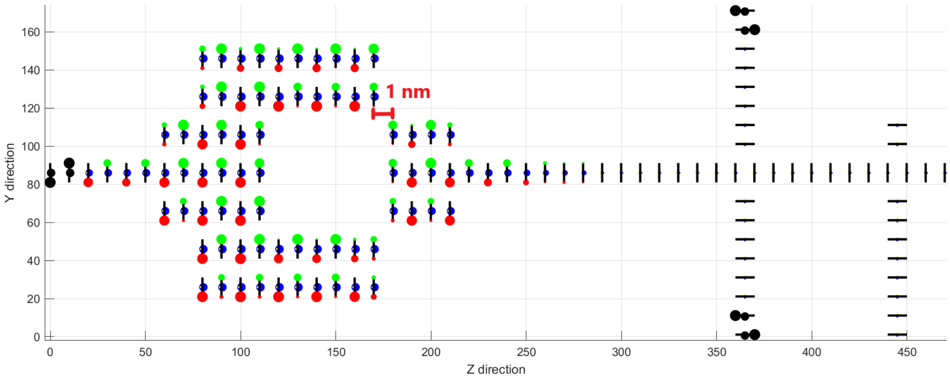

(a) $distance\_branches\_finalpart = 1\ nm$.

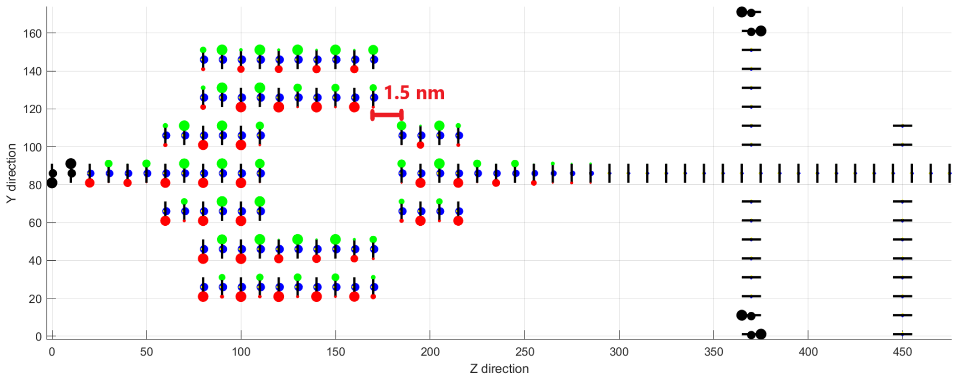

(b) $distance\_branches\_finalpart = 1.5\ nm$.

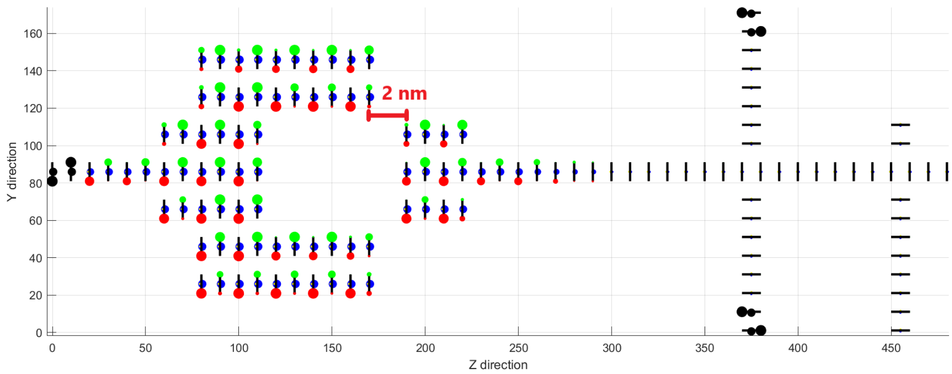

(c) $distance\_branches\_finalpart = 2\ nm$.

Figure 6.7. Reliability verification of Enhanced Inverter at different distances between the branches and its final part.

6.2 Half Adder

After the preliminary testing on the Sub-Circuit, the complete circuit layout has been defined inside SCERPA, as illustrated in Figure 6.8 and Figure 6.9, in which the merging of the different building blocks is highlighted. The simulation has been accomplished always setting a wavelength of $\lambda = 50\ nm$, as mentioned at the beginning of the chapter, and imposing all input pattern configurations according to the standard truth table of Half Adder (Table 6.2), in order to fully characterize the circuit.

Inputs		**Output**	
A	**B**	**Sum**	**Carry**
0	0	0	0
0	1	1	0
1	0	1	0
1	1	0	1

Table 6.2. Truth table of Half Adder.

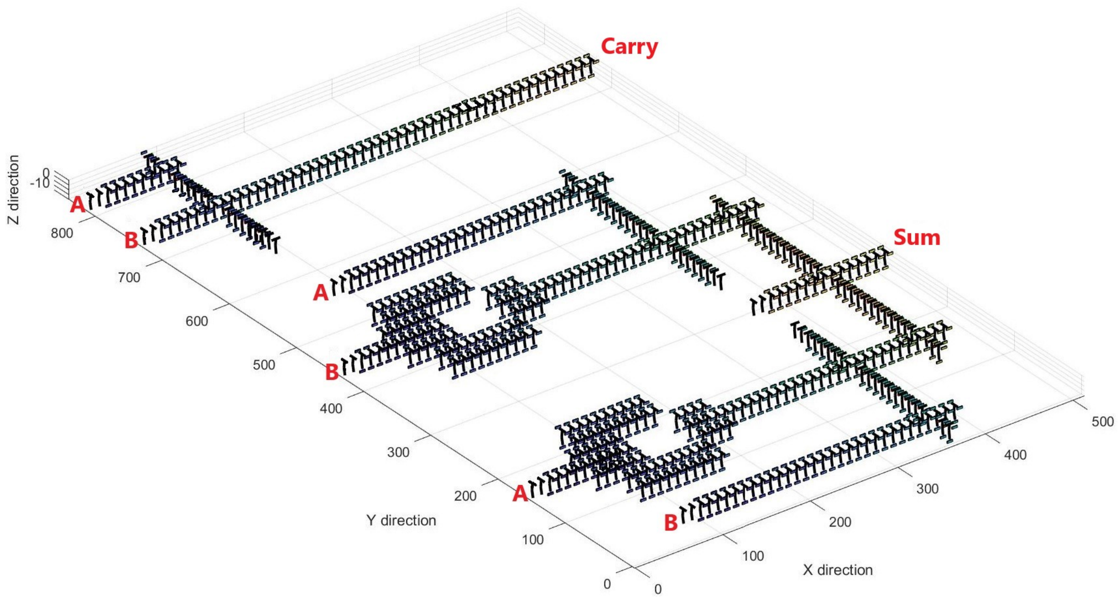

Figure 6.8. Schematic layout of Half Adder (3D view).

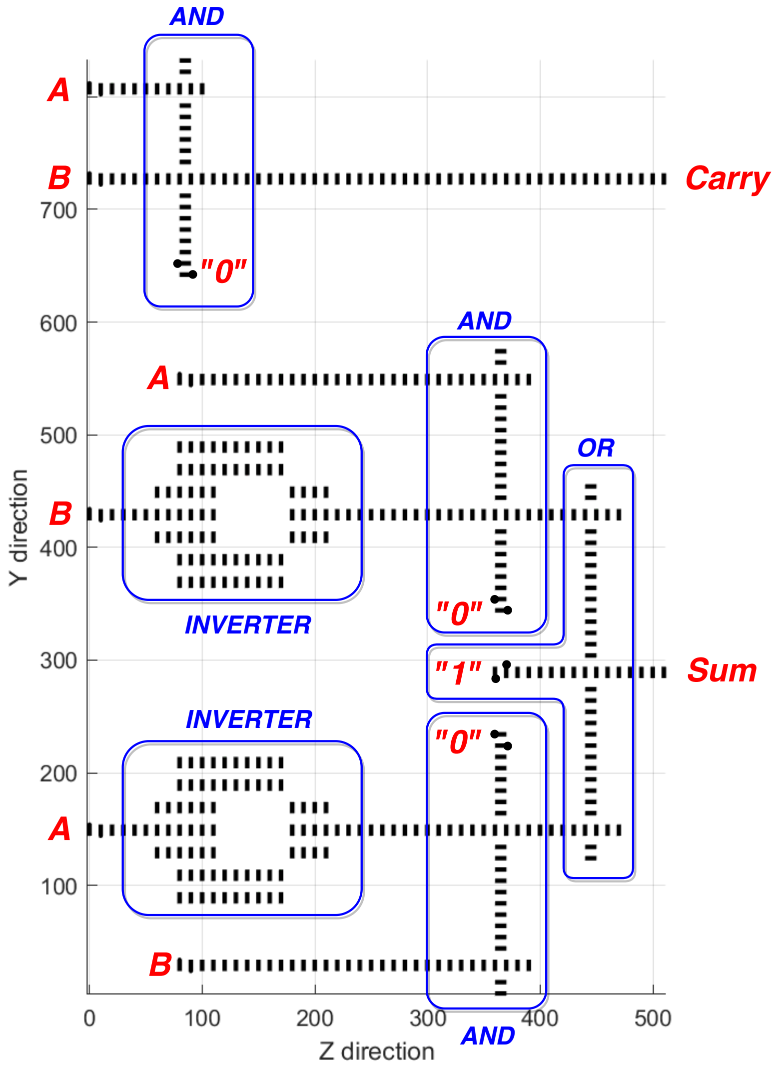

Figure 6.9. Schematic layout of Half Adder(top view).

6.2.1 Simulation Results: Half Adder

Regarding the Half Adder performance with Sinusoidal Field at $\lambda = 50\ nm$, as illustrated in Figure 6.10, good results with all input configurations are achieved.

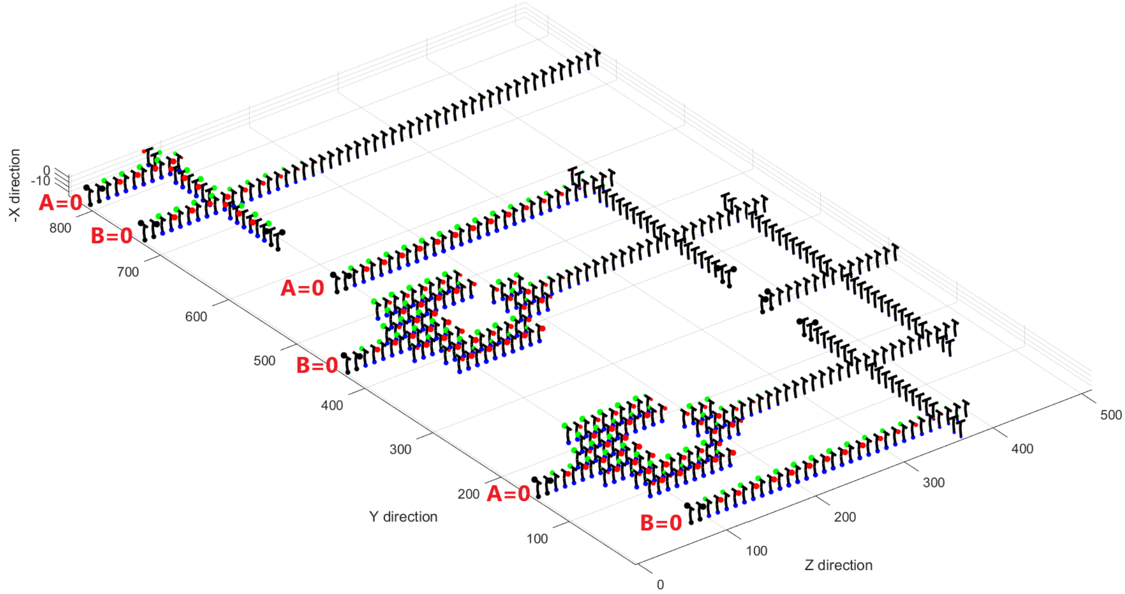

(a) Propagation of information in the initial part of HA circuit with $A = 0$, $B = 0$ input pattern.

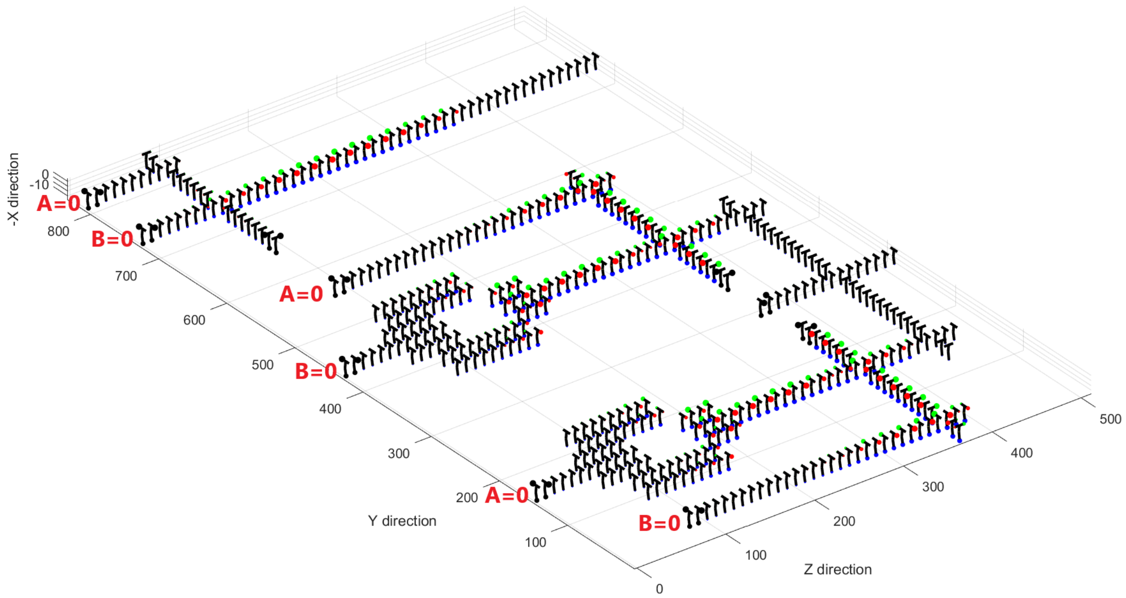

(b) Propagation of information in the central part of HA circuit with $A = 0$, $B = 0$ input pattern.

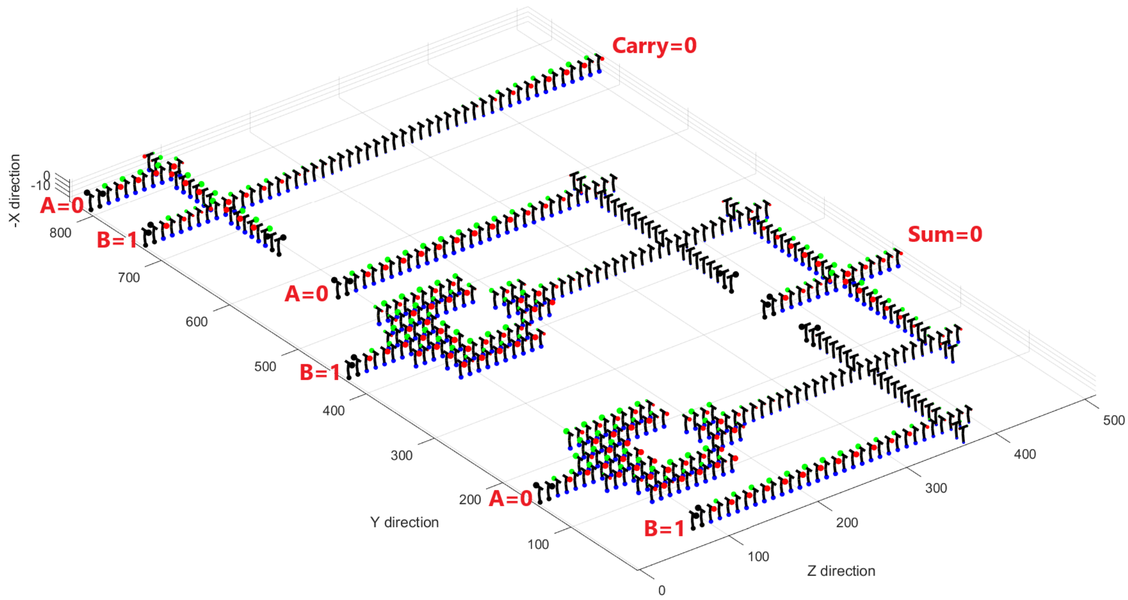

(c) Propagation of information in the final part of HA circuit with $A = 0$, $B = 0$ input pattern and corresponding output $Sum = 0$, $Carry = 0$. Propagation of information in the initial part of HA circuit with new $A = 0$, $B = 1$ input pattern.

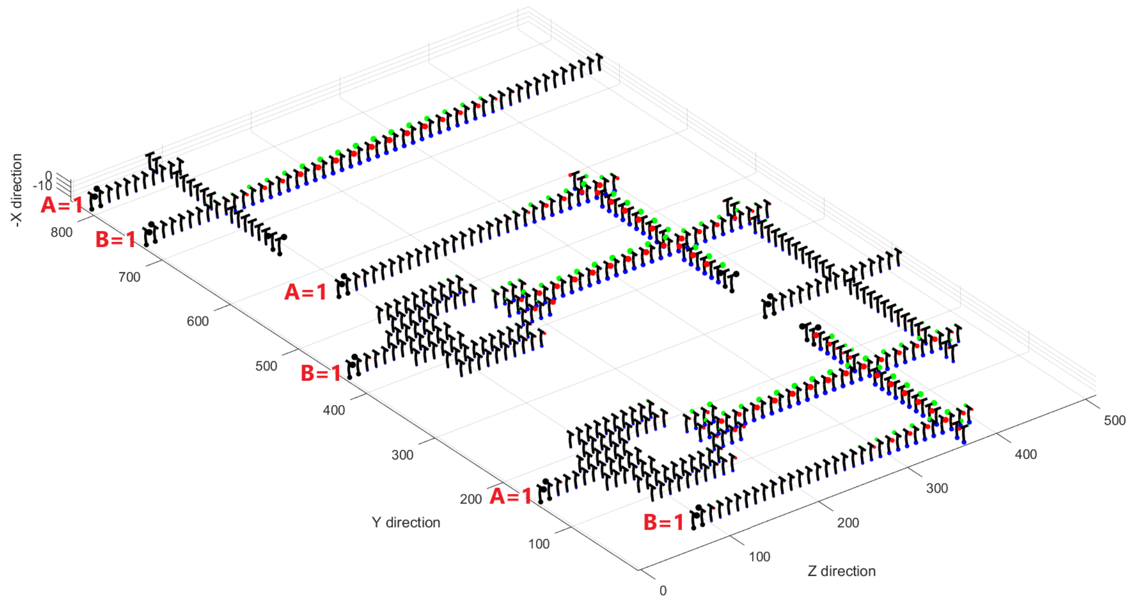

(d) Propagation of information in the central part of HA circuit with $A = 0$, $B = 1$ input pattern and switch of input configuration in $A = 1$, $B = 1$.

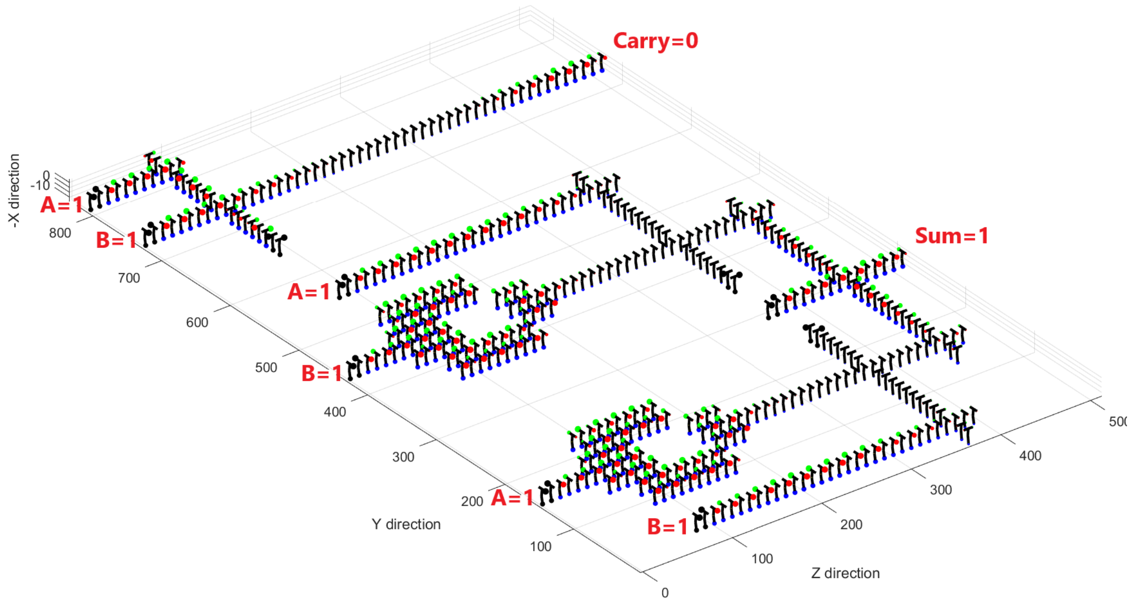

(e) Propagation of information in the final part of HA circuit with $A = 0$, $B = 1$ input pattern and corresponding output $Sum = 1$, $Carry = 0$. Propagation of information in the initial part of HA circuit with new $A = 1$, $B = 1$ input pattern.

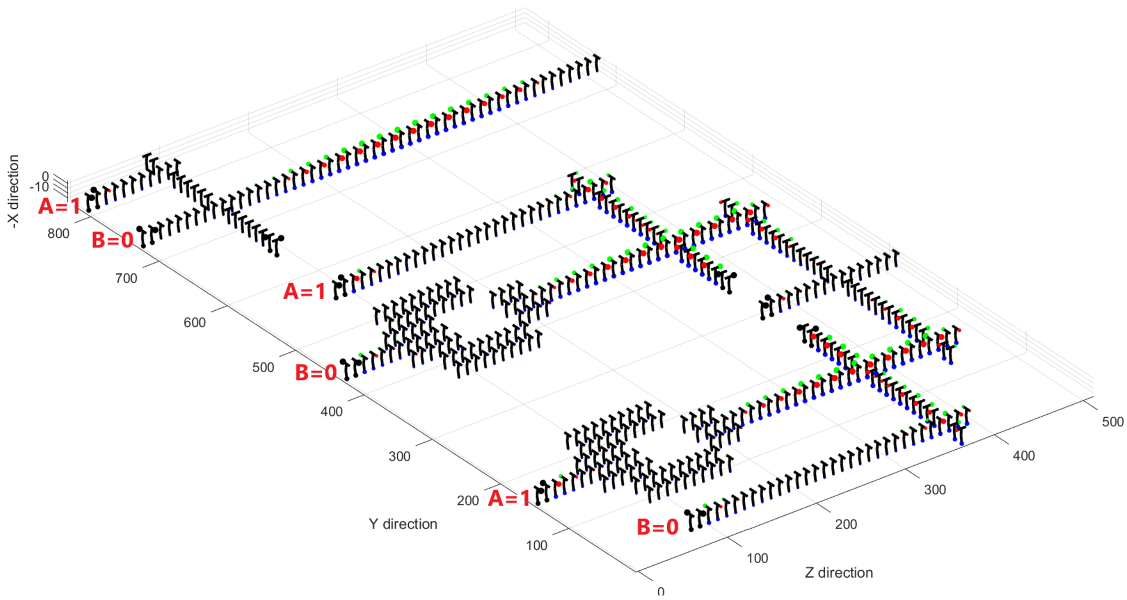

(f) Propagation of information in the central part of HA circuit with $A = 1$, $B = 1$ input pattern and switch of input configuration in $A = 1$, $B = 0$.

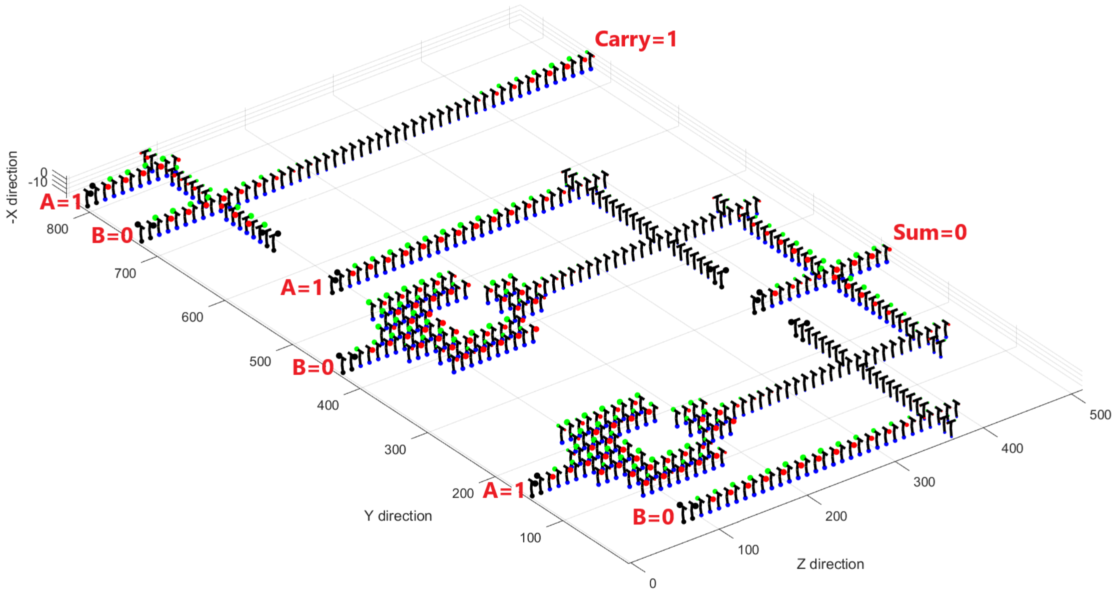

(g) Propagation of information in the final part of HA circuit with $A = 1$, $B = 1$ input pattern and corresponding output $Sum = 0$, $Carry = 1$. Propagation of information in the initial part of HA circuit with new $A = 1$, $B = 0$ input pattern.

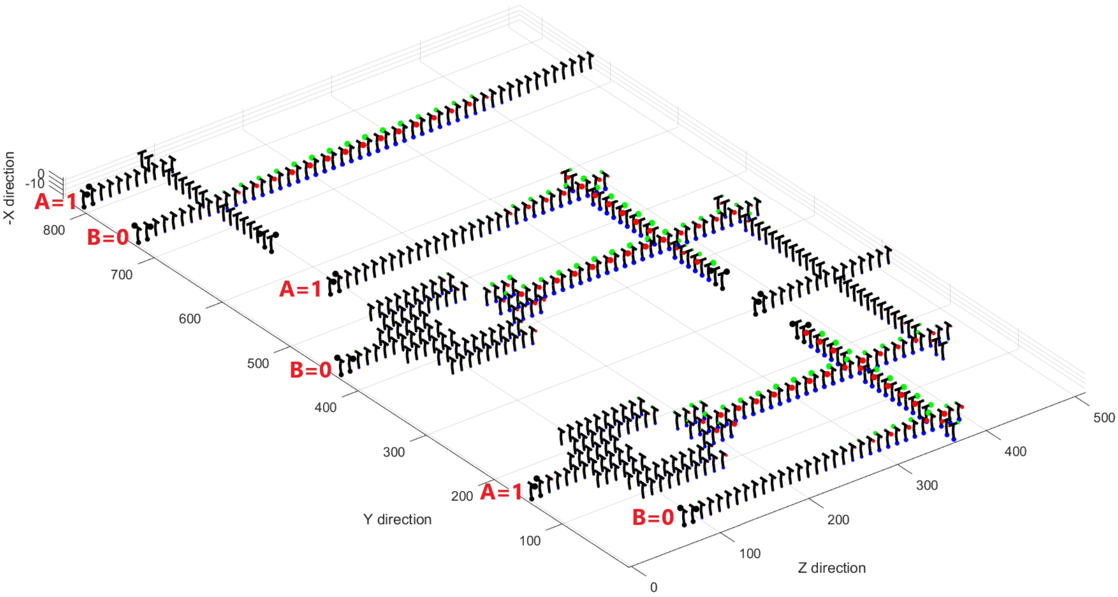

(h) Propagation of information in the central part of HA circuit with $A = 1$, $B = 0$ input pattern.

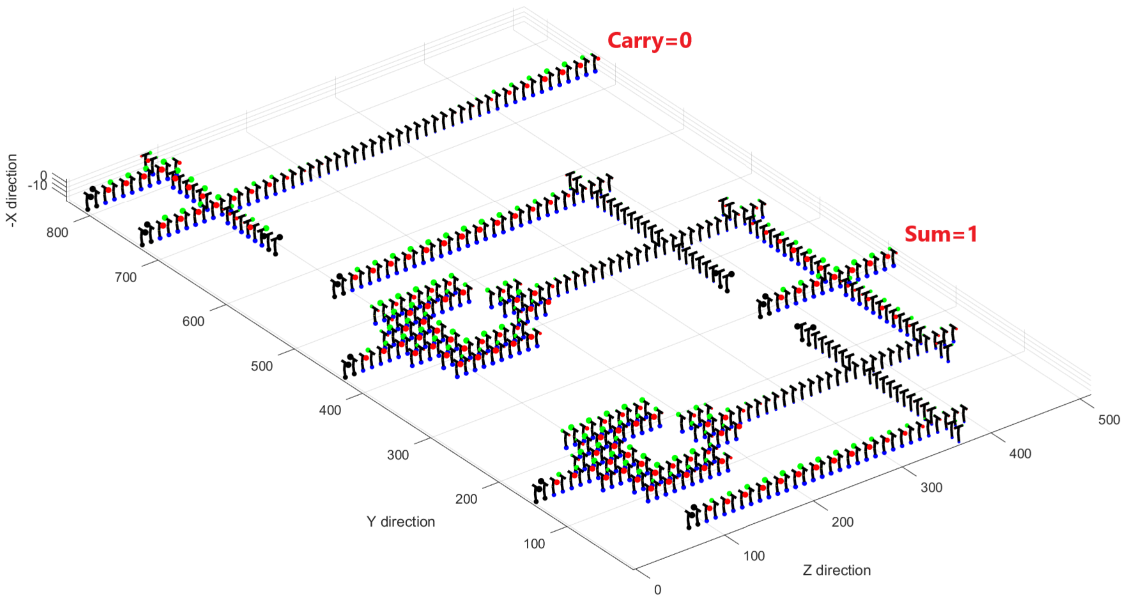

(i) Propagation of information in the final part of HA circuit with $A = 1$, $B = 0$ input pattern and corresponding output $Sum = 1$, $Carry = 0$.

Figure 6.10. Sinusoidal Clocked behaviour of Half Adder at wavelength $\lambda = 50\ nm$ and with all four input pattern configurations.

These results demonstrate the correctness of circuit implemented by SCERPA and the possibility of having a working functional device through Sinusoidal Clock mechanism at wavelength $\lambda = 50\ nm$. It is an interesting result since it demonstrates that ideally it is possible to transmit the information and perform sums at an impressive frequency of about $6\ PHz = 6 \cdot 10^{15}\ Hz$.
However, it is important to underline that this result has been obtained under very ideal conditions in which any kind of noise has been neglected, both the intrinsic one of the molecule and the one coming from the outside or generated by the other molecules. Furthermore, it has been considered that the clock is applied on the molecules, without considering neither how it is generated since today's technologies do not allow the clock generation at that frequency, nor with which physical implementation is applied to the molecules.

Chapter 7

MQCA Wire Noise Analysis

The last chapter concerns a first approach into thermal noise modelling induced in Bis-ferrocene molecules, in order to simulate a more realistic propagation of information in MQCA wire. The aim is to model a noise with a Gaussian distribution, according to the law:

$$f(x) = \frac{1}{\sqrt{2\pi\sigma^2}} \exp^{-\frac{(x-\mu)^2}{2\sigma^2}} \tag{7.1}$$

where μ is the mean value and it is supposed to be zero, while the standard deviation σ is found following the procedure described in the following.
Primarily, the so-called *Vin–Aggregated Charge Transcharacteristics* (VACT) of Bis-ferrocene molecules (obtained in [41]) has been exploited. It represents the relation between Aggregated Charges and the applied electric field, as illustrated in Figure 7.1, where it is possible to see that when the electric field applied to the MUT increases in modulus, a good charge separation between active dots is appreciable. Secondly, another element to consider is the dynamic behaviour of Aggregated Charges, resulting from the fact that these charges are not motionless but oscillate, as demonstrated in [20].

Unfortunately, specific dynamic simulation for Bis-ferrocene molecules was not carried out in [20] but only for Water and Decatriene molecules, for this reason using ad starting point these results, a reasonable *charge oscillation* values has been supposed in order to extract from the VACT the corresponding electric field variation ΔV_{in}, as depicted in Figure 7.1. Finally, imposing $\sigma = \Delta V_{in}$ thermal noise terms with Gaussian distribution are generated and added to the input voltage terms used in ideal case by SCERPA program.

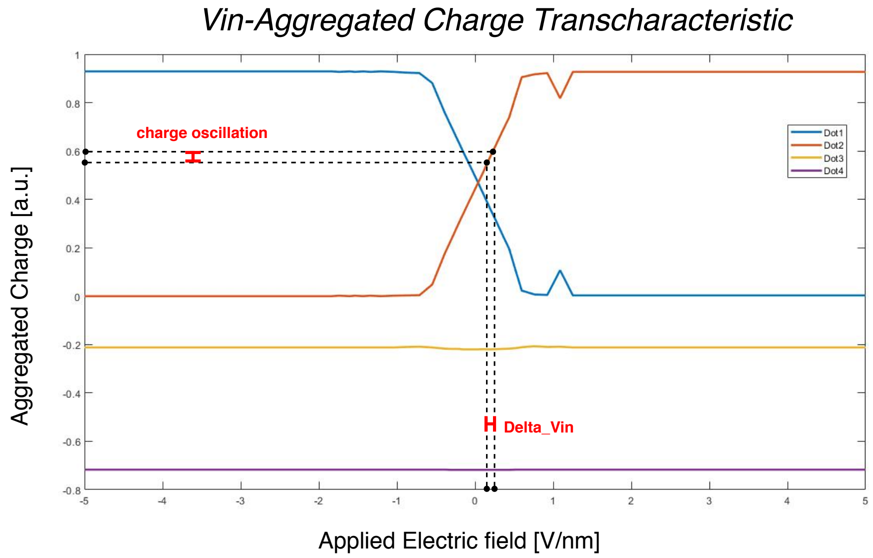

Figure 7.1. Bis-ferrocene Transcharacteristics: Aggregated Charges - Applied Electric Field relation.

7.1 Simulation Methodology and Results

A statistical approach has been accomplished for noisy MQCA Wire simulation, sending a certain number of frames in a wire with a fixed length and with a specific Sinusoidal Clock wavelength, estimating the error probability as:

$$BER_{Wire} = \frac{number\ of\ corrupted\ frames}{total\ transmitted\ frames} \tag{7.2}$$

Moreover, also the intermolecular distance $d = 8\,\text{Å}$ has been simulated to analyse the behaviour of noisy Wire when the electrostatic interactions between MQCA cells are stronger. Therefore, for simplicity's sake, having three degrees of freedom (wire length, sinusoidal clock wavelength and intermolecular distance), λ has been set in order to have the same number of activated cells even if the intermolecular distance is changed.

Wire formed by 20 molecules with Sinusoidal Clock at $\lambda = 20\ nm$ and $d = 1\ nm$

Several cases have been carried out with a wire formed by the arrangement of 20 molecules whose applied Sinusoidal Clock wavelength is equal to 20 nm, resulting in transmission of frames with length equal to about five cells. The simulations have been performed imposing a charge oscillation equal to 0.05 atomic unit (a.u.)

with corresponding $\Delta V_{in} = 81.8\ mV$. After that, the previous charge oscillation's value has been divided by an integer number n, with $n = 1,2,3,4...$, with consequent lowering of the σ which in turn leads to a reduction of noise induced in the molecules. This has been done in order to analyse the Noisy Wire performance at different noise intensities.

In the following the various BER_{Wire} attained from simulations are listed:

1. Noise obtained from charge oscillation = 0.055 a.u. $\Rightarrow$ $\sigma = \Delta V_{in} = 81.8\ mV$ and $d = 1\ nm$:
$$BER_{Wire} = \frac{50}{100} = 50\%$$
2. Noise obtained from charge oscillation = 0.0275 a.u. $\Rightarrow$ $\sigma = \Delta V_{in} = 40.9\ mV$ and $d = 1\ nm$:
$$BER_{Wire} = \frac{41}{100} = 41\%$$
3. Noise obtained from charge oscillation = 0.0183 a.u. $\Rightarrow$ $\sigma = \Delta V_{in} = 27.3\ mV$ and $d = 1\ nm$:
$$BER_{Wire} = \frac{32}{100} = 32\%$$
4. Noise obtained from charge oscillation = 0.0137 a.u. $\Rightarrow$ $\sigma = \Delta V_{in} = 20.5\ mV$ and $d = 1\ nm$:
$$BER_{Wire} = \frac{15}{100} = 15\%$$
5. Noise obtained from charge oscillation = 0.011 a.u. $\Rightarrow$ $\sigma = \Delta V_{in} = 16.4\ mV$ and $d = 1\ nm$:
$$BER_{Wire} = \frac{5}{100} = 5\%$$

Wire formed by 20 molecules with Sinusoidal Clock at $\lambda = 16\ nm$ and $d = 0.8\ nm$

In this case, always 20 molecules have been considered, with a Sinusoidal Clock Wavelength equal to 16 nm to keep constant the length of the frames (about five activated cells) with respect the case with intermolecular distance $d = 1\ nm$, as explained before.

In the following the various BER_{Wire} attained from simulations are listed:

1. Noise obtained from charge oscillation = 0.055 a.u $\Rightarrow$ $\sigma = \Delta V_{in} = 81.8\ mV$ and $d = 0.8\ nm$:
$$BER_{Wire} = \frac{6}{100} = 6\%$$

2. Noise obtained from charge oscillation = 0.0275 a.u. $\Rightarrow$ $\sigma = \Delta V_{in} = 40.9\ mV$ and $d = 0.8\ nm$:
$$BER_{Wire} = \frac{0}{100} = 0\% \quad (no\ error)$$

Afterwards, in Figures 7.2, 7.3, 7.4, 7.5, 7.6, 7.7 and 7.8 it is possible to see a charge distributions' comparison between a Wire in ideal conditions and other Wires in which the Gaussian noise has been applied, during the transmission of one frame.

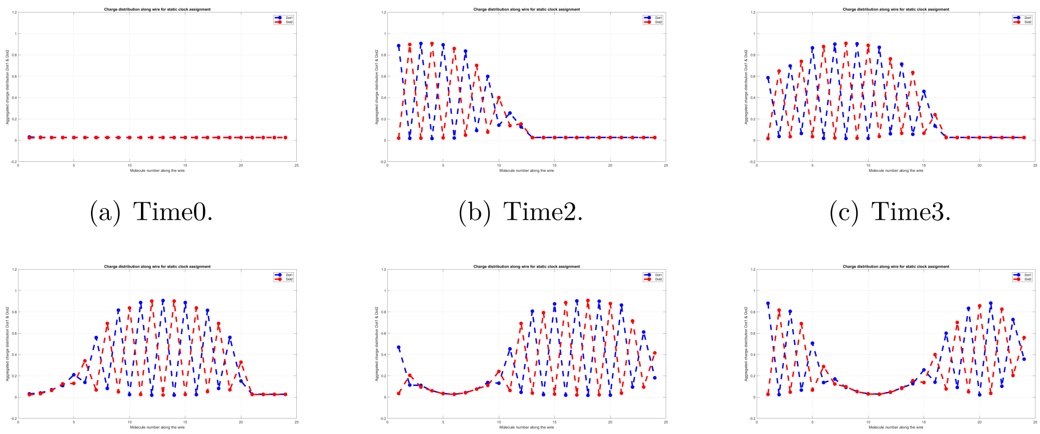

(a) Time0. (b) Time2. (c) Time3.

(d) Time4. (e) Time5. (f) Time6.

Figure 7.2. Charge distributions at different time instants of Sinusoidal Clocked Ideal Wire during transmission of one frame, with $\Delta V_{in} = 0\ mV$, $\lambda = 20\ nm$ and $d = 1\ nm$.

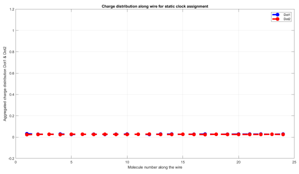

(a) Time0.

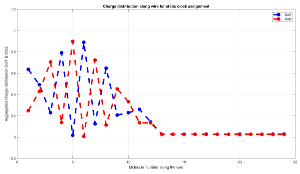

(b) Time2.

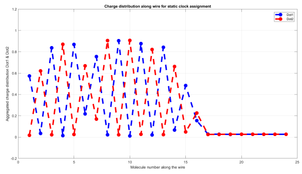

(c) Time3.

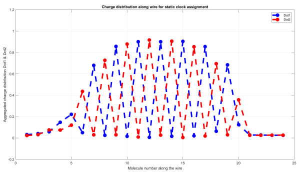

(d) Time4.

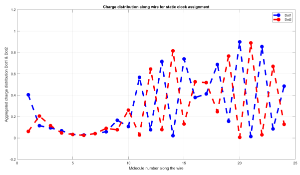

(e) Time5.

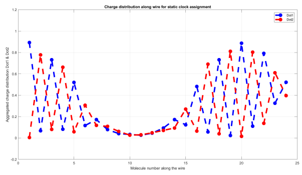

(f) Time6.

Figure 7.3. Charge distributions at different time instants of Sinusoidal Clocked Noisy Wire during transmission of one frame, with $\Delta V_{in} = 81.8\ mV$, $\lambda = 20\ nm$ and $d = 1\ nm$.

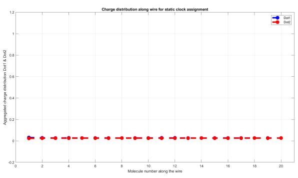

(a) Time0.

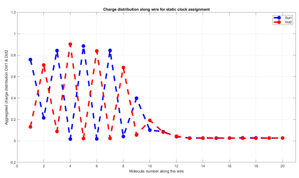

(b) Time2.

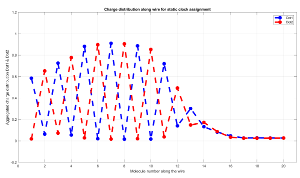

(c) Time3.

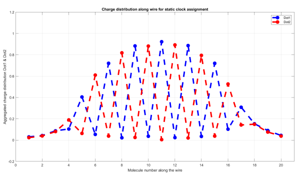

(d) Time4.

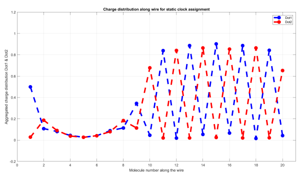

(e) Time5.

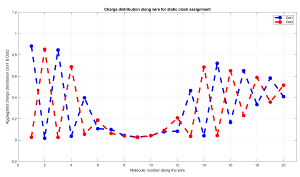

(f) Time6.

Figure 7.4. Charge distributions at different time instants of Sinusoidal Clocked Noisy Wire during transmission of one frame, with $\Delta V_{in} = 40.9\ mV$, $\lambda = 20\ nm$ and $d = 1\ nm$.

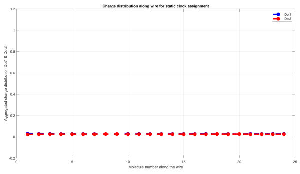

(a) Time0.

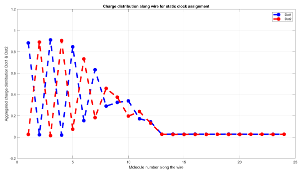

(b) Time2.

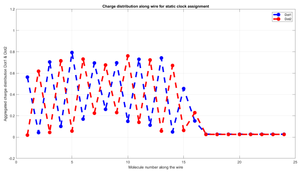

(c) Time3.

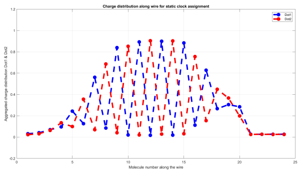

(d) Time4.

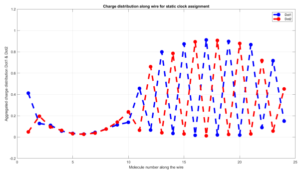

(e) Time5.

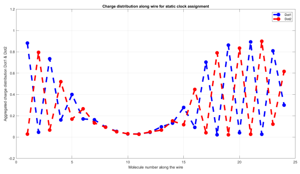

(f) Time6.

Figure 7.5. Charge distributions at different time instants of Sinusoidal Clocked Noisy Wire during transmission of one frame, with $\Delta V_{in} = 27.3\ mV$, $\lambda = 20\ nm$ and $d = 1\ nm$.

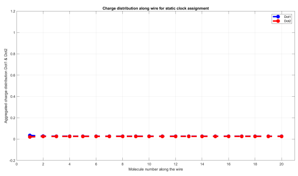

(a) Time0.

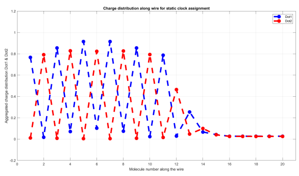

(b) Time2.

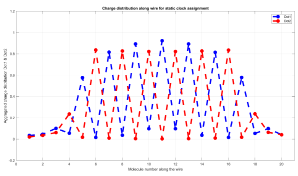

(c) Time3.

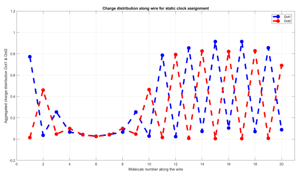

(d) Time4.

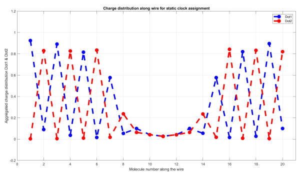

(e) Time5.

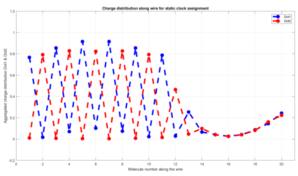

(f) Time6.

Figure 7.6. Charge distributions at different time instants of Sinusoidal Clocked Ideal Wire during transmission of one frame, with $\Delta V_{in} = 0\ mV$, $\lambda = 16\ nm$ and $d = 0.8\ nm$.

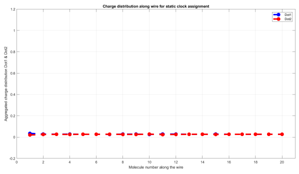

(a) Time0.

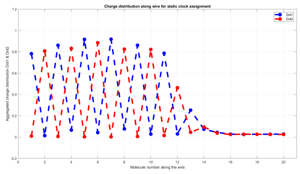

(b) Time2.

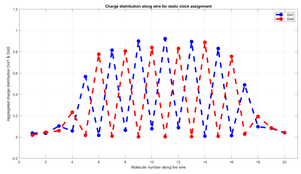

(c) Time3.

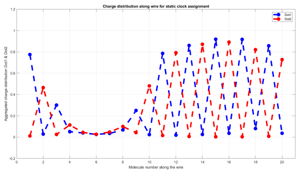

(d) Time4.

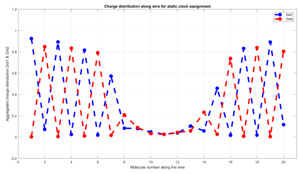

(e) Time5.

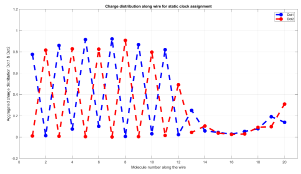

(f) Time6.

Figure 7.7. Charge distributions at different time instants of Sinusoidal Clocked Noisy Wire during transmission of one frame, with $\Delta V_{in} = 81.8\ mV$, $\lambda = 16\ nm$ and $d = 0.8\ nm$.

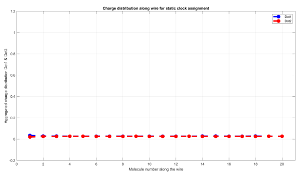

(a) Time0.

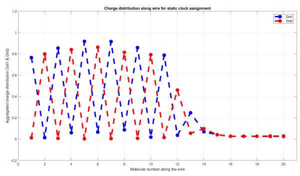

(b) Time2.

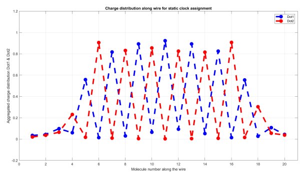

(c) Time3.

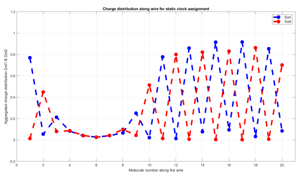

(d) Time4.

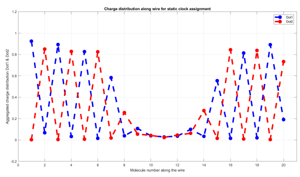

(e) Time5.

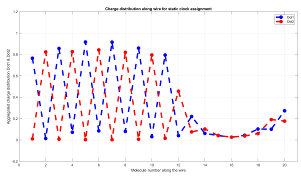

(f) Time6.

Figure 7.8. Charge distributions at different time instants of Sinusoidal Clocked Noisy Wire during transmission of one frame, with $\Delta V_{in} = 40.9\ mV$, $\lambda = 16\ nm$ and $d = 0.8\ nm$.

As expected, the noise plays a key role in information propagation and lower error probabilities in MQCA Wire with $d = 0.8\ nm$ are evaluated due to the stronger intermolecular interaction denoting a more stable device.

It is important to stress that a lot of work to do inherently to this field of research must still be performed, since only a first noise analysis has been accomplished, without considering the precise charge oscillation's range of Bis-ferrocene and any analytical model of quantum *Intermolecular Forces* (IMF) which rule interaction between molecules, such as London interaction Forces and possible instantaneous dipoles. However, important feedback results have been obtained demonstrating the possibility to transmit information even in the presence of noise. This aim is achievable through a suitable choice of molecule and an intermolecular distance sufficiently short, in order to ensure a strong electrostatic interaction.

Chapter 8

Conclusion and Future Perspectives

The primary objective of this thesis was to prove the operational feasibility of a *Sinusoidal Clock* applied to all basic QCA logic gates, including the possibility to transfer properly information and evaluation of operating conditions' limits.
In particular, for the first time, the analysis and characterization trough MATLAB® program SCERPA of sinusoidal clocked behaviour of MQCA Wire, Angle, T-shape, Majority Voter and Inverter has been proposed.

From the point of view of code design, an integration of Layout section has been performed to define the sinusoidal wave parameters, managing properly the space-time shift of this clock starting from a condition in which the structure is entirely in Reset state.
Another portion of code has been written to automatically associate the extracted samples from the clock wave with the molecules defined in the layout, resulting in the possibility to implement the Sinusoidal Clock on MQCA device simply choosing the desired structure and setting few parameters of the wave, like the wavelength, amplitude, number of time instants etc.
Whereupon code design, simulations have highlighted many limitations on information propagation, leading to an improvement of almost all device layouts and a total re-design of new Inverter able to work properly with both Three-Phase and Sinusoidal Clock mechanisms.

The lower bound of Sinusoidal Clock, from wavelength point of view, equal to $\lambda = 20\ nm$ has been found ensuring correct propagation in all MQCA structures analysed in this work.

Regarding the upper bound, no limit has been found due to slow turning on of the MQCA wire deriving from the use of this kind of Clock at high wavelengths, removing one of the metastability's causes that occurs in information propagation along the wire without any clock mechanism. In fact, in the stationary condition reached in MQCA Wire with $\lambda = 100\ \mu m$ where, at each time instant, the almost same clock voltage value (ranging from $-2\ V$ to $2\ V$) is applied in all the molecules, no error propagation occurs demonstrating the possibility, in ideal conditions, to preserve the integrity of information with arbitrarily large wavelengths.

For this reason, in the last chapter a first qualitative model of molecule's intrinsic thermal noise has been developed, in order to execute preliminary analysis and more realistic simulations, that possibly will lead in future works to the determination of the maximum wavelength limit of Sinusoidal Clock guaranteeing information integrity on all basic MQCA blocks.

In conclusion, going up to circuit level, the Half Adder has been simulated merging the previously characterized components and testing all possible input configurations, demonstrating correct behaviour and allowing the validation of all good results arising from the logic level analysis.

Concerning future perspectives, many aspects can be improved. Primarily, designing of a possible physical implementation capable to apply the sinusoidal electric field on the molecules is necessary, with consequent evaluation through FEM simulations, of real electric field values generated by the electrodes or transmission lines. A possible idea, based on concepts proposed in [24], consists of using a grid of nanowires acting as electrodes, placed above or underneath the molecules, in which time-varying signals are applied. After that, switching off and on appropriately the nanowires and summing the electric field contributions generated by them, in theory, it is possible to create a sinusoidal clock field and to simulate its propagation along the circuit.

Could be useful to create a MATLAB® script able to compute the electric field generated by nanowires and study, once their position and that of the molecules are known, their effect on MQCA block.

Secondly, in-depth study and more accurate modelling of the molecule's internal noise is required to understand the maximum wavelength applicability on MQCA Wire and to obtain, in this way, the realistic upper bound of λ in which all devices are able to work safely.

In fact, only qualitative analysis has been executed, without performing any modelling of intermolecular forces. In particular, among them, the appropriate analytical model of London Dispersion forces, defined as weak attractive forces arising from interaction between instantaneous dipoles in molecules without permanent dipolar moment [27], is fundamental to create an accurate noise model and to obtain reliable simulation results.

Finally, a further step in noise analysis is the generation of external perturbations to simulate the components or circuits in a more real environment; with consequent designing of electromagnetic shielding able to guarantee correct information propagation.

List of Acronyms

IC	Integrated Circuit
CMOS	Complementary Metal-Oxide Semiconductor
DIBL	Drain Induced Barrier Lowering
ERD	Emerging Research Devices
FCN	Field-Coupled NanoComputing
QCA	Quantum Dot Cellular Automata
MQCA	Molecular Quantum-dot Cellular Automata
NML	NanoMagnetic Logic
AQCA	Atomic Quantum Cellular Automata
CA	Cellular Automata
SEM	Scanning Electron Microscope
EBL	Electron Beam Lithography
CV	Cyclic Voltammetry
ESP	Electrostatic Potential
MUT	Molecule Under Test
$\boldsymbol{V_{IN}}$	Input Voltage
$\boldsymbol{V_{OUT}}$	Output Voltage
SET	Single Electron Transistor
SCERPA	Self Consistent Electrostatic Potential Algorithm
FEM	Finite Element Method
VACT	Vin–Aggregated Charge Transcharacteristics
IMF	Intermolecular Forces

Bibliography

[1] Li C; Fan W; Lei B; Zhang D; Han S; Tang T; et al. "Multilevel memory based on molecular devices." In: *Journal of Applied Physics Letters.* vol. 84.no. 11 (2004).

[2] Giorgio Alemanno. "Analysis and development of a structure for nanocomputing based on organic molecules". Master thesis. Torino, Italia: Politecnico di Torino, December 2018.

[3] Neal G. Anderson and Sanjukta Bhanja (Eds.) *Field-Coupled Nanocomputing: Paradigms, Progress, and Perspectives.* LNCS. Vol. vol. 8280. Berlin, Verlag, Heidelberg: Springer, 2014.

[4] Yuri Ardesi. "Energy Analysis and Bistability Study of Molecular FCN". Master thesis. Torino, Italia: Politecnico di Torino, December 2017.

[5] Semiconductor Industry Association. *International Technology Roadmap for Semiconductors 2.0.* 2015 edition. URL: http://www.itrs2.net/.

[6] A. Aviram. "Molecules for memory, logic, and amplification". In: *Journal of the American Chemical Society* vol. 110 (1988), 5687–5692.

[7] N. S. Hush; A. T. Wong; G. B. Bacskay; and J. R. Reimers. "Molecular switches: the critical-field in electricfield activated bistable molecules". In: *Journal of the American Chemical Society* vol. 112 (1990), 4192–4197.

[8] Suhaib Ahmed Bisma Bilal and Vipan Kakkar. "Quantum Dot Cellular Automata: A New Paradigm for Digital Design". In: *International Journal of Nanoelectronics and Materials* vol. 11 (January 2018), pp. 87–98.

[9] Perez-Martinez F. Farrer I. Anderson D. Jones G. Ritchie D. Chorley S. Smith C. "Demonstration of a quantum cellular automata cell in a GaAs/AlGaAs heterostructure." In: *Journal of Applied Physics.* vol. 91 (2007), 032102–032103.

[10] Bernstein Gary H. Alexandra Imre V. Metlushko A. Orlov L. Zhou L. Ji György Csaba and Wolfgang Porod. "Magnetic QCA systems." In: *Microelectronics Journal* vol. 36.no. 7 (2005), pp. 205–208.

[11] Macucci M. Gattobigio M. Bonci L. Iannaccone G. Prins F. Single C. Wetekam G. Kern D. "A QCA cell in silicon-on-insulator technology: theory and experiment." In: *Superlattices Microstruct.* vol. 34 (2003), 205–211.

[12] Mitic M. Cassidy M. Petersson K. Starrett R. Gauja E. Brenner R. Clark R. Dzurak A. Yang C. Jamieson D. “Demonstration of a silicon-based quantum cellular automata cell.” In: *Journal of Applied Physics.* vol. 96 (2006), pp. 013503–013503.

[13] Single C. Prins F. Kern D. “Simultaneous operation of two adjacent double dots in silicon.” In: *Journal of Applied Physics.* vol. 78 (2001), 1421–1423.

[14] A. Pulimeno; M. Graziano; A. Sanginario; V. Cauda; D. Demarchi and G. Piccinini. “Bis-ferrocene molecular QCA wire: ab-initio simulations of fabrication driven fault tolerance”. In: *IEEE Transactions on Nanotechnology* vol. 12 (2013), 498–507.

[15] A. Pulimeno; M. Graziano; D. Demarchi and G. Piccinini. “Towards a molecular QCA wire: simulation of write-in and read-out systems”. In: *Solid State Electronics* Elsevier, vol. 77 (2012), pp. 101–107.

[16] Leonardo Doffo. “Analysis and development of a structure for nanocomputing based on organic molecules”. Master thesis. Torino, Italia: Politecnico di Torino, July 2016.

[17] Pulimeno A.; Graziano M.; Abrardi C.; Demarchi D.; Piccinini G. “Molecular QCA: a write-in system based on electric fields”. In: *IEEE Nanoelectronics Conference (INEC)* (June 2011).

[18] Pulimeno A.; Graziano M.; Antidormi A.; Wang R.; Zahir A.; Piccinini G. “Understanding a Bisferrocene Molecular QCA Wire”. In: *Field-Coupled Nanocomputing* Neal G. Anderson and Sanjukta Bhanja (Eds.); Springer; Berlin, Verlag, Heidelberg; vol. 8280 (2014), 307–338.

[19] Pulimeno A.; Graziano M.; Piccinini G. “Molecule Interaction for QCA Computation”. In: *IEEE NANO2012 12th International Conference on Nanotechnology* Birmingham (UK) (August 2012), 20–23.

[20] Alessandro Gaeta. “Molecular QCA timing: simulation and analysis of charge time evolution”. Master thesis. Torino, Italia: Politecnico di Torino, July 2018.

[21] Joyce RA; Qi H; Fehlner TP; Lent CS; Orlov AO; Snider GL.r. “A system to demonstrate the bistability in molecules for application in a molecular QCA cell”. In: *IEEE nanotechnology materials and devices conference* vol. 2 (June 2009), pp. 9–45.

[22] R. Wang; A. Pulimeno; M. Ruo Roch; M. Graziano and G. Piccinini. “Effect of a Clock System on Bis-ferrocene Molecular QCA”. In: *IEEE Transactions on Nanotechnology* vol. 15.no. 4 (July 2016).

[23] Ruiyu Wang; Michele Chilla; Alessio Palucci; Mariagrazia Graziano and Gianluca Piccinini. “An effective algorithm for clocked Field-Coupled Nanocomputing paradigm”. In: *IEEE nanotechnology materials and devices conference* (July 2016).

[24] Kevin Hennessy and Craig S.Lent. "Clocking of molecular quantum-dot cellular automata". In: *American Vacuum Society* (25 June 2001). DOI: 10.1116/1.1394729.

[25] G. Ji L. Orlov A. Bernstein G.H. Porod W. Imre A. Csaba. "Majority logic gate for magnetic quantum-dot cellular automata." In: *Science* vol. 311.no. 5758 (2006), pp. 205–208.

[26] C. S. Lent; B. Isaksen and M. Lieberman. "Molecular quantum-dot cellular automata". In: *Journal of the American Chemical Society* vol. 125 (2003), 056–1063.

[27] Mohamad Mohebifar; Erin R. Johnson and Christopher N. Rowley. "Evaluating Force-Field London Dispersion Coefficients Using the Exchange-Hole Dipole Moment Model". In: *J. Chem. Theory Comput.* (November 2017), 6146–6157. DOI: 10.1116/1.1394729.

[28] Craig S. Lent and Beth Isaksen. "Clocked Molecular Quantum-Dot Cellular Automata". In: *IEEE Transactions on Electron Devices* vol. 50 (2003), 1890–1896.

[29] H. Qi; S. Sharma; Z. Li; G.L. Snider; A.O. Orlov; C.S. Lent and T.P. Fehlner. "Molecular quantum cellular automata cells. Electric field driven switching of a sil- icon surface bound array of vertically oriented two-dot molecular quantum cellular automata". In: *Journal of the American Chemical Society* vol. 125 (July 2016), pp. 5250–15259.

[30] Yuhui Lu. "Molecular quantum-dot cellular automata: From molecular structure to circuit dynamics". In: *Journal of Applied Physics.* vol. 102 (2007).

[31] Yuhui Lu and Craig S Lent. "A device architecture for computing with quantum dots". In: *Proceedings of the IEEE* vol. 85 (April 1997), pp. 541 –557.

[32] Yuhui Lu and Craig S Lent. "Metric for characterizing the bistability of molecular quantum-dot cellular automata". In: *Journal of Nanoelectronics.* vol. 19.no. 15 (2008).

[33] Massimo Macucci. *Quantum Cellular Automata: Theory, Experimentation and Prospects.* Covent Garden, London: Imperial College Press, 2006.

[34] Usha Mehta and Vaishali Dharer. *Quantum-dot Cellular Automata (QCA): A Survey.* Nirma University, Ahmedabad, India.

[35] Cowburn R. P. and M. E. Welland. "Room temperature magnetic quantum cellular automata." In: *Science* vol. 287.no. 5457 (2000), pp. 619–624.

[36] Singh ; U.C.; Kollman; P.A. "An approach to computing electrostatic charges for molecules". In: *Journal of Computational Chemistry* vol. 5 (1984), pp. 129–145.

[37] Mariagrazia Graziano; Ruiyu Wang; Massimo Ruo Roch; Yuri Ardesi; Fabrizio Riente; Gianluca Piccininii. "Characterisation of a bis-ferrocene molecular QCA wire on a non-ideal gold surface". In: *Micro and Nano Letters* vol. 14 (2019), pp. 22–27.

[38] Lorenzo Polsinelli. "Simulation of nanoelectronic systems". Master thesis. Torino, Italia: Politecnico di Torino, 2016-2017.

[39] A. Orlov A. Imre G. Csaba L. Ji W. Porod and G. H. Bernstein. "Magnetic Quantum-Dot Cellular Automata: Recent Developments and Prospects". In: *Journal of Nanoelectronics and Optoelectronics* vol. 3.no. 1 (2008), pp. 1–14. DOI: 10.1166/jno.2008.004.

[40] C. S. Lent; P. D. Tougaw; W. Porod and G. H. Bernstein. "Quantum cellular automata". In: *Journal of Nanoelectronics.* vol. 4 (1993), pp. 49 –57.

[41] Yuri Ardesi. Azzurra Pulimeno. Mariagrazia Graziano. Fabrizio Riente and Gianluca Piccinini. "Effectiveness of Molecules for Quantum Cellular Automata as Computing Devices". In: *Journal of Low Power Electronics and Applications* vol. 8.no. 24 (July 2018). DOI: 10.3390/jlpea8030024.

[42] R.Jayalakshmi and R.Amutha. "A Theoretical Study on the Implementation of Quantum Dot Cellular Automata". In: *4th International Conference on Advances in Electrical, Electronics, Information, Communication and Bio-Informatics (AEEICB-18)).* Tamil Nadu, India, 2018.

[43] Wang Ruiyu. "Analysis and Modulation of Molecular Quantum-dot Celluar Automata (QCA) Wire". PhD thesis. Torino: Politecnico di Torino, March 2017.

[44] John Timler and Craig S. Lent. "Power gain and dissipation in quantumdot cellular automata". In: *Journal of Applied Physics.* vol. 91 (2002). DOI: 10.1063/1.1421217.

[45] G. Toth and C.S. Lent. "Quasi-adiabatic Switching for Metal-Island Quantum-dot Cellular Automata". In: *Journal of Applied Physics* vol. 85 (1999), pp. 2977–2984.

[46] C.S. Lent; P.D. Tougaw and W. Porod. "Quantum cellular automata: the physics of computing with arrays of quantum dot molecules". In: *PHYSCOMP 94 Proceedings* (1994), pp. 5–13.

[47] P.G. Cozzi V. Arim; M. Iurlo; L. Zoli; S. Kumar; M. Piacenza; F. Della Sala; F. Matino; G. Maruccio; R. Rinaldi; F. Paolucci; M. Marcaccio and A.P. Bramanti. "Toward quantum-dot cellular automata units: thiolated-carbazole linked bisferrocenes". In: *Nanoscale* vol. 4 (2012), 813–823.

[48] Mary Mehrnoosh Eshaghian Wilner. *Bio-Inspired and Nanoscale Integrated Computing.* Hoboken, New Jersey: John Wiley and Sons, Inc., 2009.

[49] L. Zoli. “Active bis-ferrocene molecules as unit for molecular computation”. PhD thesis. 2010.